NAVAL POSTGRADUATE SCHOOL
Monterey, California

THESIS

A FINE RESOLUTION MODEL OF THE COASTAL EASTERN BOUNDARY CURRENT SYSTEMS OFF IBERIA AND MOROCCO

by

Antonio S. Martinho

March 2001

Thesis Advisor: Mary L. Batteen
Second Reader: R. T. Williams

Approved for public release; distribution is unlimited.

REPORT DOCUMENTATION PAGE

Form Approved
OMB No. 0704-0188

1. AGENCY USE ONLY *(Leave blank)*	2. REPORT DATE March 2001	3. REPORT TYPE AND DATES COVERED Master's Thesis

4. TITLE AND SUBTITLE A Fine Resolution Model of the Coastal Eastern Boundary Current Systems off Iberia and Morocco

5. FUNDING NUMBERS

6. AUTHOR(S)
Martinho, Antonio S.

7. PERFORMING ORGANIZATION NAME(S) AND ADDRESS(ES)
Naval Postgraduate School
Monterey, CA 93943-5000

8. PERFORMING ORGANIZATION REPORT NUMBER

9. SPONSORING / MONITORING AGENCY NAME(S) AND ADDRESS(ES)

10. SPONSORING / MONITORING AGENCY REPORT NUMBER

11. SUPPLEMENTARY NOTES
The views expressed in this thesis are those of the author and do not reflect the official policy or position of the Department of Defense or the U.S. Government.

12a. DISTRIBUTION / AVAILABILITY STATEMENT
Approved for public release; distribution is unlimited.

12b. DISTRIBUTION CODE

13. ABSTRACT *(maximum 200 words)*

To investigate the role of wind forcing, bottom topography and thermohaline gradients on classical as well as unique features in the northern Canary Current system (NCCS), four experiments are conducted with a sigma coordinate primitive equation model. The first experiment, which investigates the pressure gradient force error, shows that velocity errors inherent in three dimensional sigma coordinate models can be successfully reduced from ~1 m/s to less than 0.5 cm/s in the NCCS. The second experiment, which investigates the effect of annual wind forcing on a flat bottom, accurately portrays classical eastern boundary current features as well as unique NCCS features associated with a large embayment (i.e., the Gulf of Cadiz), poleward spreading of Mediterranean Outflow, and the generation of Meddies. The additional effect of bottom topography in Experiment 3 shows that topography plays important roles in intensifying and trapping the equatorward current near the coast, in weakening the subsurface poleward current and in intensifying eddies off the capes of Iberia. The use of full instead of horizontally averaged thermohaline gradients in Experiment 4 highlights the development of the Iberian Current off the Portugal west coast, a feature not seen in the previous experiments. This shows that thermohaline gradients play an important role for the formation of the Iberian Current.

14. SUBJECT TERMS	15. NUMBER OF PAGES
Primitive equation model, northern Canary Current System, currents, meanders, eddies, Meddies, filaments, undercurrent, POM	116
	16. PRICE CODE

17. SECURITY CLASSIFICATION OF REPORT	18. SECURITY CLASSIFICATION OF THIS PAGE	19. SECURITY CLASSIFI- CATION OF ABSTRACT	20. LIMITATION OF ABSTRACT
Unclassified	Unclassified	Unclassified	UL

NSN 7540-01-280-5500

Standard Form 298 (Rev. 2-89)
Pescribed by ANSI Std. 239-18

THIS PAGE INTENTIONALLY LEFT BLANK

Approved for public release; distribution is unlimited

THE ROLE OF THE PLANETARY BETA EFFECT ON CURRENTS AND MEDDIES IN THE NORTHERN CANARY CURRENT SYSTEM

Antonio S. Martinho
Lieutenant, Portuguese Navy
B.S., Portuguese Naval Academy, 1992

Submitted in partial fulfillment of the
requirements for the degree of

MASTER OF SCIENCE IN PHYSICAL OCEANOGRAPHY

from the

NAVAL POSTGRADUATE SCHOOL
March 2001

Author: Antonio Costa Neves Santos Martinho

Antonio S. Martinho

Approved by: Mary L. Batteen

Mary L. Batteen, Thesis Advisor

R. T. Williams

R. T. Williams, Second Reader

Roland W. Garwood, Chairman
Department of Oceanography

THIS PAGE INTENTIONALLY LEFT BLANK

ABSTRACT

To investigate the role of wind forcing, bottom topography and thermohaline gradients on classical as well as unique features in the northern Canary Current system (NCCS), four experiments are conducted with a sigma coordinate primitive equation model. The first experiment, which investigates the pressure gradient force error, shows that velocity errors inherent in three dimensional sigma coordinate models can be successfully reduced from ~1 m/s to less than 0.5 cm/s in the NCCS. The second experiment, which investigates the effect of annual wind forcing on a flat bottom, accurately portrays classical eastern boundary current features as well as unique NCCS features associated with a large embayment (i.e., the Gulf of Cadiz), poleward spreading of Mediterranean Outflow, and the generation of Meddies. The additional effect of bottom topography in Experiment 3 shows that topography plays important roles in intensifying and trapping the equatorward current near the coast, in weakening the subsurface poleward current and in intensifying eddies off the capes of Iberia. The use of full instead of horizontally averaged thermohaline gradients in Experiment 4 highlights the development of the Iberian Current off the Portugal west coast, a feature not seen in the previous experiments. This shows that thermohaline gradients play an important role for the formation of the Iberian Current.

THIS PAGE INTENTIONALLY LEFT BLANK

TABLE OF CONTENTS

THIS PAGE INTENTIONALLY LEFT BLANK

LIST OF FIGURES

LIST OF TABLES

THIS PAGE INTENTIONALLY LEFT BLANK

I. INTRODUCTION

The Canary Current System (CCS) on the eastern boundary of the central North Atlantic is a classical eastern boundary current (EBC) system. Stretching from ~10°N to ~45°N along the coasts of northwest Africa and the Iberian Peninsula (IP), it marks the closing eastern boundary of the North Atlantic Gyre. Typical of other EBCs, the mean equatorward Canary Current (CC) is a broad (~1000 km), relatively slow (~10-30 cm/s), yearlong surface flow extending to depths of ~500 m (Wooster *et al.*, 1976). The portion of the CC that stretches along the coast of the IP is often referred to as the Portugal Current (e.g., Tomczak and Godfrey, 1994).

As in other EBCs, a poleward undercurrent exists near the coast beneath the CC (e.g., Meincke *et al.*, 1975; Fiuza, 1980) as a relatively narrow (~10-40 km) and weak (~2-10 cm/s) flow, which is strongest between ~100 and ~600 m depth. The depth and strength of the undercurrent varies seasonally and latitudinally. In winter it shoals to the north near Cabo da Roca (see Figure 1 for geographic locations, and Figure 2a for bathymetric contours and coastline geometry for the region), and forms a third flow component commonly referred to as the Iberian Current (IC) (Haynes and Barton, 1990). A narrow (25-40 km), relatively weak (~20-30 cm/s), seasonal surface current, the IC is found trapped near the coast against the shelf break (Fiuza, 1980; Frouin *et al.*, 1990; Haynes and Barton, 1990) and can occasionally be seen as far south as Cabo de Sao Vincente (Batteen *et al.*, 2000).

A unique feature that distinguishes the CCS from other EBCs is the existence of Mediterranean Outflow (MO) through the Strait of Gibraltar into the adjacent Gulf of

Cadiz. A large embayment, the Gulf of Cadiz's pronounced east-west coastline orientation results in weaker upwelling in the Gulf of Cadiz than to the north or south of the Gulf of Cadiz, due to the dominant equatorward trade wind direction. The Gulf of Cadiz also creates a large separation between the two west coast upwelling regimes so that no continuous flow between the two appears to exist (Barton, 1998).

The salty MO plume that exits the Mediterranean Sea through the Strait of Gibraltar is diluted, thickens, and becomes vertically differentiated into two distinct cores as it flows westward into the Gulf of Cadiz (Iorga and Lozier, 1999). At ~7°W in the Gulf of Cadiz, both a shallow core at depths of ~600-900 m and a deeper core at ~1100-1200 m exist. Both cores continue to flow westward along the southern coast of Spain and turn poleward around Cabo de Sao Vincente (Amber and Howe, 1979; Iorga and Lozier, 1999). A third, shallower, poleward core of Mediterranean water has also been traced from the Strait of Gibraltar northward to ~38.5°N off western Portugal (Amber, 1982). In addition, a climatological cyclonic circulation in the southwestern Gulf of Cadiz acts to spread salty MO south of ~34°N (Iorga and Lozier, 1999).

The northern CCS (NCCS) is influenced predominantly by equatorward, upwelling favorable winds produced by the eastern half of the Azores High. Located in the northeastern part of the Atlantic Ocean, the Azores High is a semi-permanent subtropical high pressure system similar in nature and behavior to the North Pacific Subtropical High (Nelson, 1977). As such, the center of the Azores High migrates meridionally with the seasons, reaching its southernmost extent near 27°N in March and ridging north to ~33°N by August. The building and migration of the Azores High cause wind stress values over the NCCS region to vary temporally, resulting in both alongshore

and cross-shore variability of the predominantly equatorward winds along the west coast of the IP and the northwest coast of Africa. The east-west pressure contrast between Portugal and the center of the Azores High during summer is ~8 mb. In winter, this pressure gradient weakens to ~1 mb. As a result of this seasonally changing pressure gradient, considerably stronger northerly and northwesterly winds occur in the NCCS region in summer, while northerly and northwesterly winds become weaker to even slight southerly off the Iberian Peninsula in winter (Batteen *et al.*, 2000). The shift in maximum wind stress also causes upwelling favorable winds to shift from ~27°N near the Canary Islands in January, to ~43°N off Portugal by July (Fiuza, 1982).

Like other classical EBCs, observations of the sea surface in the NCCS region have shown highly energetic mesoscale features such as jet-like surface currents, meanders, eddies and filaments over the broad climatological mean flow of the CC. Satellite sea surface images have shown nearshore upwelling during periods of upwelling favorable winds with several narrow filaments of cooler water extending off the coast of the Iberian Peninsula (Fiuza and Sousa, 1989) and Cape Ghir in northwest Africa (Van Camp *et al.*, 1991; Hagen *et al.*, 1996). In these images, upwelling filaments often extend ~80-150 km offshore, with alongshore spacing of ~80-100 km between filaments (Haynes *et al.*, 1993), and often terminate with dipole eddy pairs (Fiuza *et al.*, 1982; Barton, 1998). Observations have also shown anticyclonic and cyclonic pairs of mesoscale eddies on the order of 100 km off the IP coast (Fiuza, 1984; Stammer *et al.*, 1991). These mesoscale features have been observed during periods of predominantly upwelling favorable winds and appear to be located near prominent coastline irregularities such as capes. These observations provide evidence that wind forcing along

with coastline irregularities appear to be important mechanisms in the formation and sustainment of many of the mesoscale features found in the NCCS domain and other EBC regions (Batteen *et al.*, 2000).

Unique to the NCCS is the generation of anticyclonic submesoscale coherent vortices (SCVs) or Meddies. Numerical studies suggest that baroclinic instability of the northward dense plume of salty MO along the IP continental slope leads to the generation of Meddies (Kase *et al.*, 1989). As a result of numerous observations over the past decade, the primary generation region of Meddies is widely accepted to be near Cabo de Sao Vincente, off southwest Portugal. Several different trajectories of Meddies have been observed, including a southwestward movement into the Canary Basin, and westward translations south of the Azores (Richardson and Tychensky, 1998).

Over the last two decades numerous modeling studies have focused on the driving mechanisms of complex mesoscale activities in EBC regions, including upwelling filaments, highly energetic eddies, and meandering jets. For the California Current System, the classical EBC system, baroclinic instability, wind forcing, and coastline irregularities have been investigated as possible generation mechanisms (e.g., Ikeda *et al.*, 1984a, b; Batteen, 1997).

For the NCCS, Batteen *et al.*, (2000) used the results of four numerical experiments of increasing complexity to investigate the classical and unique features of the NCCS. All four experiments were run on a ∃-plane. Experiment 1 included seasonal wind forcing on a straight coast, while Experiments 2 and 3 added the effects of irregular coastline geometry to the seasonal wind forcing. The most complex experiment, Experiment 4, added the effects of both thermohaline gradients and annual MO to the

seasonal wind forcing and irregular coastline geometry. Consistent with previous studies, wind forcing was shown to be a key generative mechanism for EBC mesoscale features, while capes were shown to be key areas for enhanced upwelling, extensive filaments, maximum current velocities and enhanced growth of cyclonic meanders and eddies. Unique features of the NCCS, including the development of anticyclonic meanders and eddies in an embayment like the Gulf of Cadiz and the generation of Meddies from MO, were also highlighted .

Another study by Batteen and Murray (2000) investigated the role of planetary beta on classical as well as unique features in the NCCS. Four numerical experiments were conducted with varying Coriolis parametrizations (f-plane or beta-plane). The first two experiments used a closed boundary and annual salinity forcing for the MO. The latter two experiments used an open Mediterranean Sea at the Strait of Gibraltar and seasonal forcing for MO to permit a more accurate investigation of the subsurface spreading of MO and Meddies. All four experiments used seasonal climatological winds and seasonal thermohaline gradients along the western boundary to force the model. Experiments run on a $\exists$-plane (Experiments 2 and 4) accurately portrayed classical eastern boundary current (EBC) mesoscale features. In addition, these experiments depicted unique NCCS features associated with a large embayment (the Gulf of Cadiz), poleward spreading of MO, and the generation of Meddies. Experiments run on an *f*-plane (Experiments 1 and 3) showed the unrealistic dominance of a continuously strengthening equatorward jet that inhibited the development of classical EBC and unique NCCS features. The complex upper layer and subsurface flow regimes of Experiment 4

most realistically portrayed currents, mesoscale features and Meddies similar to NCCS observations.

The objective of this study is to build on previous studies by incorporating the effects of bottom topography . The Princeton Ocean Model (POM), a bottom following sigma coordinate model, was chosen for this study because it has been widely used to simulate coastal processes associated with continental shelf flows and bottom boundary layer dynamics. The results of several numerical experiments (see Table 1) are explored. Each experiment includes the effects of thermohaline forcing at all three open boundaries, and uses a beta plane. In Experiment 1 velocity errors produced by the pressure gradient force error, an error inherent in all three-dimensional sigma coordinate models, are investigated using the horizontally averaged climatology with bottom topography and no wind forcing. In Experiment 2 the horizontally averaged annual climatology is used with annual wind forcing on a flat bottom. Experiment 3 is the same as Experiment 2 except that bottom topography has been incorporated. To explore the role of bottom topography on the NCCS, the results of Experiment 3 are compared with the results of Experiment 2. Experiment 4 is the same as Experiment 3 except that full annual climatology is used instead of the horizontally averaged annual climatology. To determine the role of the full climatology, results of Experiment 4 are compared with the results of Experiment 3.

This study is organized as follows. In section 2 we describe the numerical model and the specific experimental conditions. The results of the numerical experiments are presented in section 3. A summary is presented in section 4.

II MODEL DESCRIPTION

A. DATA SETS

The topographic data were obtained from the Institute of Geophysics and Planetary Physics, University of California San Diego (Sandwell D.T. and W.F. Smith, 1996). The data set has a resolution of 2 minutes (e.g., 1/30 of a degree) and is a compilation of 30 years of data soundings obtained by ships. Where the ships' data is sparse, altimetry information was used to interpolate soundings .

Annual temperature and salinity values were obtained from Levitus and Boyer (1994) and Levitus et al. (1994). The data uses a 1 by 1 degree horizontal resolution at the vertical levels shown in Table 2.

For wind forcing, climatological wind fields were obtained from the European Centre for Medium Range Weather Forecasts (ECMWF) near-surface wind analyses (Trenberth et al., 1990). The data uses a 2.5 by 2.5 degree grid.

B. PRE-PROCESSING

The original topography (Figure 2a) was interpolated with a two-dimensional (2D) linear interpolation filter to the resolution used in the POM model, i. e., 3 by 3.7 km near the coast and 6 by 7.4 km away from the coast (Figure 2b), with a total of 287 by 241 points. The highest resolution was used where the values of the 'slope parameter' (defined by Mellor, 1998, as $\frac{|\delta H|}{2 * \overline{H}}$, where $\overline{H}$ is the average depth and δH is the difference in depth between two adjacent cells), were the largest in both the latitude and

longitude directions. Since over much of the topography the slope parameter was larger than 0.2, which is the suggested maximum value to be used in sigma coordinate models (Mellor, 1998), the topography had to be smoothed with a linear 2D low-pass filter in order to meet this criterium. The new depth of each point calculated with this filter was a non-weighted average of 15 by 15 points surrounding the point. Subsequently depths greater than 2500 m were reassigned to depths of 2500 m, land was assigned the depth of 10 m (to avoid divisions by zero in the model) and the Strait of Gibraltar was closed. The new topography is shown in Figure 2c.

The annual temperature and salinity values were interpolated for the horizontal spatial resolution of the model and for the 21 vertical sigma levels (Table 3 and Figure 3) with a three-dimensional (3D) linear interpolation scheme. This had to be done separately for smoothed topography and for flat bottom due to the change in vertical levels for flat bottom and for topography. Temperature fields at sigma level one and several cross-sections are shown in Figures 4a to 4g.

The daily seasonal winds were averaged over time in order to obtain the annual non-weighted average wind vector field (Figure 5). The wind vectors were interpolated for the horizontal spatial resolution of the model with a 2D linear interpolation scheme. The components of the wind stress were then calculated.

C. BRIEF MODEL DESCRIPTION

The Princeton Ocean Model, POM, a well documented model (e.g., Blumberg and Mellor, 1987; Mellor, 1996), was used in the model studies. POM is a primitive equation, free surface model with a second-moment turbulence closure scheme (Mellor and

Yamada, 1982) that, through the use of bottom-following sigma levels, can realistically simulate processes associated with continental shelf flows and bottom boundary layer dynamics in local domains (e.g, bays, estuaries and coastal regions). Recently, the model has been used sucessfully to simulate decadal processes in entire ocean basins (see Ezer and Mellor, 1994, 1997).

As described earlier, the resolution of the horizontal orthogonal grid varies between 3 by 3.7 km and 6 by 7.4 km (Figure 2b). The variable grid allows the use of more (less) points in regions of large (small) gradients.

The 21 sigma levels used are shown in Figure 3 and Table 3. The sigma values range from zero at the surface to minus one at the bottom with the vertical grid spacing proportional to the ocean depth. The vertical resolution has been chosen to be higher near the surface and the bottom in order to resolve both the Surface Boundary Layer (SBL) and the Bottom Boundary Layer (BBL), which are important in coastal regions. To eliminate the time constraints for the vertical grid related to the higher resolution near surface, bottom and shallow waters, an implicit vertical time differencing scheme is used.

The prognostic variables of the model are potential temperature, salinity, density, the three components of velocity, surface elevation, turbulence kinetic energy and length scale. The model has a split time step for the external and internal modes. The external mode solves the equations for the vertically integrated momentum equations. It also provides the sea surface and barotropic velocity components, and has a time step of 6 seconds. The internal mode solves the complete 3D equations and has a time step of 180 seconds.

A Smagorinsky formulation (Smagorinsky et al., 1965) is used for the horizontal diffusion in which the horizontal viscosity coefficients depend on the grid size, the velocity gradients and a coefficient. In this study a value of 0.2 was assigned to this coefficient, consistent with other POM studies (e.g, Ezer and Mellor, 1997) .

C. INITIALIZATION, FORCING AND BOUNDARY CONDITIONS

The model was initialized with annual temperature and salinity values obtained from Levitus and Boyer (1994) and Levitus et al. (1994). Due to the short time of the model runs (less than 60 days), zero salinity and temperature fluxes have been prescribed at the ocean surface. The climatological surface temperature (Figure 4a) shows a decrease in temperature from the southwestern to the northeastern corner of the domain. The gradient increases to the north (which will be shown to be important for the formation of the Iberian Current). A cross-section for salinity at 36°N (Figure 4d). shows the Mediterranean Water signature at ~1200 m depth with salinity values of ~36.1 psu. In the upper 300 m the North Atlantic Ocean waters are found, with the characteristic high salinity values. A cross-section for temperature at the same location (Figure 4e) shows below ~1000 m depth a downward sloping of the isotherms approaching the coast which is consistent with the presence of warm Mediterranean Waters and of a poleward flow. In a cross-section near ~41.5°N (northern boundary) the signature of the Mediterranean Water is found at ~1000 m depth with a much less zonal extent but with the same value for the maximum salinity (Figure 4f). The waters at 41.5°N are generally ~0.1 to 0.2 psu less haline than the waters at 36°N. The temperatures for the 41.5°N cross-section (Figure

4g) still show a strong Mediterranean Water influence but now at ~1000 m depth, consistent with the high salinity values found at this location. A cross-section of salinity at the southern boundary (Figure 4b) shows the Mediterranean signature at ~1200 m depth with salinity values of ~ 35.7 psu, much less than the ones found on the northern boundary. The temperature signature (Figure 4c) is also less strong than in the northern boundary case (the vertcal gradient of temperature near the coast is much higher in the southern boundary case).

The model was forced from rest with the annual ECMWF wind fields, which were interpolated for the model grid. As expected, the wind stress is stronger in the southern region of the model domain and weaker off Iberia and in the Gulf of Cadiz (Figure 5).

Correct specification of the open boundary conditions (BC) is very important to achieve realistic results, with no reflections, clamping, spurious currents or numerical alteration of the total volume of water in the model. The problem is that there is not a general criteria that can give the answer to what boundary conditions are the best for a specific model or study. For models with a free surface, such as used here, one of the important criteria is that the BCs should be transparent to the waves. In this model, a gradient boundary condition (Chapman, 1985), which allows geostrophic flow normal to the boundary, worked best for the elevation. For the baroclinic velocity components normal to the boundary, an explicit wave radiation scheme based on the Sommerfeld radiation condition was used. For inflow situations, the model was forced with annual temperature and salinity values obtained from Boyer (1994) and Levitus et al. (1994), while in outflow situations an advection scheme was used.

For the barotropic velocity components, a Flather radiation plus Roed local solution (FRO) was used. Palma and Matano (2000) showed good results with the FRO during BC tests to determine the BCs response to an alongshelf wind stress. Matano (1998) also showed that the FRO BC had good reflection properties and results in a test that determined the BC response to the combined action of wind forcing and wave radiation. His tests were executed with the barotropic version of POM and compared with benchmark results (no boundary conditions).

III. RESULTS FROM MODEL SIMULATIONS

A. EXPERIMENT 1 – PRESSURE GRADIENT FORCE ERROR

In Experiment 1 (see Table 1), the model was initialized with the horizontally averaged annual climatological temperatures and salinities. A realistic coastline and realistic topography were used, and there was no wind or thermohaline forcing.

With the horizontal averages of the climatology and no forcing, we should expect that nothing will happen, i.e., the initial state of rest should be mantained with time. Due to pressure gradient force errors, however, this will not be the case and there will be resultant velocities as the result of these errors.

Velocity errors induced by the pressure gradient force are unavoidable in 3D sigma coordinate models. There are two types of sigma coordinate errors, the sigma error of the first kind (SEFK) and of the second kind, as defined by Mellor (1998). The first one goes to zero prognostically by advecting the density field to a new state of equilibrium. The second one, a vorticity error, is the most important because it does not vanish with time, and is present in both 2D and 3D cases.

There are several techniques to reduce the pressure gradient errors:

1 – Smoothing the topography can reduce both SEFK and SESK. In particular, the slope parameter should not be greater than 0.2 (Mellor, 1998). Greater values of this parameter can induce currents over 1 m/s.

2 – Using the highest possible resolution can reduce the errors, since, the pressure gradient error decreases with the square of the horizontal and vertical grid size (Mellor et al., 1994).

3 – Subtracting the horizontally averaged density before the computation of the baroclinic integral reduces the SESK (Mellor, 1998).

4 - Using a curvilinear grid that follows the bathymetry reduces the SESK (Mellor, 1998).

In this study the first three techniques were used. The last technique, the use of a curvilinear grid, could not be used, because the geography of the Gulf of Cadiz would have given rise to singularity points.

The results of Experiment 1 are shown in Figures 6 and 7. In Figure 6 the velocity has been plotted versus time. The velocity error is shown to increase faster in the first 3 days, and become almost constant after day 7. The size of the error reduces to less than 0.5 cm/s by day 10. To show where the errors are present in the model domain, the velocity field at sigma level 1 is shown in Figure 7. As expected, maximum velocities of ~0.5 cm/s are found within ~30 km from the coast where the slope parameter is the largest. Experiment 1 has shown that with the use of the three techniques, the pressure gradient error has been considerably reduced. Before the use of these techniques, model runs showed pressure gradient errors of ~ 1 m/s in the coastal regions (not shown).

B. EXPERIMENT 2 – WIND FORCING ON A FLAT BOTTOM

In Experiment 2 (see Table 1), the model was initialized with the horizontally averaged annual climatological temperatures and salinities. A realistic coastline and flat

bottom (constant depth of 2500 meters) were used, and the model was forced with annual climatological winds.

By day 10, a quasi-steady state for the kinetic energy has been achieved (not shown). The strong winds at the southward end of the model have caused cooler temperatures associated with strong upwelling in the coastal region south of Cape Beddouzza (e.g., Figure 8). Throughout the model domain, there are predominantly southward currents except in a zonal oceanic region between 32.5 N and 34.5 N where there is a slight northward component due to the Ekman transport (e.g, see wind stress, Figure 5). The stronger currents tend to be found near coastline features, e.g., off Cabo da Roca and off Cape Ghir, with maximum speeds of ~50 cm/s in the coastal region between Cape Beddouzza and Cape Ghir (e.g., Figure 9a). Between 1000 m depth (Figure 9b) and the bottom (Figure 9c), the flow is predominantly barotropic throughout the domain (e.g., compare Figures 9b and 9c). The coastal current at these depths is poleward, in the opposite direction of the surface flow.

By day 20, the offshore extent of the coastal upwelled waters has increased, particularly off the coastal area south of Cape Ghir where the offshore extent is ~120 km. The coldest waters are found south of Cape Ghir and Cabo da Roca (e.g., Figure 10). Off the Iberian coast and south of Cape Beddouzza, the waters are about 1°C colder than at day 10. The maximum surface velocities are found in the coastal region near Cape Bedouzza (not shown).

By day 30, the temperature fields (Figure 11) show that the upwelled waters have propagated farther westward. The offshore extension of the 17°C isotherm is at ~300 km off Cape Ghir and at ~60 km off Iberia. The minimum offshore extension is in the Gulf of

Cadiz region. The surface temperatures near the coast are very similar to the ones at day 30. A filament is present off Cape Ghir with an offshore extension of ~55 km (e.g., Figure 7). Figure 12 shows the presence of disorganized flow near this area, which means that some of the mean kinetic energy has been converted to eddy kinetic energy.

By day 40, there is evidence of filament activity off Cabo da Roca, the southwest tip of Iberia, and off Cape Ghir (Figure 13). The development of mesoscale features is also evident in almost all of the coastal domain with the more developed features near coastline irregularities, i.e., Cabo da Roca, Cabo de Sao Vicente, Cape Ghir and Cape Beddouzza. The development of some smaller features in the region of the Gulf of Cadiz is also discernible (Figure 14).

Also apparent in the model results is the development of two anticyclonic eddies at ~1200 m depth (e.g., Figure 15), one off Cabo de Sao Vicente and another one off Cabo da Roca. A cross-section of salinity at 37.42°N, near the southern anticyclonic eddy (e.g., Figure 16) shows a salty core of 35.87 psu at 1100 m depth, which is associated with the signature of Mediterranean water (present in the initial annual climatology). It has been suggested (e.g., Kase et al., 1989) that the Meddies are generated by the basic instability of the equatorward coastal jet and the poleward undercurrent. The deep origin, salty signature, depth and anticyclonic rotation of the eddy west of Cabo Sao Vicente is consistent with observations of Meddies in this region (e.g., Richardson and Tychensky, 1998). The Meddy observed off Cabo da Roca is consistent with the results of Kase et al., (1989), who observed eddies in the Mediterranean Outflow off Iberia.

The continuing westward propagation of upwelled water with time, as seen in Figures 8, 10, 11 and 13, is consistent with the results of McCreary et al. (1987) and

Batteen et al. (1989). They showed that, due to the beta effect, the surface coastal jet does not necessarily have to be confined to within a Rossby radius of deformation of the coast.

The results in this experiment are also consistent with the ones obtained by Batteen et al. (2000) with a primitive equation model with biharmonic diffusivity, based on the hydrostatic, Boussinesq and rigid lid aproximations. In particular they were able to reproduce a realistic equatorward current, a poleward undercurrent, Meddies and other mesoscale features (eddies, meanders and filaments).

C. EXPERIMENT 3 – ROLE OF TOPOGRAPHY

In Experiment 3 (see Table 1), the model was initialized with the horizontally averaged annual climatological temperatures and salinities. A realistic coastline and bottom topography were used along with forcing by the annual climatological winds.

By day 10, the velocities in the coastal areas in the bottom topography Experiment 3 (e.g., Figure 17a) are roughly twice the ones in the flat bottom Experiment 2 (e.g., Figure 9a). The velocities in Experiment 3 also have the highest magnitudes at ~15 km offshore (near the shelf break) instead of at the coast as in the flat bottom Experiment 2. As in the flat bottom experiment, the strongest currents are found in the coastal region south of Cape Beddouzza. The temperatures at the surface are also very similar for the two experiments (e.g., compare Figures 8 and 18), both in the location of the strongest upwelling regions (south of Cape Beddouzza) and in the horizontal extent of the upwelled waters. One of the main differences between the experiments occurs off Figueira da Foz where the upwelled waters are present farther from the coast in

Experiment 3. The main reason for this phenomena is the location of a topographic feature at this location. Below the surface, at intermediate sigma level 10, the coastal velocities are still equatorward but are about 50% of the ones at surface (Figure 17b) while near the bottom the equatorward velocities decrease to 10% of the surface values (Figure 17c).

By day 20, a comparison of the 17°C isotherm in both experiments (e.g, see Figures 10 and 19) shows that the extent of the upwelled waters is much less than in the flat bottom case (Figure 10) particularly off Cape Ghir. This can be explained by the presence of the bottom topography which traps the flow and opposes the tendency for westward propagation due to the planetary beta effect. In Experiment 3 the surface temperatures are also colder than in Experiment 2 in the region of Gulf of Cadiz where the winds are not as strong.

The plot of total kinetic energy for Experiment 3 (e.g. Figure 20a) shows a steady and rapid increase of the kinetic energy for the first 25 days. During this period the flow develops currents but no mesoscale features. Between days 25 and 35, the kinetic energy decreases to about 1/3 of the maximum value. This loss consistent with (Røed, 1999) can be explained by a transfer of kinetic energy to available gravitational energy and then to eddy gravitational energy and eddy kinetic energy (e.g., Figure 20b). This explanation is supported by the development of eddies at ~ day 30. The eddies develop at Cabo da Roca, Cabo Sao Vicente and off Figueira da Foz (e.g, Figure 21). The surface temperature (e.g, Figure 22) is similar to experiment 2 with the waters being ~1°C colder in the coastal area south of Cape Ghir. Off Cape Ghir the extent of the upwelled waters is also smaller. Note that the filament present in this region in Experiment 2 is now absent

in Experiment 3. This shows that the trapping of the currents due to topography is much stronger than the combined effect of coastline irregularities and the planetary beta effect. Note the presence of relatively strong eddies near the capes off Iberia, which were much weaker in Experiment 2. This shows that the bottom topography plays an important role in their intensification.

Unlike Experiment 2 which had meanders throughout the coastal domain by day 40 (e.g see Figure 14), the only evidence of mesoscale phenomena in this experiment are two eddies, one off Cabo da Roca and the other off Figueira da Foz (e.g, Figures 23a and 23b). The eddy off Cabo da Roca is centered at ~38.82°N, 10.44°W, with a diameter of 70 km and a core temperature of 14.4°C. Off Cape Ghir and off the coast of Portugal between Cabo da Roca and Cabo Sao Vicente, the flow is mantained much closer to shore in the experiment with topography (e.g., compare Figures 13 and 23a). The opposite situation is shown in the Gulf of Cadiz where the slope of topography is much less than in the rest of the coastal domain.

The poleward undercurrent is much weaker in Experiment 3 then in Experiment 2. For example, at day 30, it is less than 1cm/s (Figure 24a) at 1200 meters depth in Experiment 3, while in Experiment 2 the current was 6 to 7 cm/s at the same depth (see Figure 24b). The core of the undercurrent in Experiment 3 is also much deeper. For example, at day 30 the core is at ~2300 m depth while in Experiment 2 it is at ~1200 m depth.

Meddy formation also occurs much later in Experiment 3 than in Experiment 2. Instead of having Meddies form by day 30 as in Experiment 2, Meddies do not form until ~ day 60. The Meddies form off Cabo da Roca and off Figueira da Foz (Figure 25);

however, unlike Experiment 2, no Meddy forms off Cabo Sao Vicente. As Experiment 2 showed, the sharpness of the coastline is likely necessary to the formation of Meddies off Cabo Sao Vicente. In Experiment 2 the Meddies also appeared to be generated due to the curvature of the Mediterranean outflow back on itself, consistent with the theory suggested by Pichevin and Nof (1996). It is speculated that the smoothing of topography also smoothed the irregularities of the coastline at 1200 depth.

D. EXPERIMENT 4 – THE ROLE OF BOTTOM TOPOGRAPHY WITH FULL CLIMATOLOGY

In Experiment 4 (see Table 1), the model was initialized with the full annual climatological temperatures and salinities. A realistic coastline and bottom topography were used along with forcing by the annual climatological winds.

By day 10, the currents are very similar to the ones found on Experiment 3 (i.e., compare Figures 26 and 17a), except ~80 km offshore of Iberia where there is poleward flow, and warmer temperatures off Cabo Sao Vicente, which are advected poleward (see the 18°C isotherm, Figure 27) . Since this is a region of weak wind stress, the Ekman transport is not able to overcome the geostrophic adjustment of density due to the thermohaline gradients from the full temperature and salinity fields. Even though the Gulf of Cadiz is also an area of weak wind stress, this phenomena is not present due to the fact that the horizontal variation of temperature (density) is much smaller (Figure 4a) compared to the Ekman transport. The difference in temperatures in coastal areas between Experiments 3 and 4 (Figures 18 and 27, respectively) reflect the different

climatologies used. To the south, i.e., off Cape Ghir, the temperatures are similar in both experiments while in the northern area, i.e., off Figueira da Foz, Experiment 4 temperatures are ~1.5°C colder than those of Experiment 3. The temperature differences between the waters in upwelling regions and adjacent waters for both experiments are approximately constant.

Again in day 20, similar patterns are shown for the velocities for the two experiments (Figures 28 and 29). The strongest currents are found in the coastal area south of ~34°N except for ~80 km offshore of Iberia, where the currents have a poleward component in Experiment 4. A comparison of cross-sections of the meridional velocity component for Experiments 3 and 4 (e.g., Figures 30 and 31), at 32.8°N shows a much more developed poleward undercurrent in Experiment 4 with a well defined core at ~800 m depth (Figure 30) and velocities 20% stronger than in experiment 3 (Figure 31). In Experiment 4 the equatorward current is narrower and reaches ~1400 m depth, compared to ~1000 m depth in Experiment 3.

A comparison of cross-sections of meridional velocity off Cabo Roca for Experiments 3 and 4 shows the presence of the Iberian current in Experiment 4 (Figure 32) but not in Experiment 3 (Figure 33). The Iberian Current is a seasonal shoaling of the poleward undercurrent off Iberia (Haynes and Barton, 1990), usually seen in winter time, when the seasonal wind stress is also weaker off Iberia. This shows that the horizontal variability of density is important for the formation of the Iberian Current. At this location, the undercurrent in Experiment 4 has its core at ~800m with a maximum value of 27 cm/s, while the equatorward current is trapped within the first 400 m depth and has an offshore extent of ~70 km (Figure 32). In Experiment 3 the undercurrent is much

weaker with a magnitude of ~6 cm/s, does not have a well defined core and is found much deeper. Above the undercurrent, the equatorward current is 25% stronger than in the previous case, reaches 1500 m depth and is ~140 km wide. As a result, a much stronger along shelf variability is present in Experiment 4 than in Experiment 3. Consistent with Batteen et al., 2000, and Batteen and Murray (2000), the Iberian Current is seen as far south as Cabo Sao Vicente 37.4°N (e.g., Figure 34).

By day 30, as in Experiment 3, there is a 20% decrease in the coastal surface velocities compared to those at day 20 (compare Figures 35 and 28), which could be due to two factors: first, the geostrophic adjustment produces velocities in opposition (but smaller in magnitude) to the main flow, resulting in a reduction of the speeds; second, the horizontal variability of density contributes to the enhancement of the poleward alongshore variability, giving rise to a greater enhancement and surfacing of the undercurrent, which subsequently reduces the flow surface speeds.

A cross section at 32.8°N (Figure 36) shows a strong undercurrent with a speed of ~20 cm/s with a core depth at ~500 m depth for Experiment 4, a core of similar magnitude but with a much deeper location is shown for Experiment 3, at 1000 m depth (Figure 37). Off Iberia, the horizontally opposing flows of the equatorward coastal and the poleward Iberian current produced horizontal shear that could decrease the overall speeds (Figure 35). A cross-section at 32.8°N for Experiment 3 at day 40 (Figure 38) shows that the undercurrent has a shallower core at ~750 m depth and a weaker (from 69cm/s to 55 cm/s, a reduction of 20%) surface equatorward current.

The meanders present off Figueira da Foz and Cabo da Roca in Experiment 4 are consistent with those in Experiment 3 . The extent of the upwelled waters is very similar

in Experiments 3 and 4 (Figures 62 and 19) in the coastal regions south of Cabo Sao Vicente; however, to the north there are differences in extent as well in value due mainly to differences between the two climatologies.

By day 40, surface velocities are similar to the ones at day 30, except for the stronger surface poleward flow off Iberia and north of Figueira Foz (Figures 40 and 35). By day 60, a Meddy has formed off Cabo da Roca; however, as in Experiment 3, no Meddy forms off Cabo Sao (Figure 41). As in Experiment 3, the Meddy forms at ~ day 60, compared to ~ day 40 in Experiment 2.

Surface temperature and velocity fields at day 60 are shown for Experiment 4 (Figure 42), Experiment 3 (Figure 43) and Experiment 2 (Figure 44). While all three experiments show similar features, i.e., surface equatorward flow, upwelling, meanders and eddies, notable differences are apparent. A comparison of the flat bottom (Figure 44) and topography (Figure 43) with the same climatology shows the effect of planetary beta acting alone in the flat bottom Experiment 2 (Figure 44) versus competing with the topographic beta effect in Experiment 3. The effect of the full climatology is evident in Experiment 4 (Figure 42), which shows the thermal gradient from north to south, the tightening of the currents near the coast and slightly weaker surface currents due to the effect of thermohaline gradients.

THIS PAGE INTENTIONALLY LEFT BLANK

IV. SUMMARY

The objective of this study was to investigate the roles of wind forcing, bottom topography and thermohaline gradients on classical as well as unique features in the northern Canary Current System. Toward this end, four numerical experiments were run, all on a beta-plane, with a sigma coordinate numerical model, i.e., the Princeton Ocean Model. The first experiment investigated the pressure gradient force error. The second experiment investigated the effect of annual wind forcing on a flat bottom. The third experiment investigated the additional effect of topography. The fourth experiment was used to determine the additional role of the full annual climatology.

Experiment 1, used to evaluate the pressure force gradient error, showed that velocity errors inherent in three dimensional sigma coordinate models could be sucessfully reduced from ~1 m/s to ~0.5cm/s using three techniques: smoothing the topography, using the highest possible resolution, and subtracting the area averaged density before the computation of the baroclinic integral. The results showed that the highest velocities (~0.5cm/s) were concentrated near the coast where the values of the slope parameter were the highest.

Experiment 2 produced an offshore surface equatorward meandering jet, realistic surface and subsurface poleward currents, upwelling, meanders, eddies and filaments. In addition, these experiments depicted unique NCCS features, including the geographical separation of the Gulf of Cadiz region from the west coast upwelling regimes, poleward

spreading of the Mediterranean Outflow, and the development and propagation of Meddies from the Cabo Sao Vicente and Cabo da Roca regions.

A comparison between Experiments 2 and 3 showed that the bottom topography plays an important role in trapping and intensifying the equatorward current near the coast. The poleward undercurrent also weaker and had a deeper core depth in Experiment 3. Stronger eddies occurred off Cabo da Roca and Cape Ghir in Experiment 3. No formation of Meddies off Cabo Sao Vicente in Experiment 3 occurred. It was speculated that since Meddies did form off Cabo Sao Vicente in Experiment 2, consistent with observations, that the sharpness of the coastline is likely to be necessary to the formation of Meddies.

In Experiment 4, the additional effect of the full annual climatology produced an offshore surface equatorward meandering jet, realistic surface and subsurface currents, upwelling, meanders and filaments. The effect of the full climatology produces the tightening of the currents near the coast and slightly weaker currents due to the effect of thermohaline gradients. As in Experiment 3, there was no development of eddies of Cabo Sao Vicente but only off Cabo da Roca. Only Experiment 4 showed the Iberian Current off the Portugal coast showing that thermohaline gradients are essential to the formation of this current.

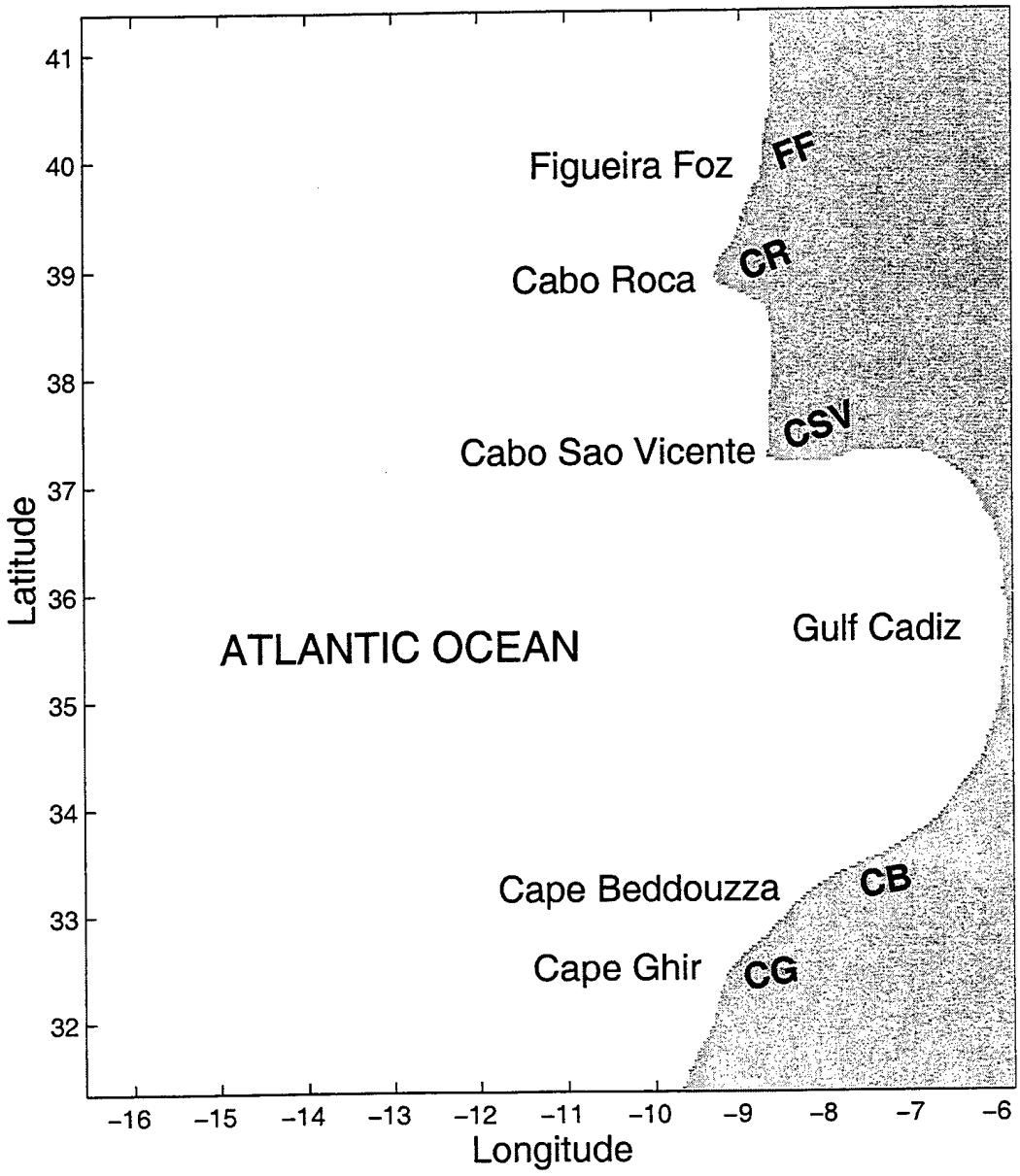

Figure 1. The model domain for the northern Canary Current System (NCCS) is bounded by 31.5°N to 41.5°N, 6°W to 16.5°W. Geographical locations (with abbreviated names used in the following figures) and prominent features are labeled. The model domain has a closed boundary along the entire coast and three open boundaries.

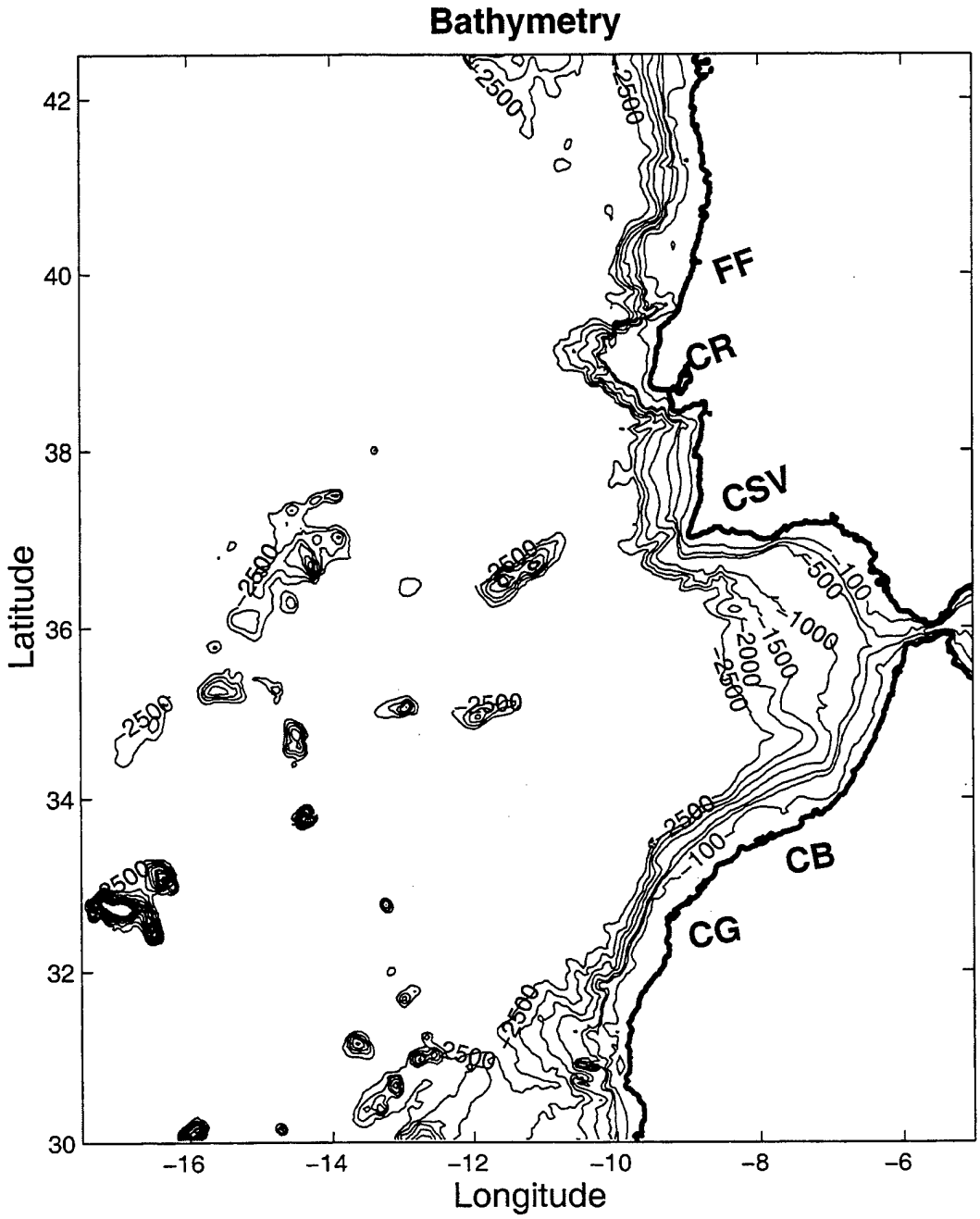

Figure 2a. Original topography (from Sandwell D.T. and W.F. Smith, 1996), with a resolution of 2 minutes (i.e., 1/30 of a degree).

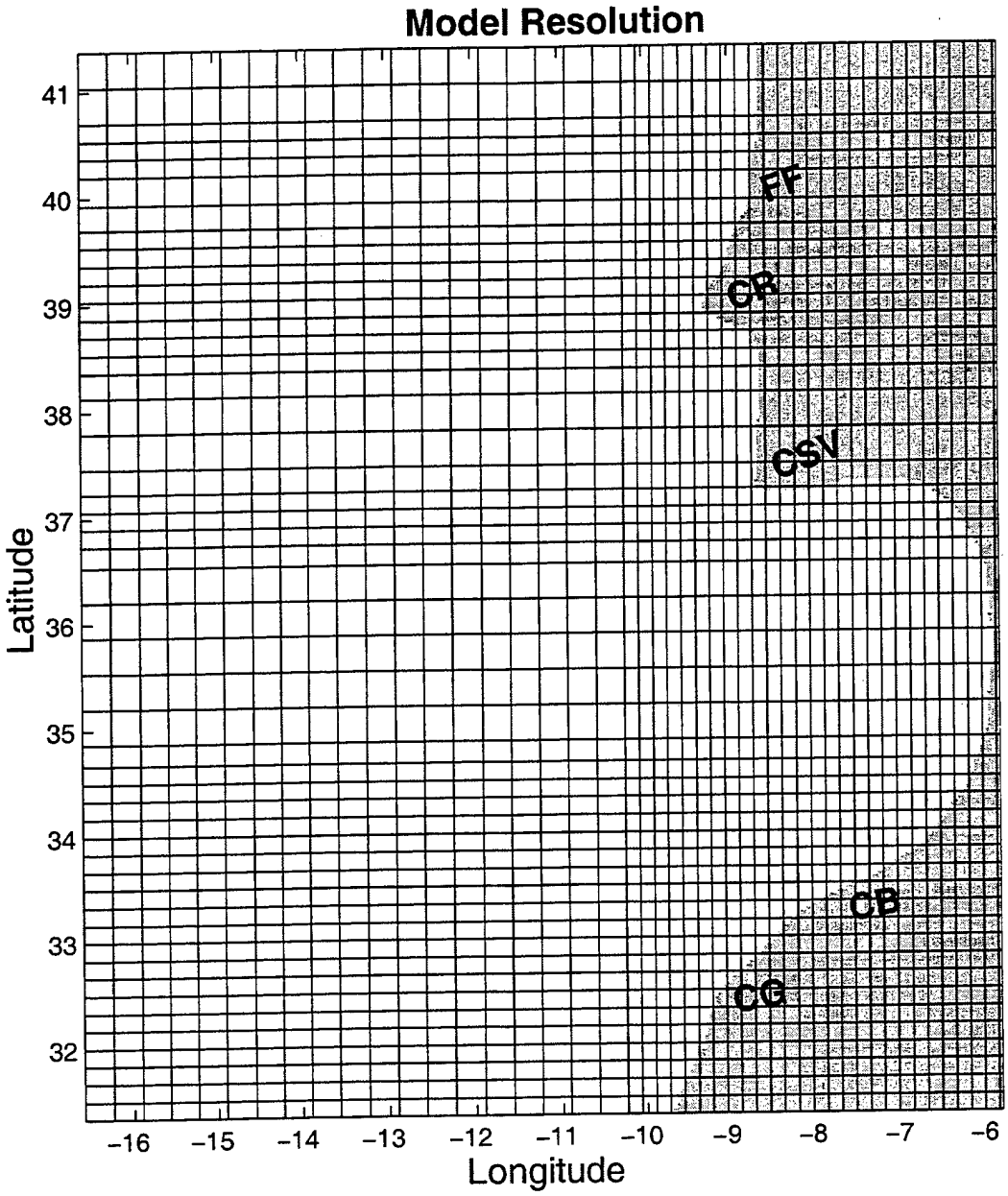

Figure 2b. Grid lines with every fifth grid line plotted.

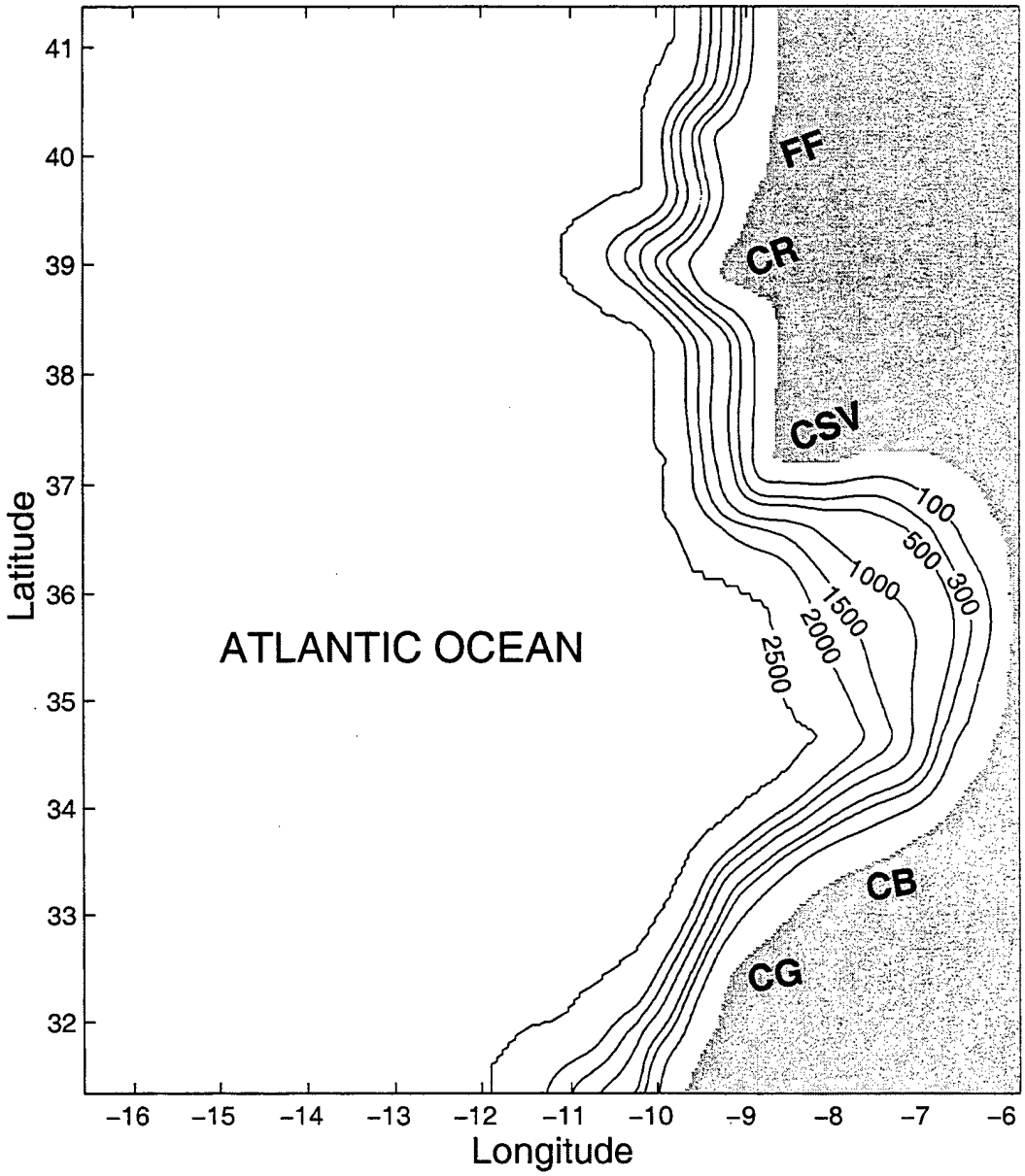

Figure 2c. Smoothed topography obtained after applying a linear two-dimensional low-pass filter and reassigning 2500 m depth to depths greater than 2500 m.

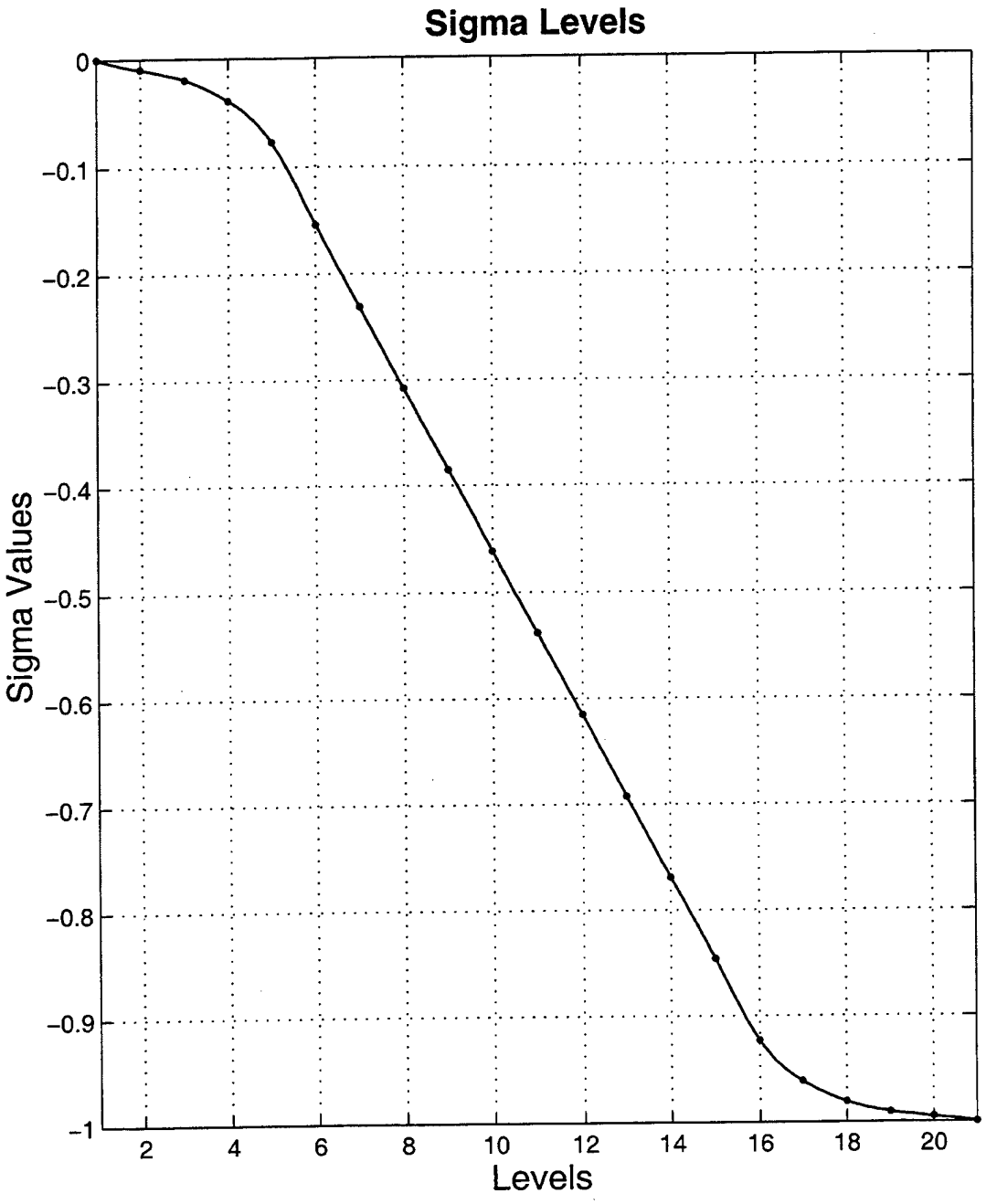

Figure 3. Plot of the 21 sigma levels.

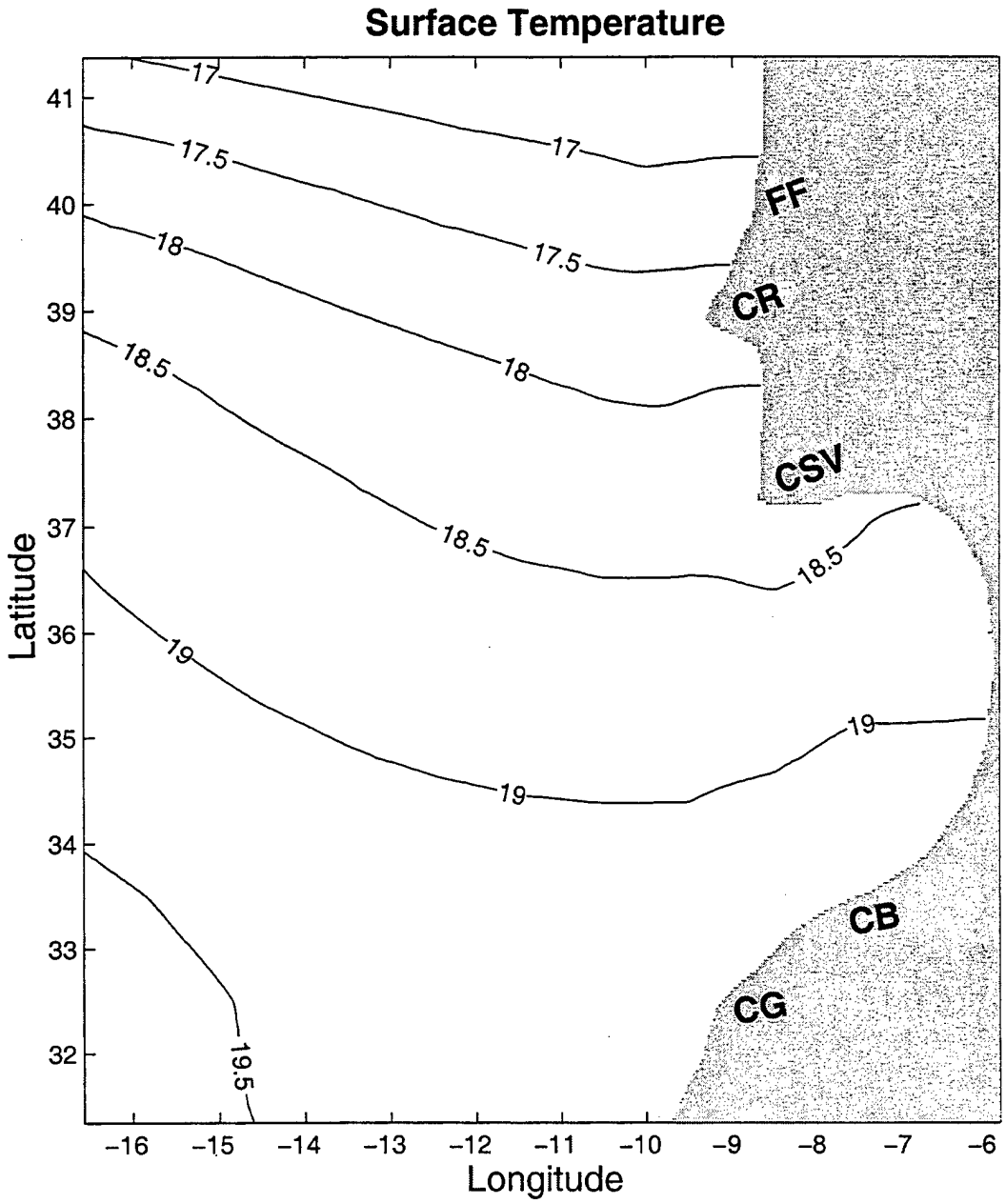

Figure 4a. Levitus annual climatological surface temperature.

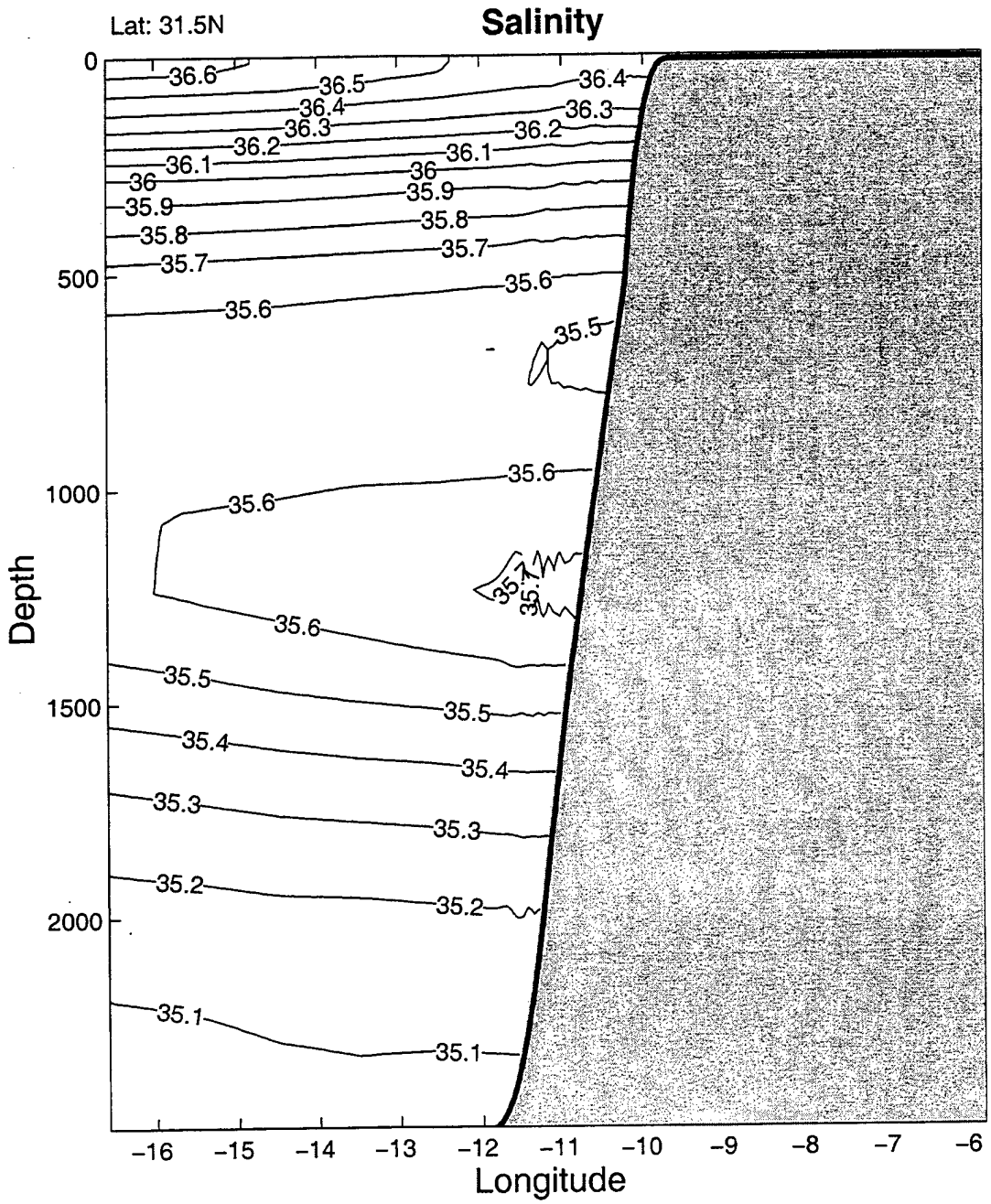

Figure 4b. Cross-section at 31.5°N of Levitus annual climatological salinity.

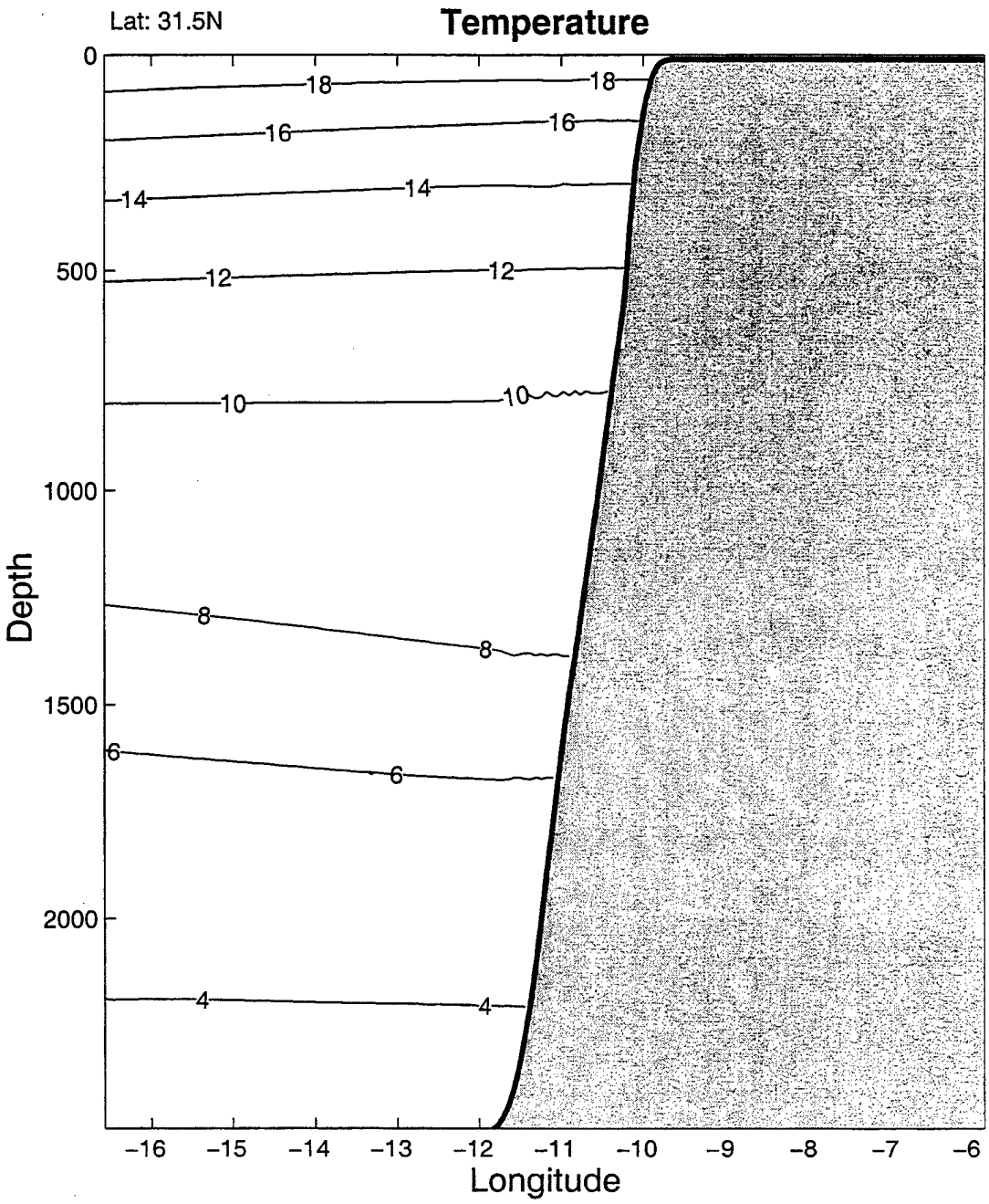

Figure 4c. Cross-section at 31.5°N of Levitus annual climatological temperature.

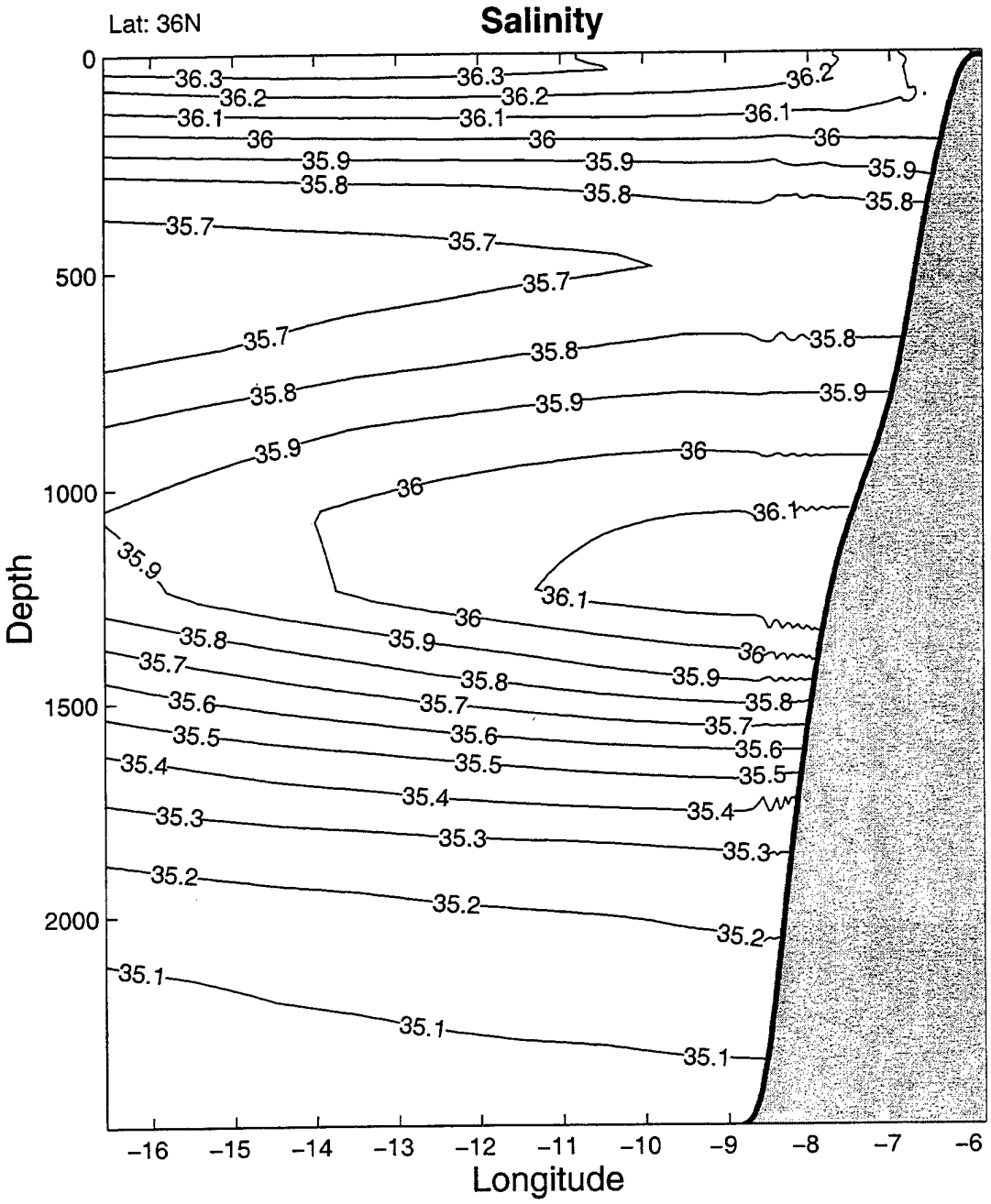

Figure 4d. Cross-section at 36°N of Levitus annual climatological salinity.

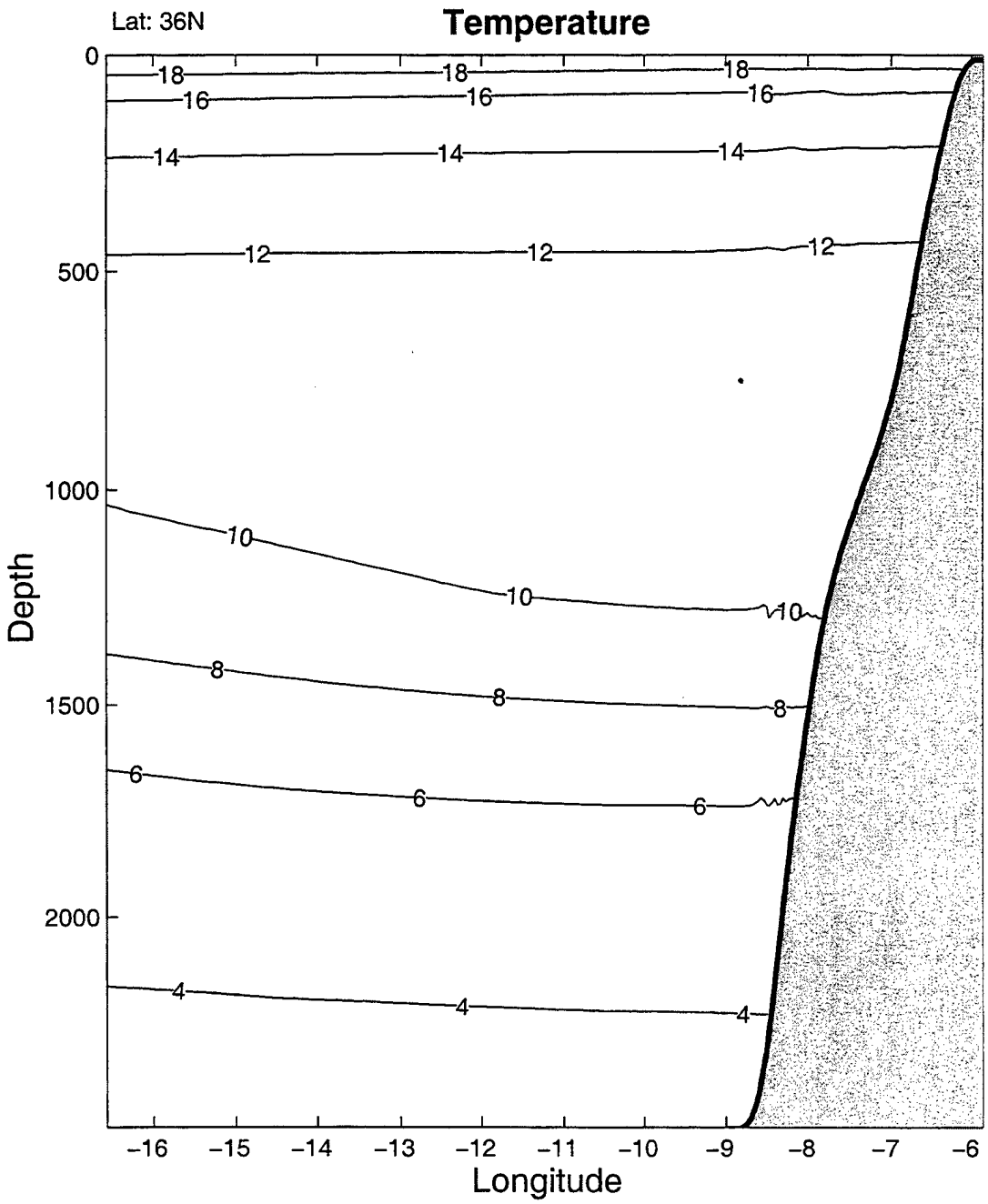

Figure 4e. Cross-section at 36°N of Levitus annual climatological temperature.

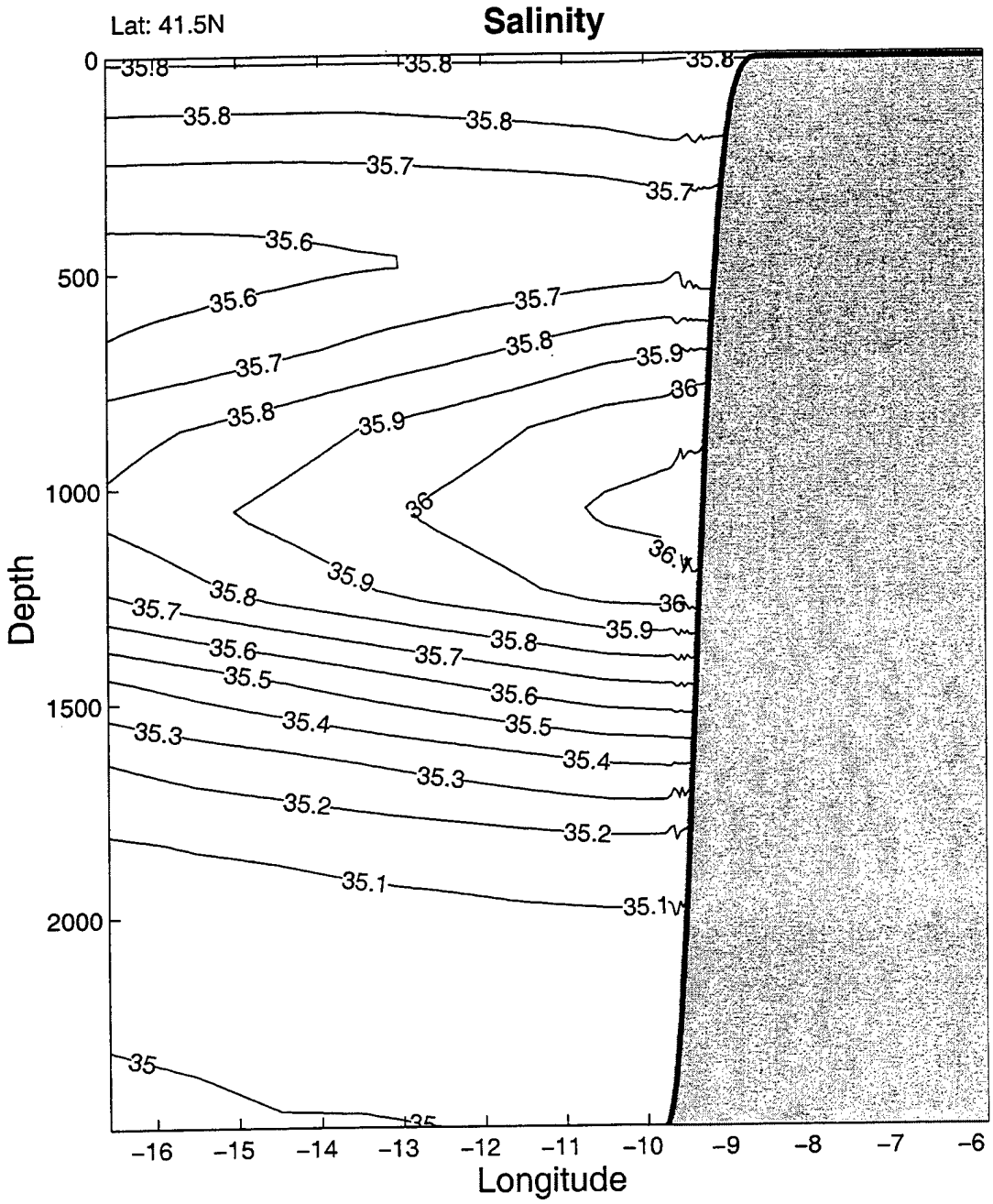

Figure 4f. Cross-section at 41.5°N of Levitus annual climatological salinity.

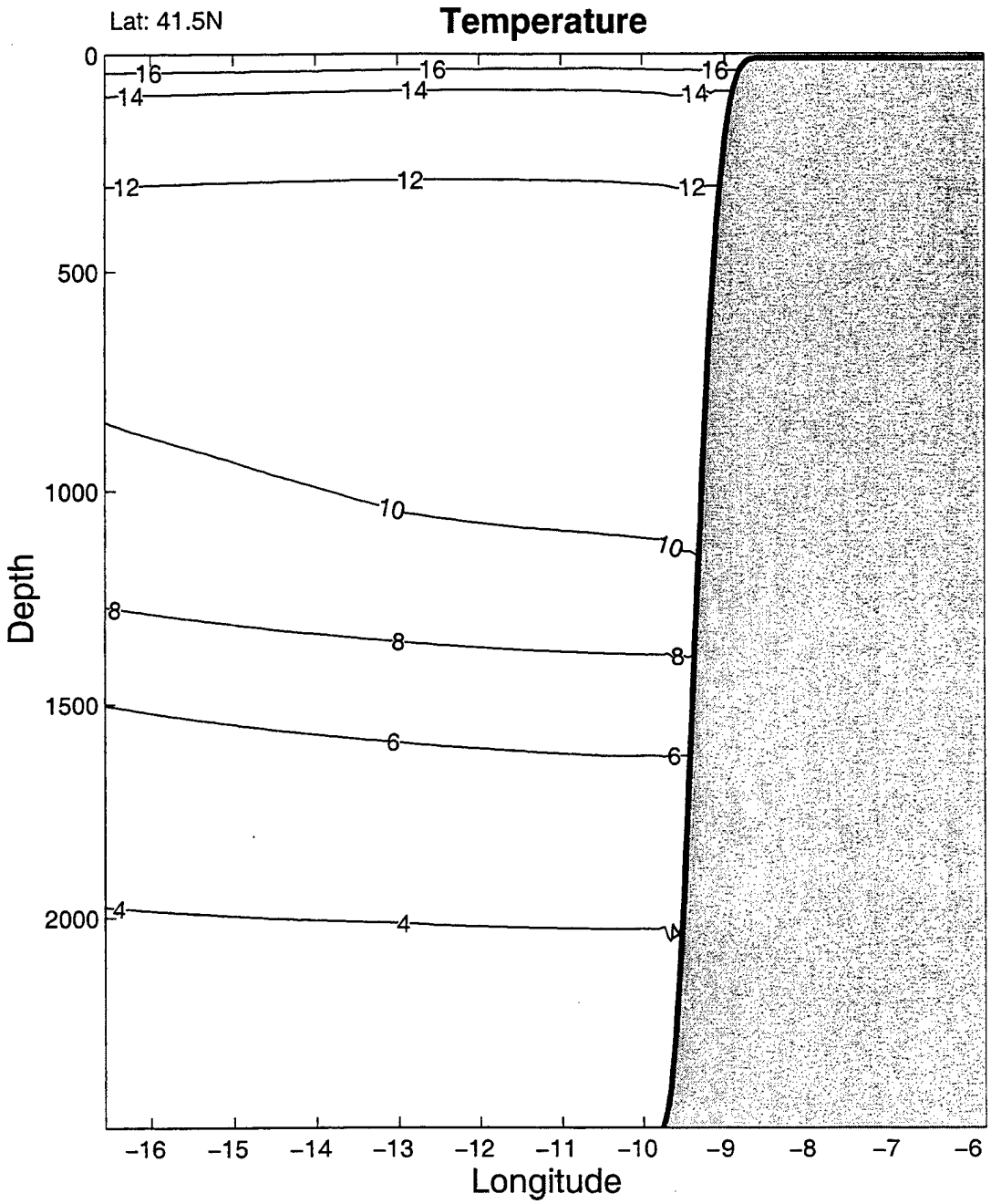

Figure 4g. Cross-section at 41.5°N of Levitus annual climatological temperature.

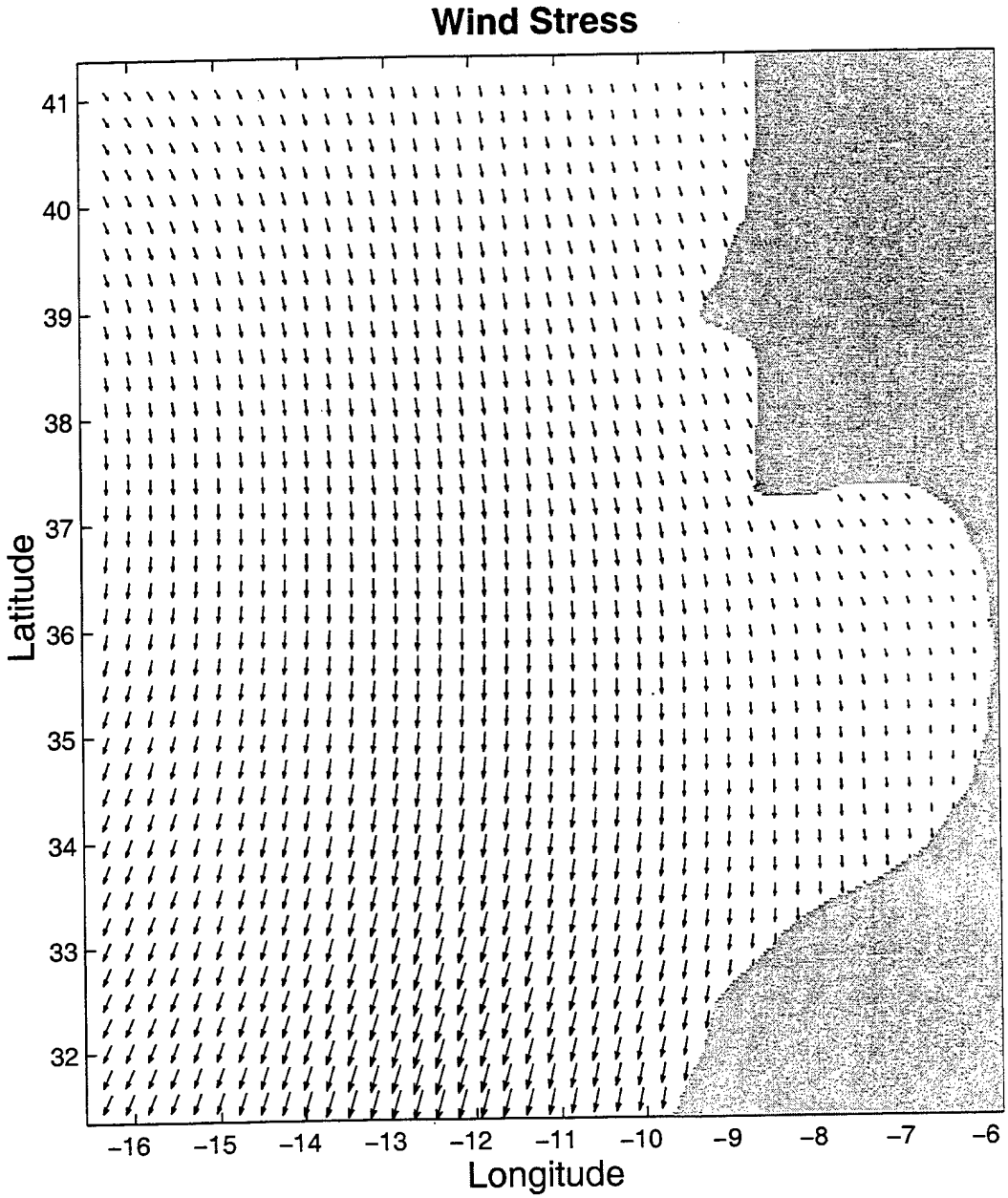

Figure 5. Wind stress in Pascal calculated from annual climatological ECMWF winds obtained from Trenberth et al. (1990).

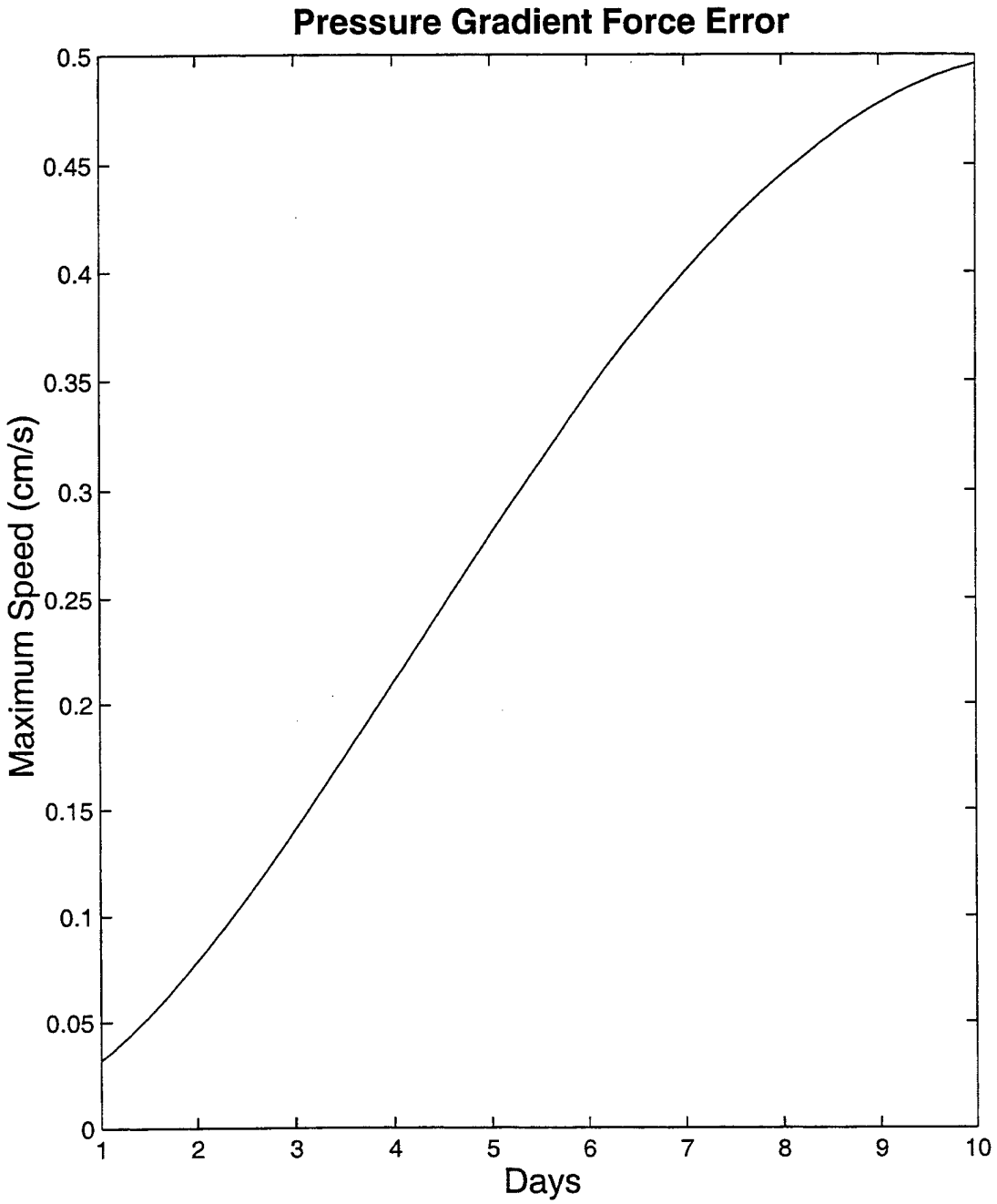

Figure 6. Plot of the maximum velocity error versus time due to the pressure gradient force error for Experiment 1.

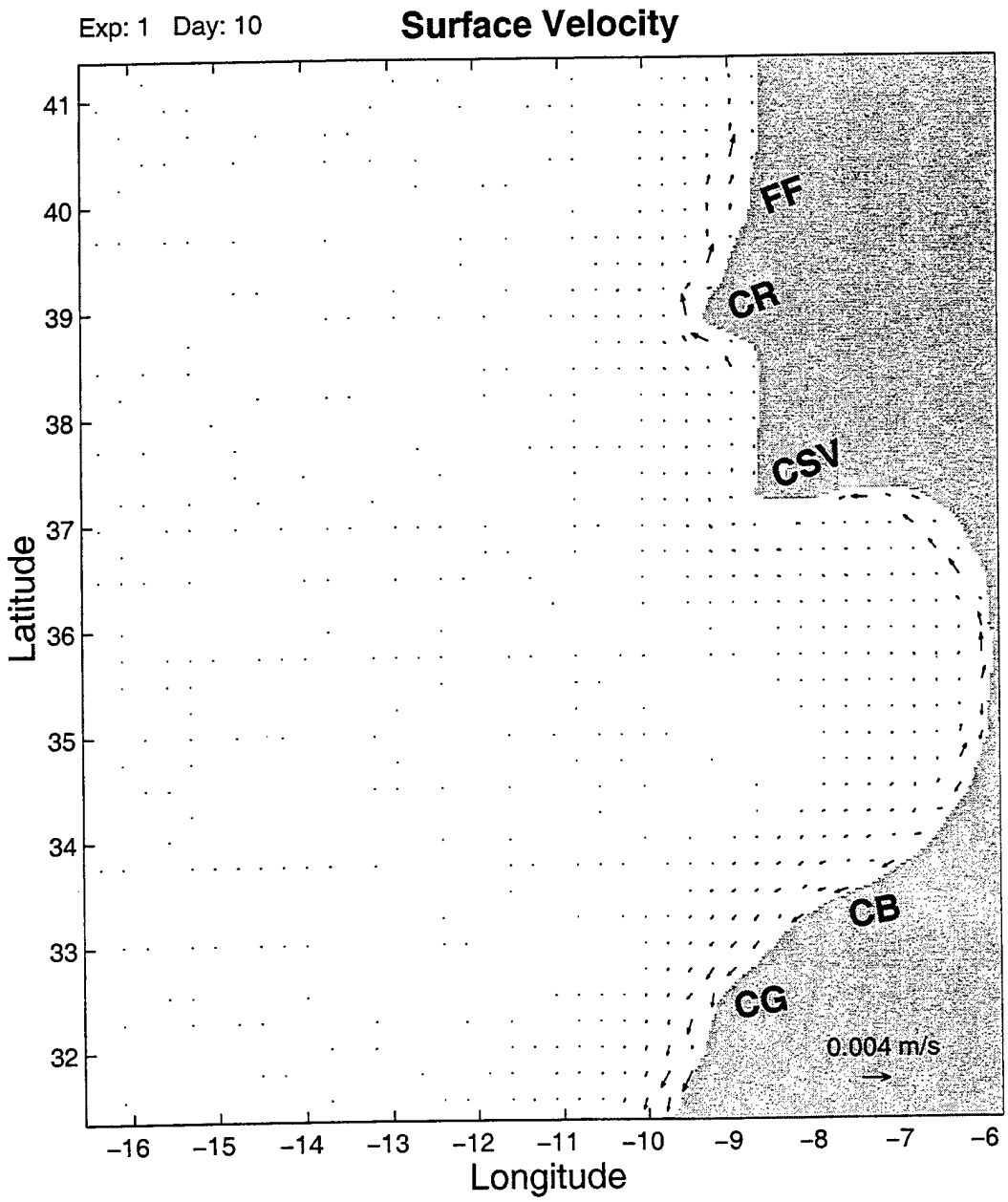

Figure 7. Surface velocity error due to the pressure gradient force error on day 10 for Experiment 1.

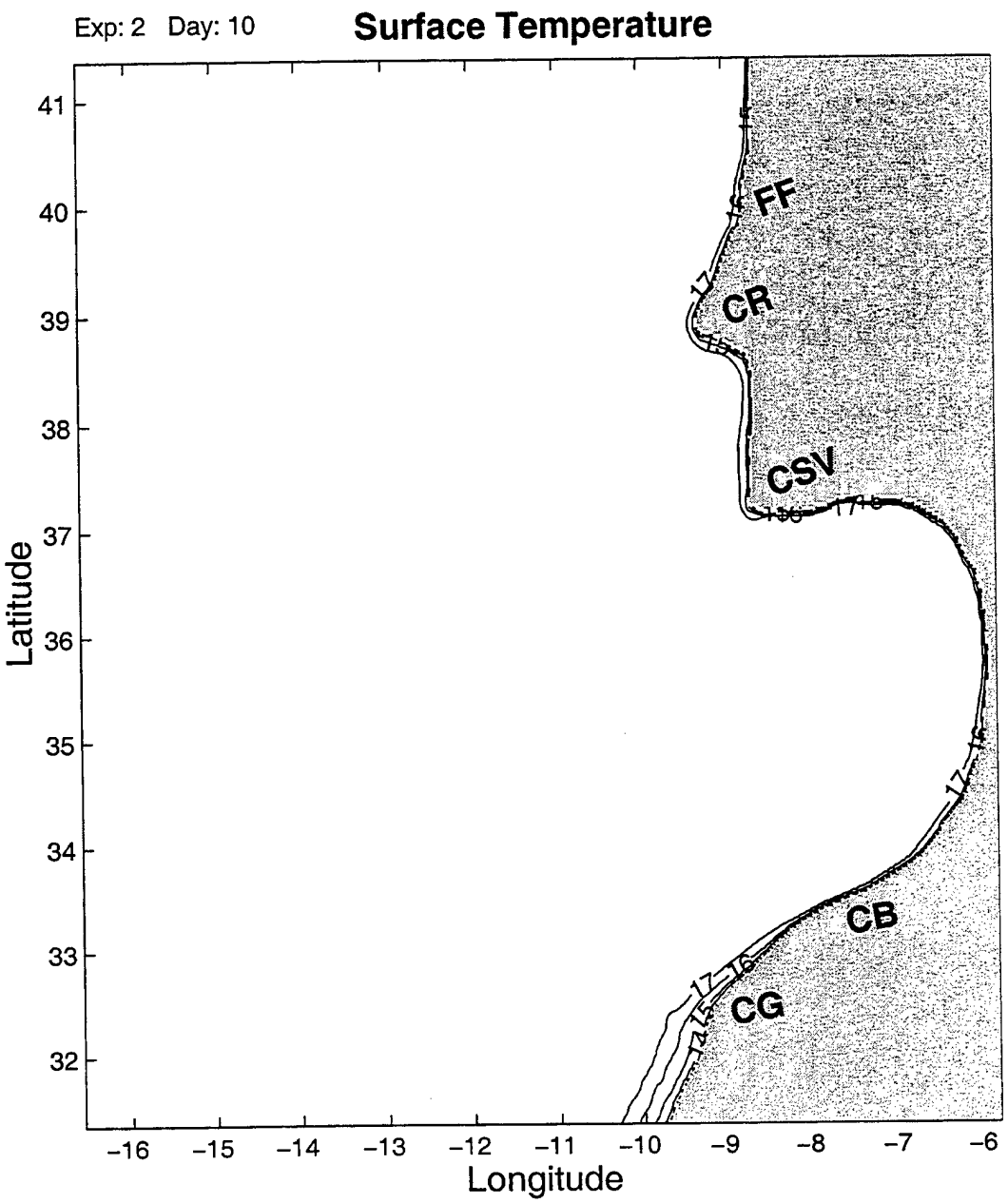

Figure 8. Surface temperature contours for Experiment 2 on day 10. Contour interval is 1°C.

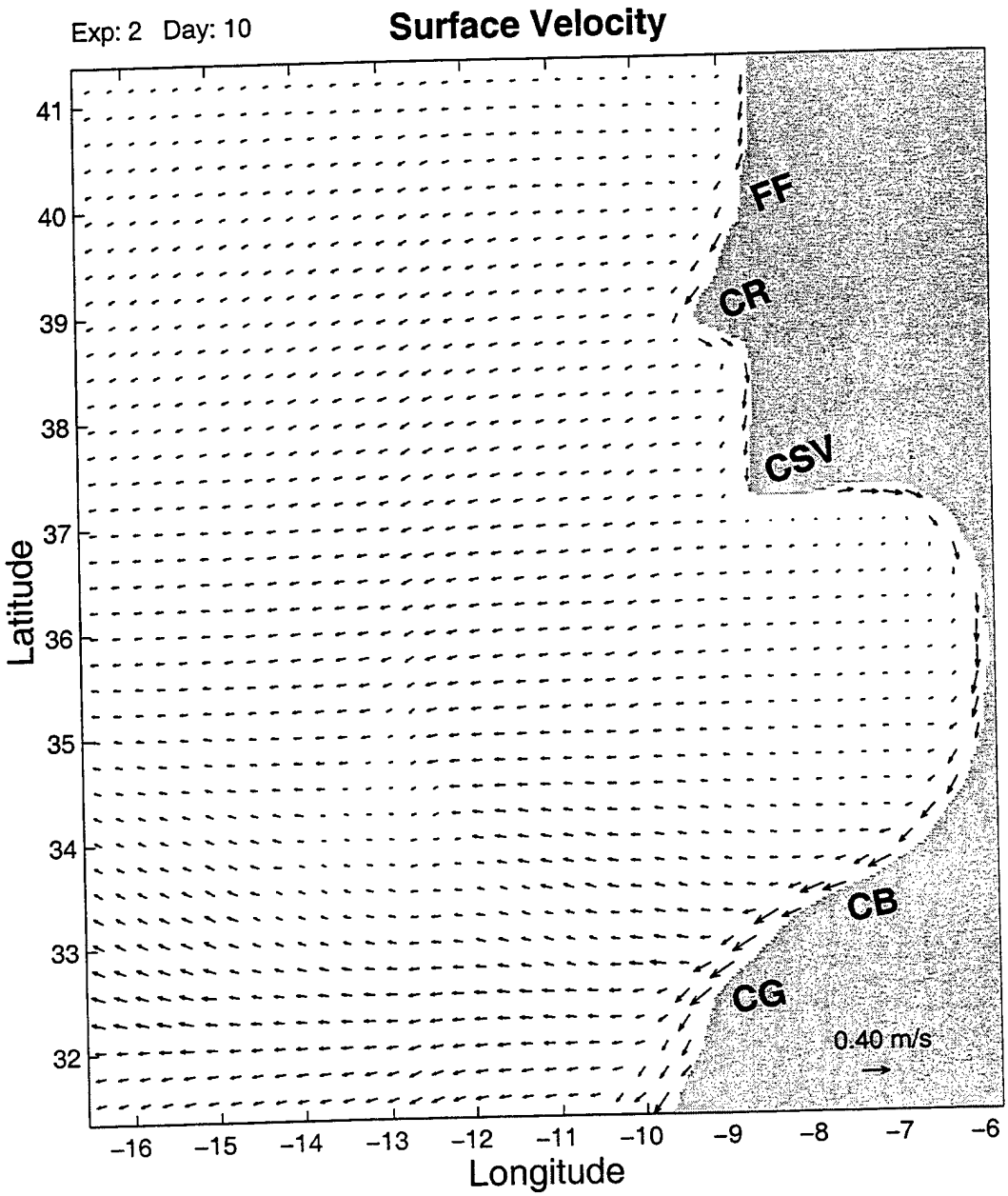

Figure 9a. Surface velocity vectors for Experiment 2 on day 10.

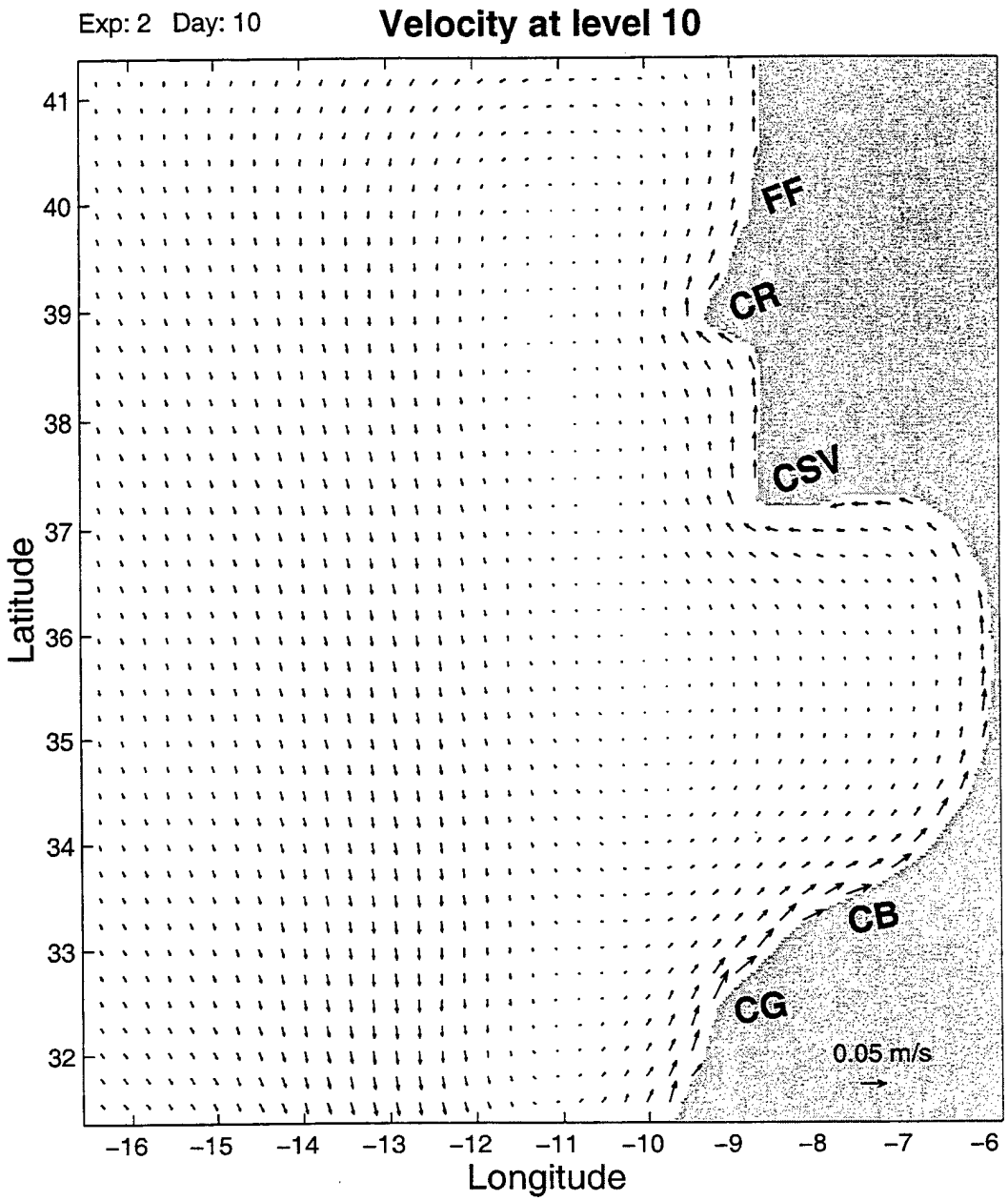

Figure 9b. Velocity vectors at sigma level 10 for Experiment 2 on day 10.

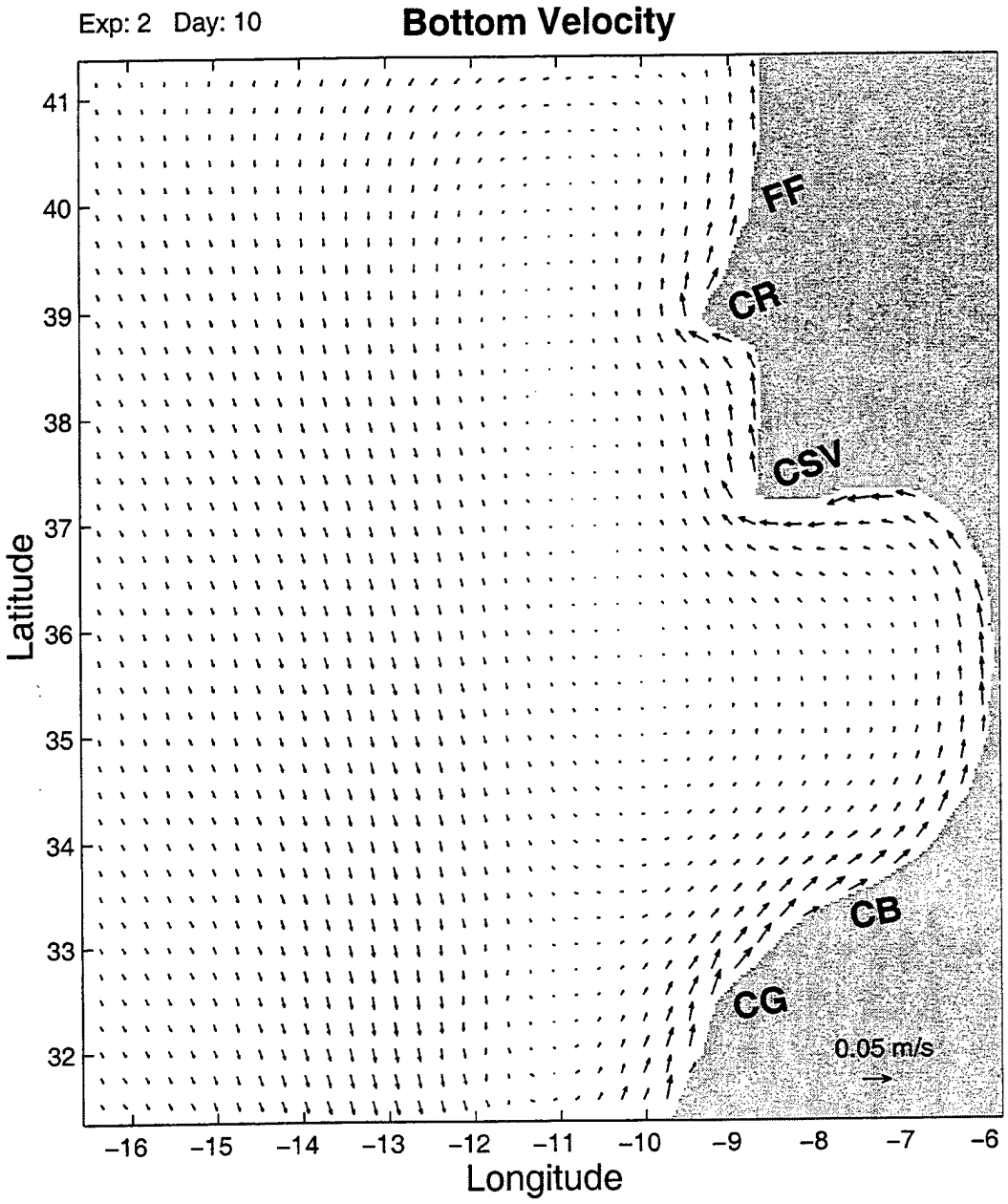

Figure 9c. Velocity vectors at sigma level 20 for Experiment 2 on day 10.

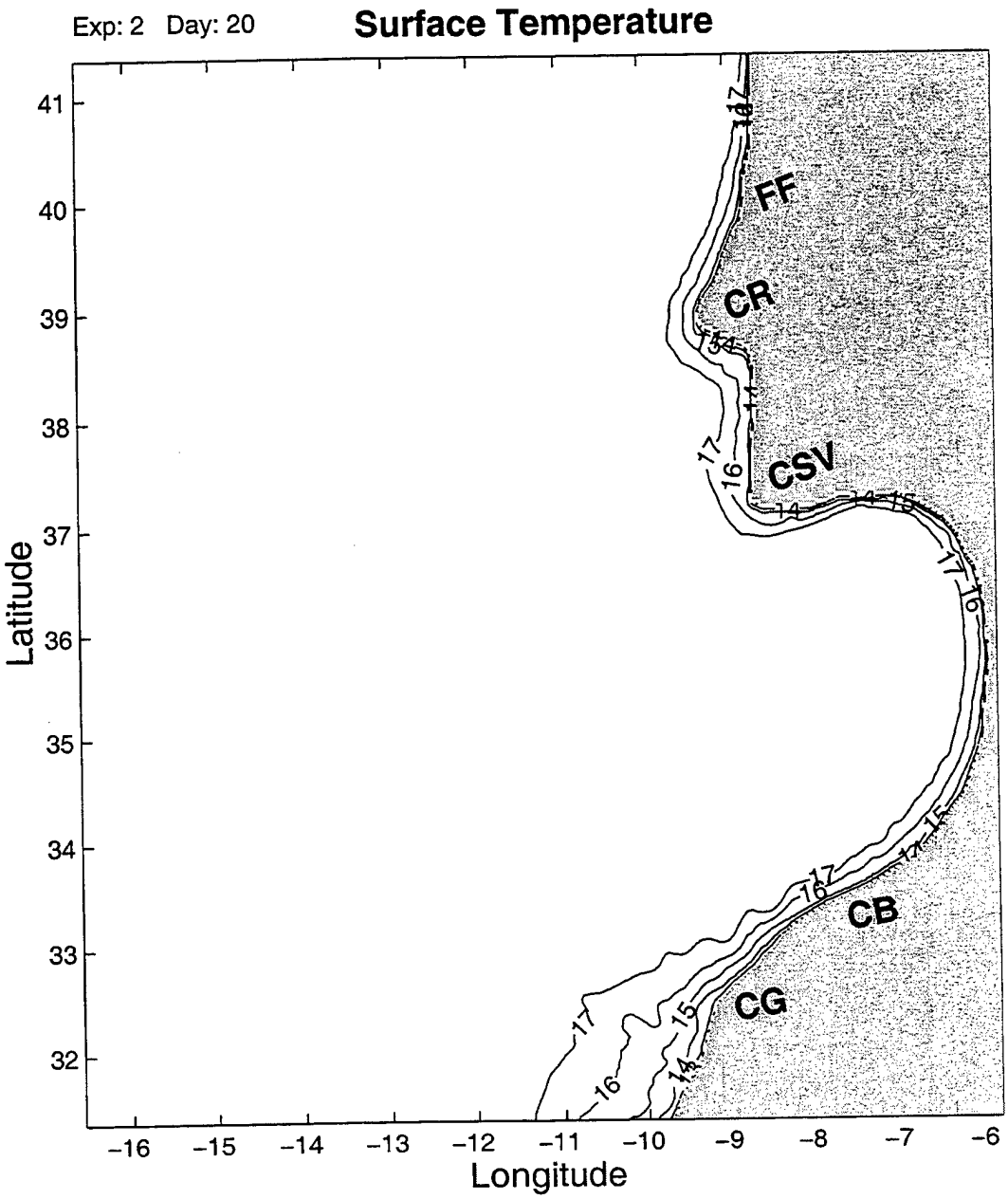

Figure 10. Surface temperature contours for Experiment 2 on day 20. Contour interval is 1°C.

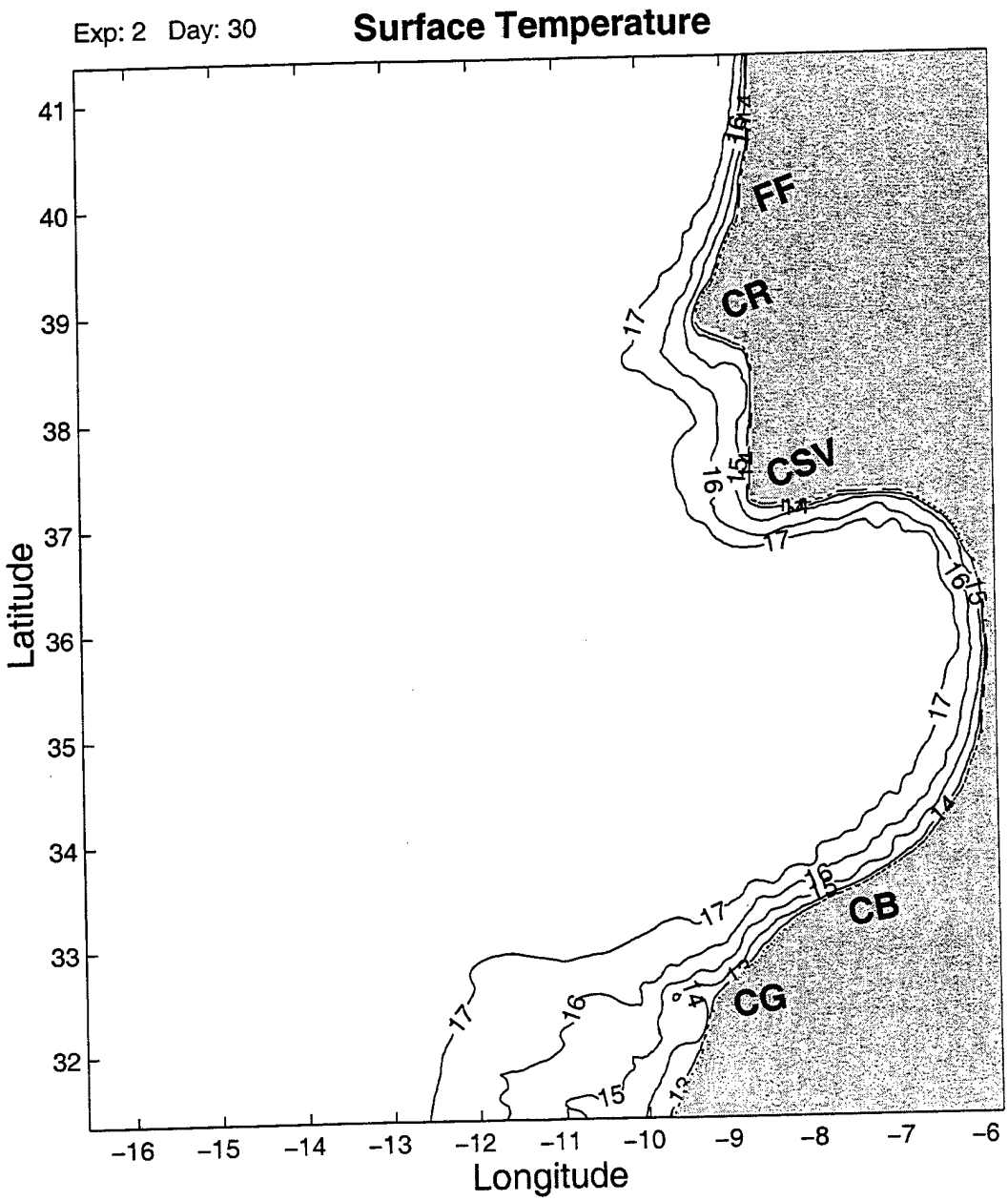

Figure 11. Surface temperature contours for Experiment 2 on day 30. Contour interval is 1°C.

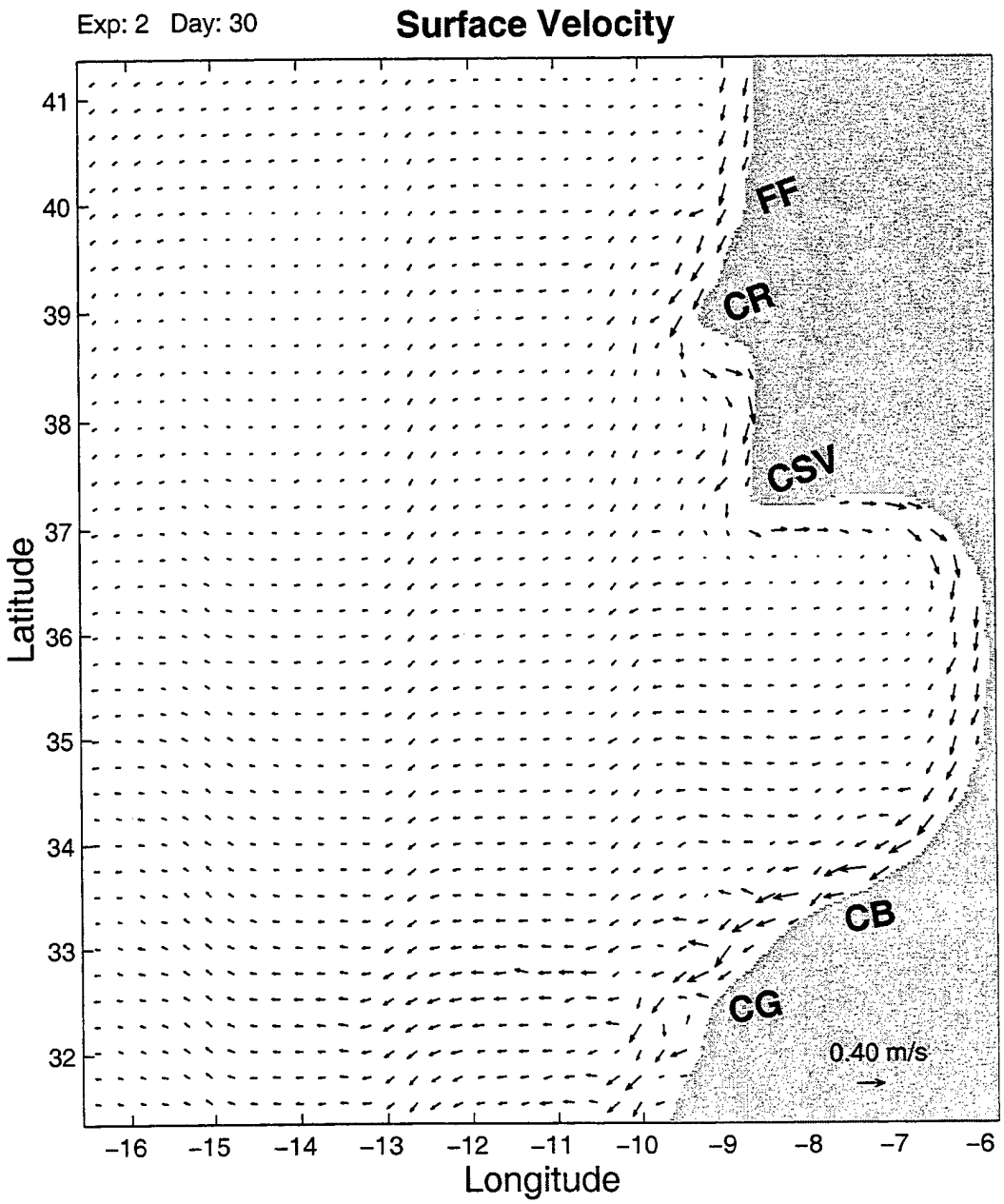

Figure 12. Surface velocity vectors for Experiment 2 on day 30.

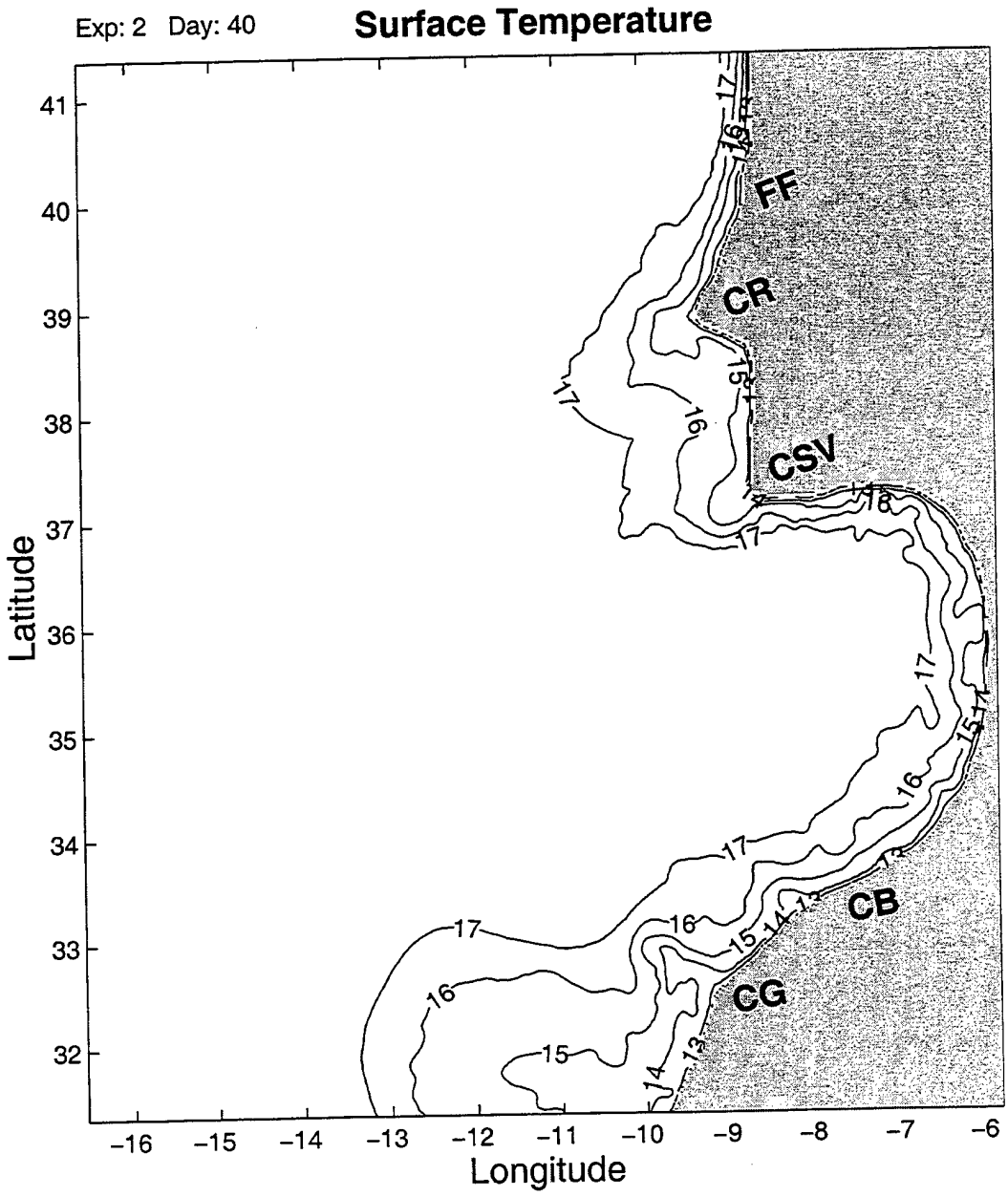

Figure 13. Surface temperature contours for Experiment 2 on day 40. Contour interval is 1°C.

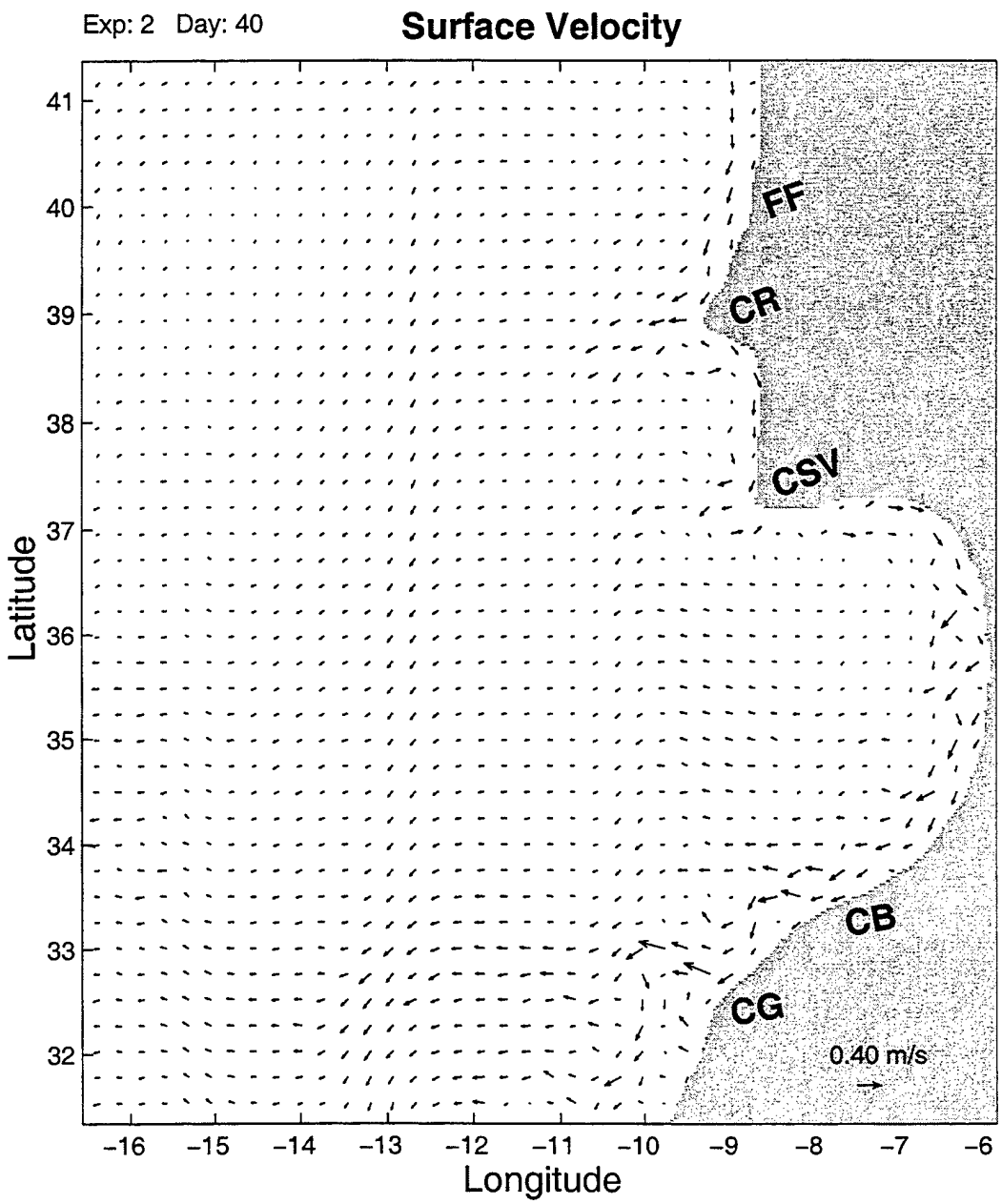

Figure 14. Surface velocity vectors for Experiment 2 on day 40.

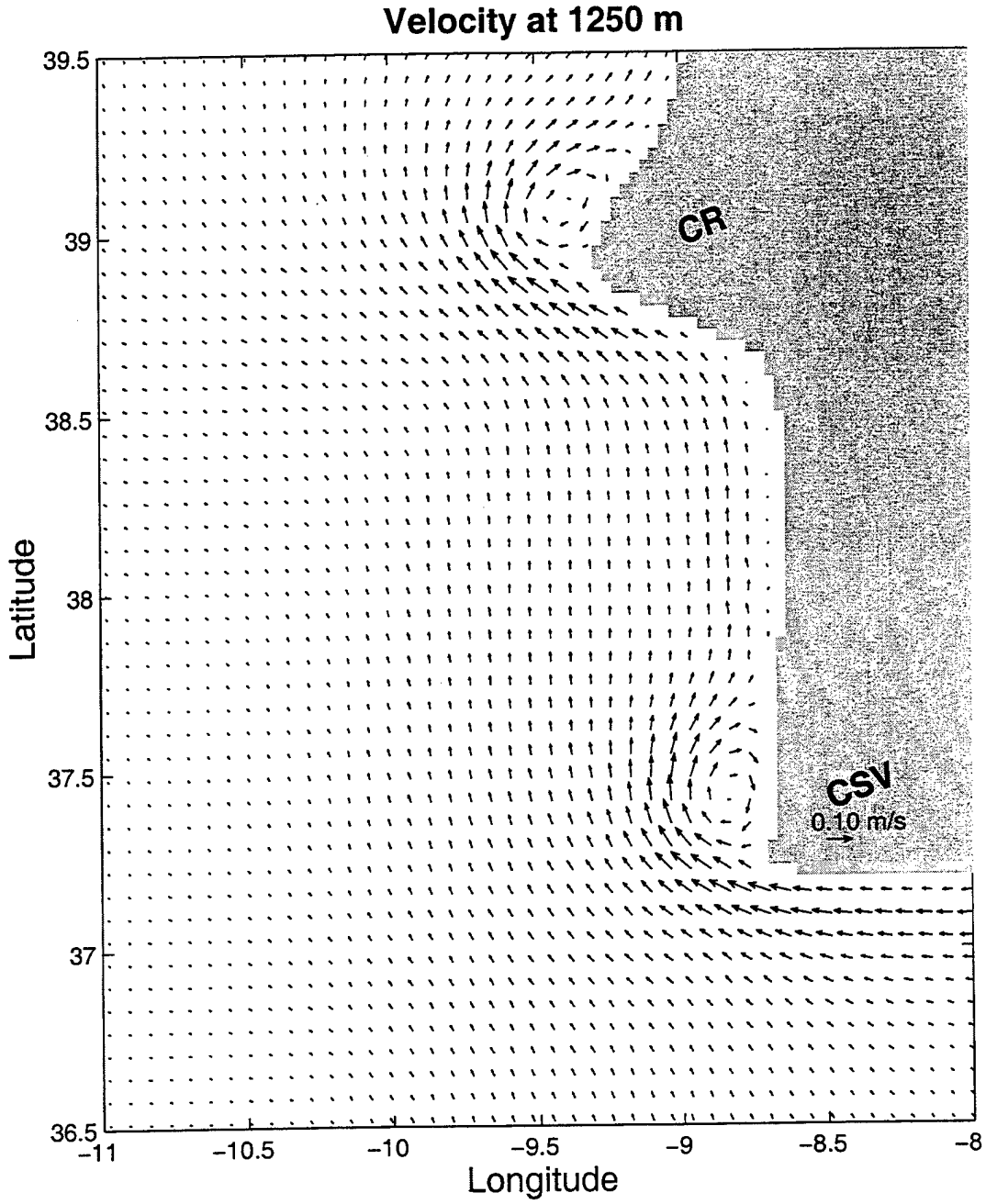

Figure 15. Velocity vectors at 1200 m depth for Experiment 2 on day 40.

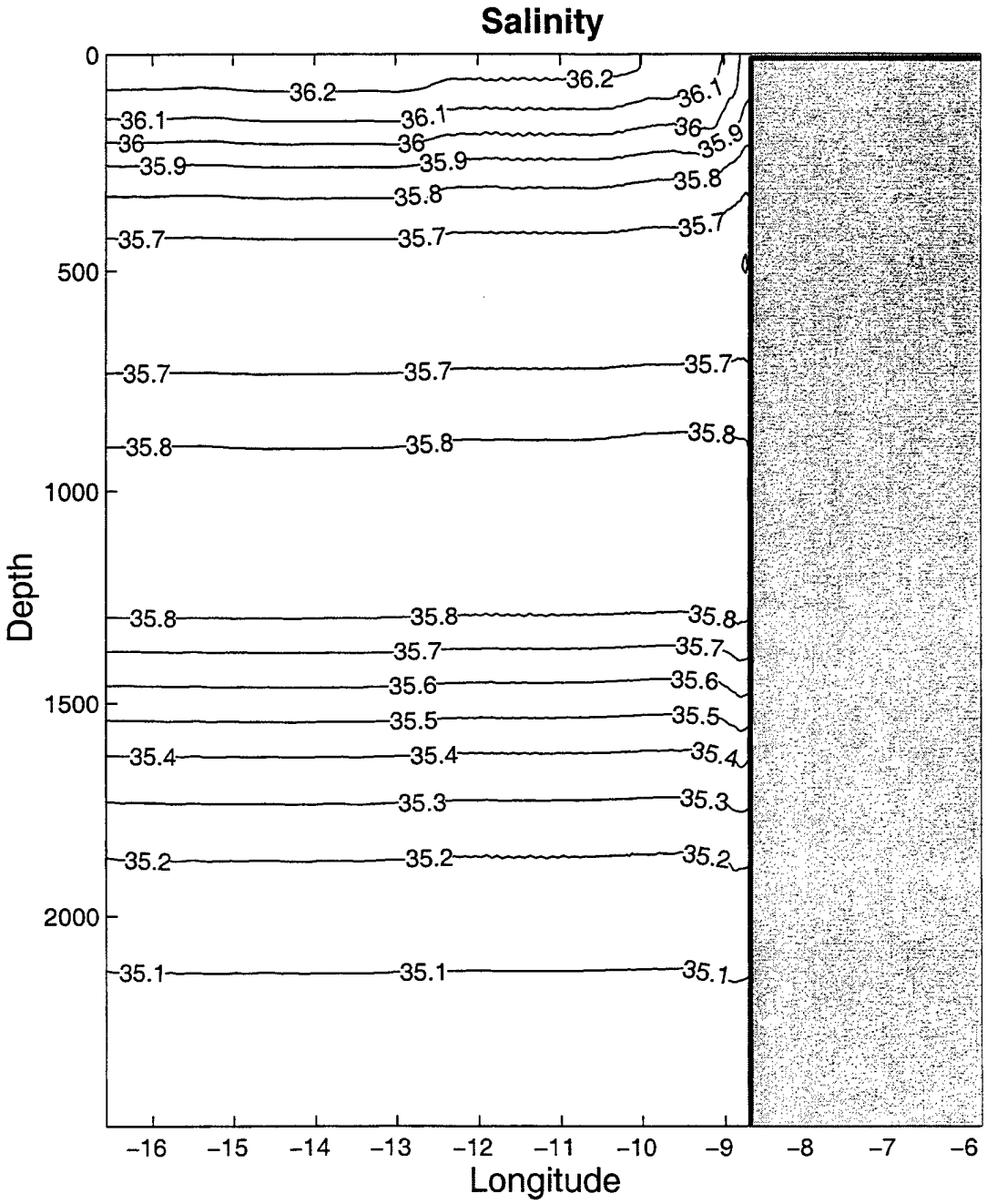

Figure 16. Cross-section at 37.4°N of salinity for Experiment 2 on day 40.

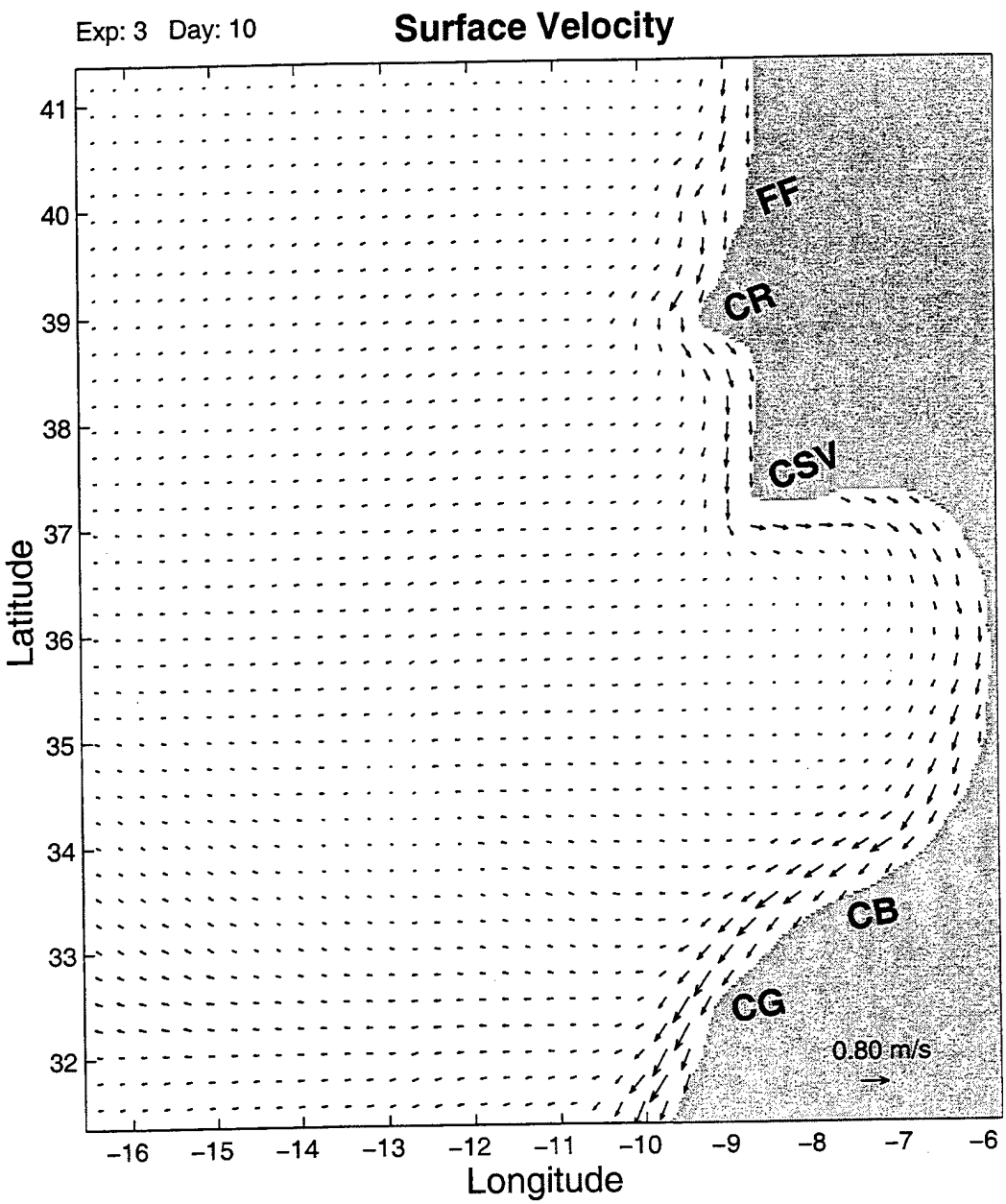

Figure 17a. Surface velocity vectors for Experiment 3 on day 10.

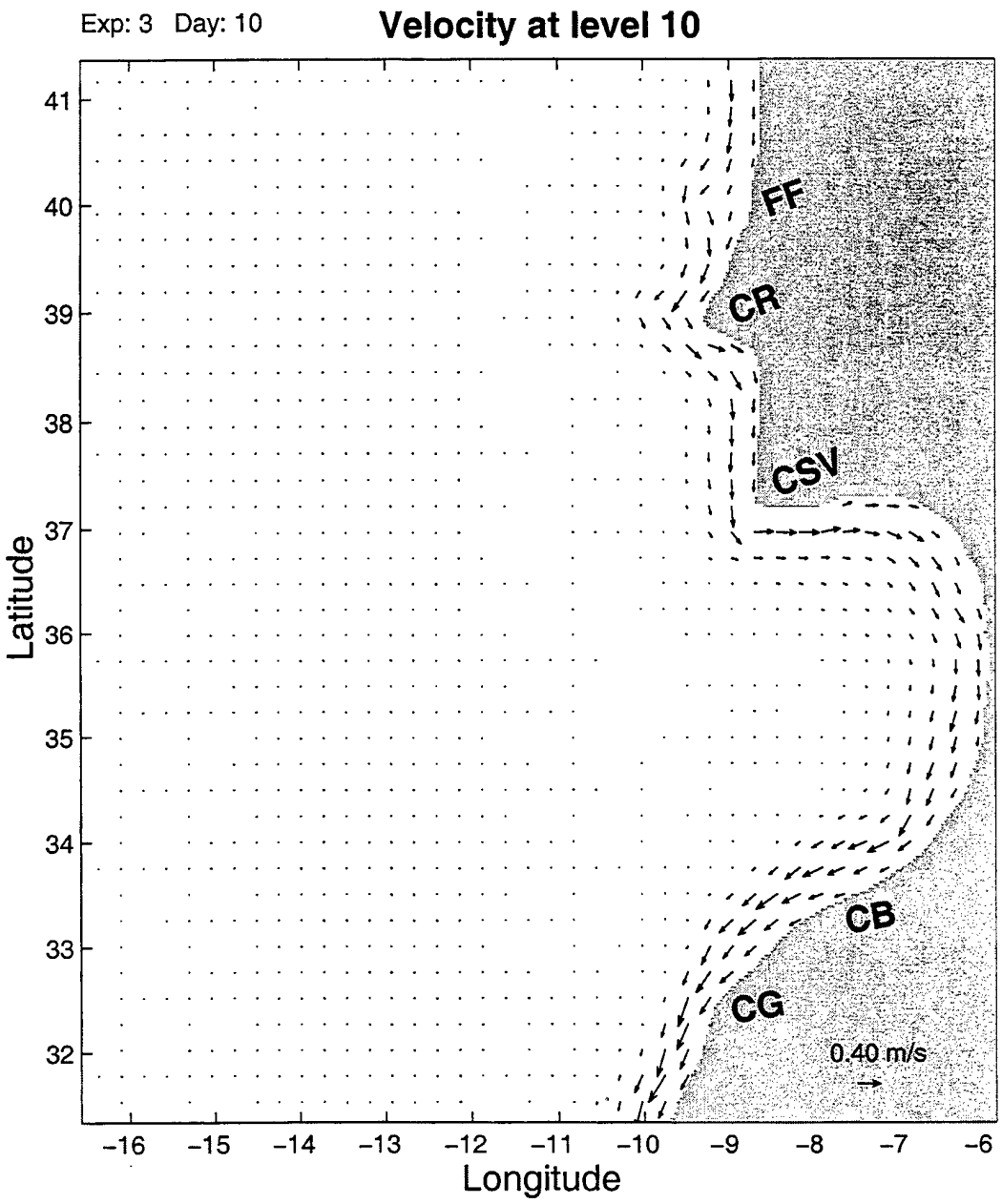

Figure 17b. Velocity vectors at sigma level 10 for Experiment 3 on day 10.

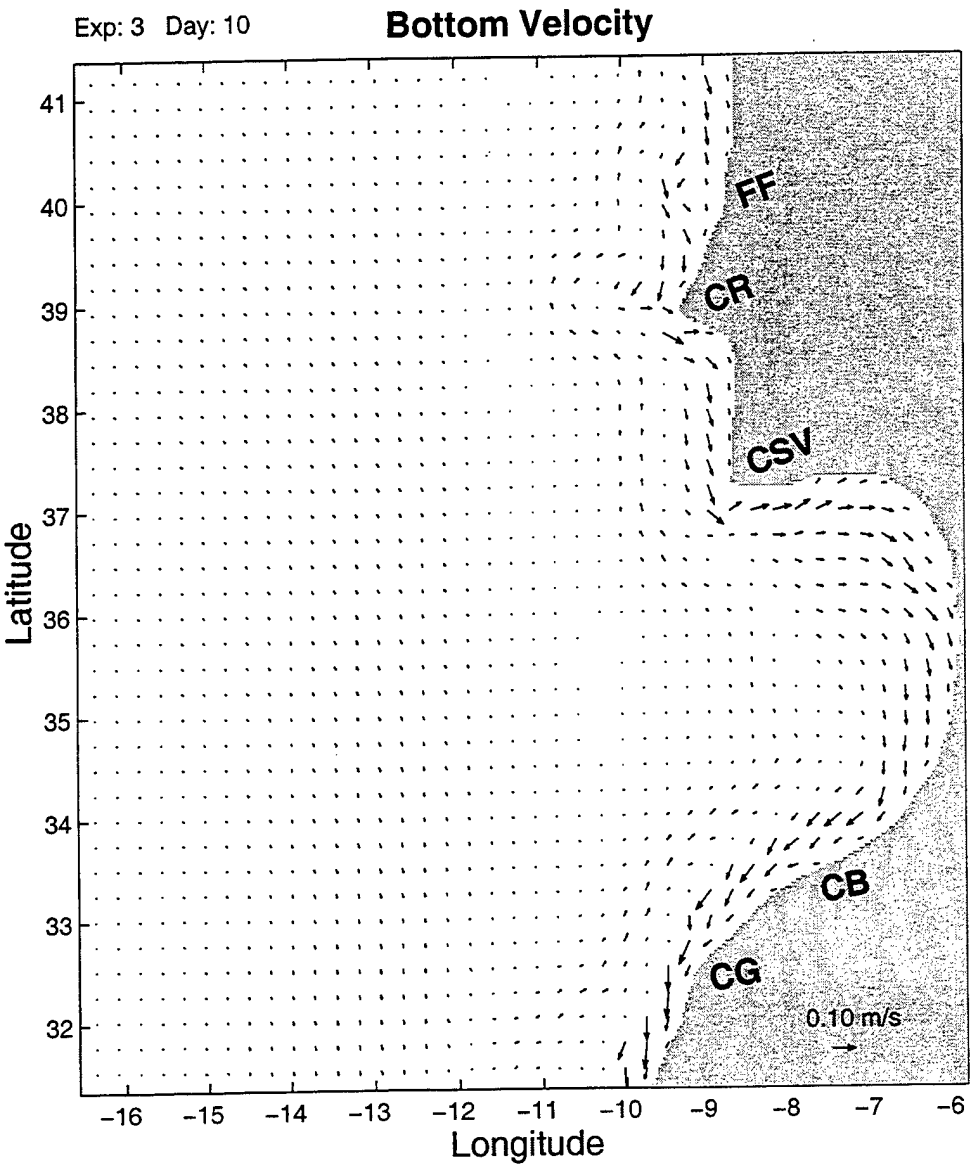

Figure 17c. Velocity vectors at sigma level 20 for Experiment 3 on day 10.

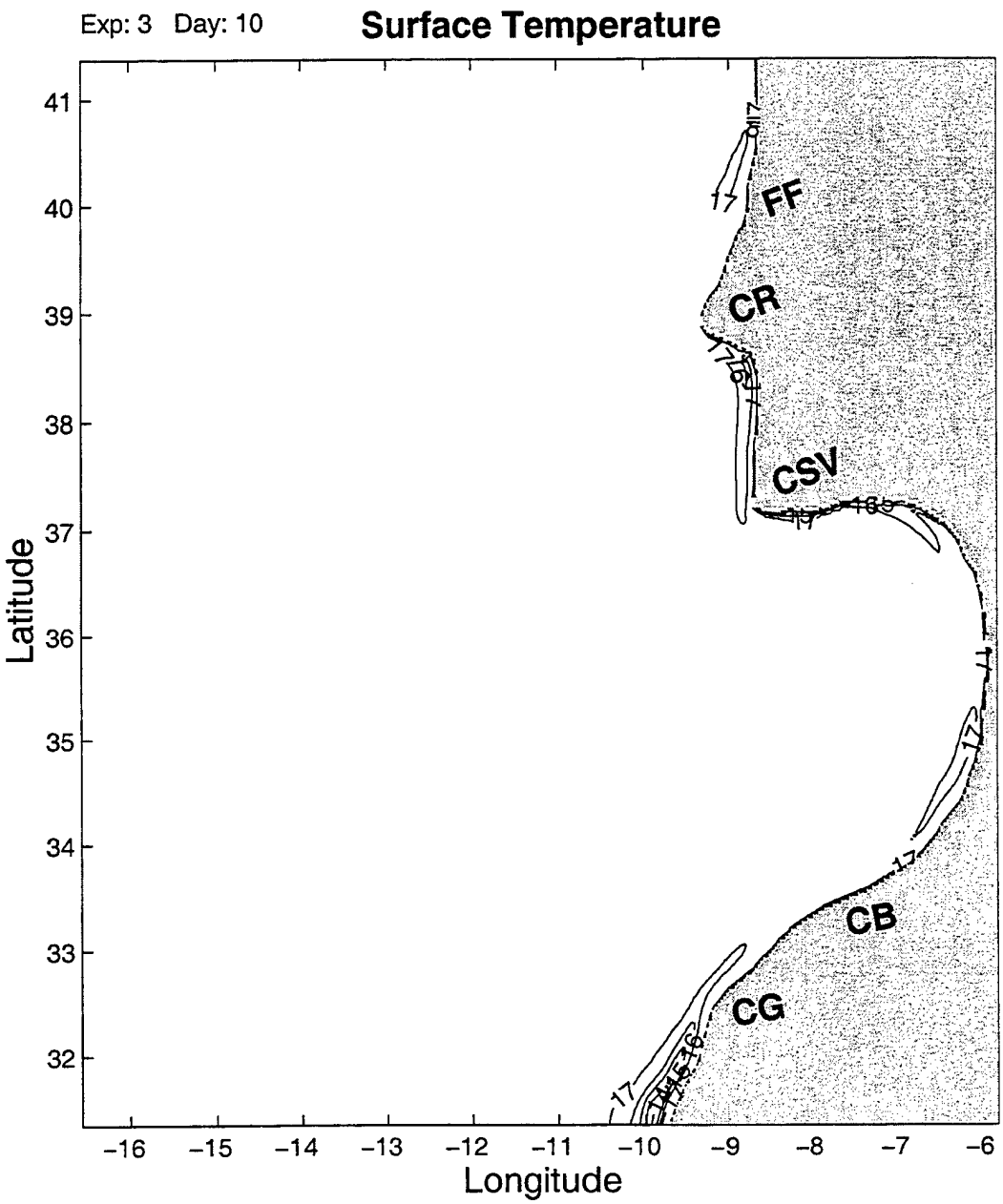

Figure 18. Surface temperature contours for Experiment 3 on day 10. Contour interval is 1°C.

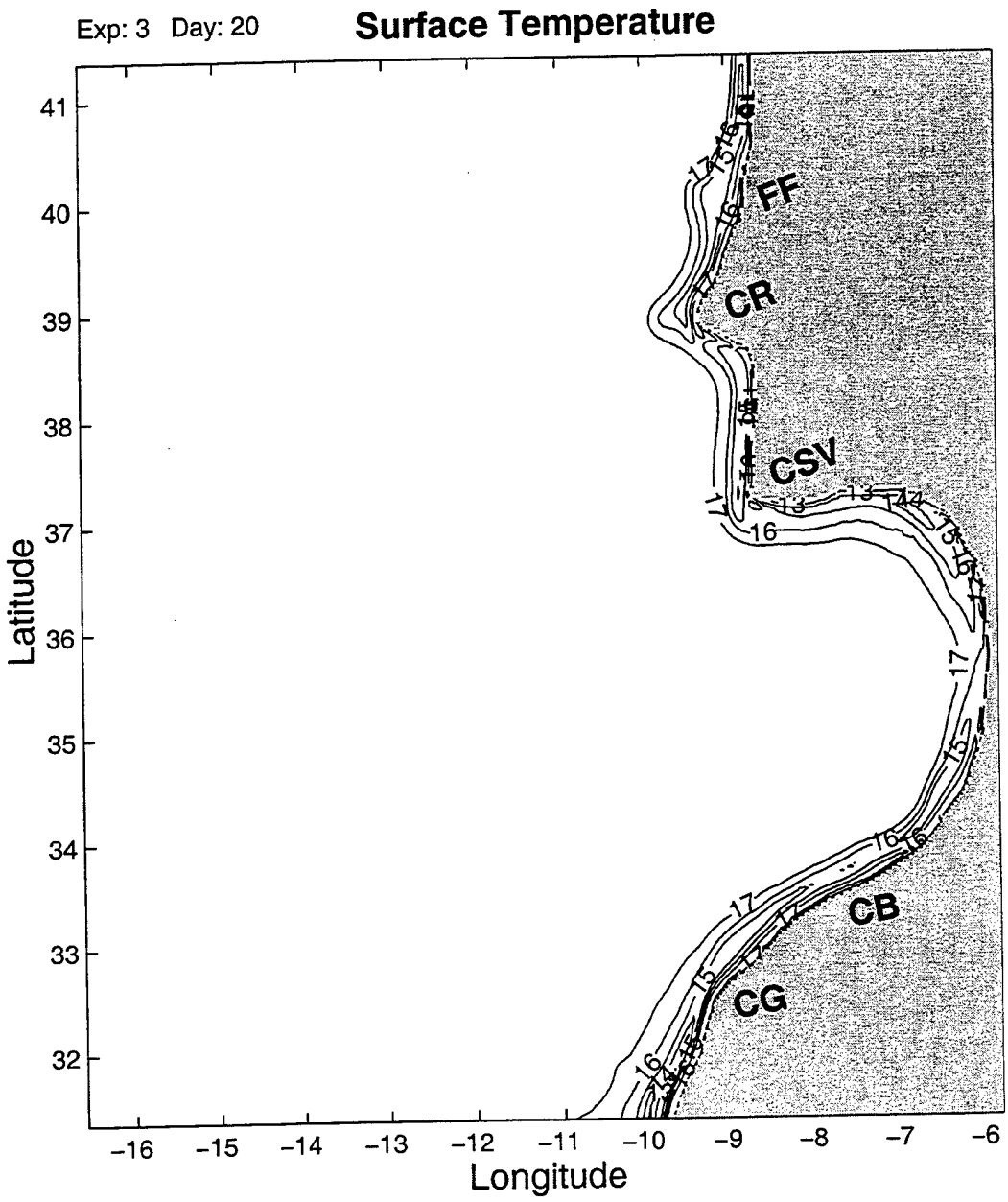

Figure 19. Surface temperature contours for Experiment 3 on day 20. Contour interval is 1°C.

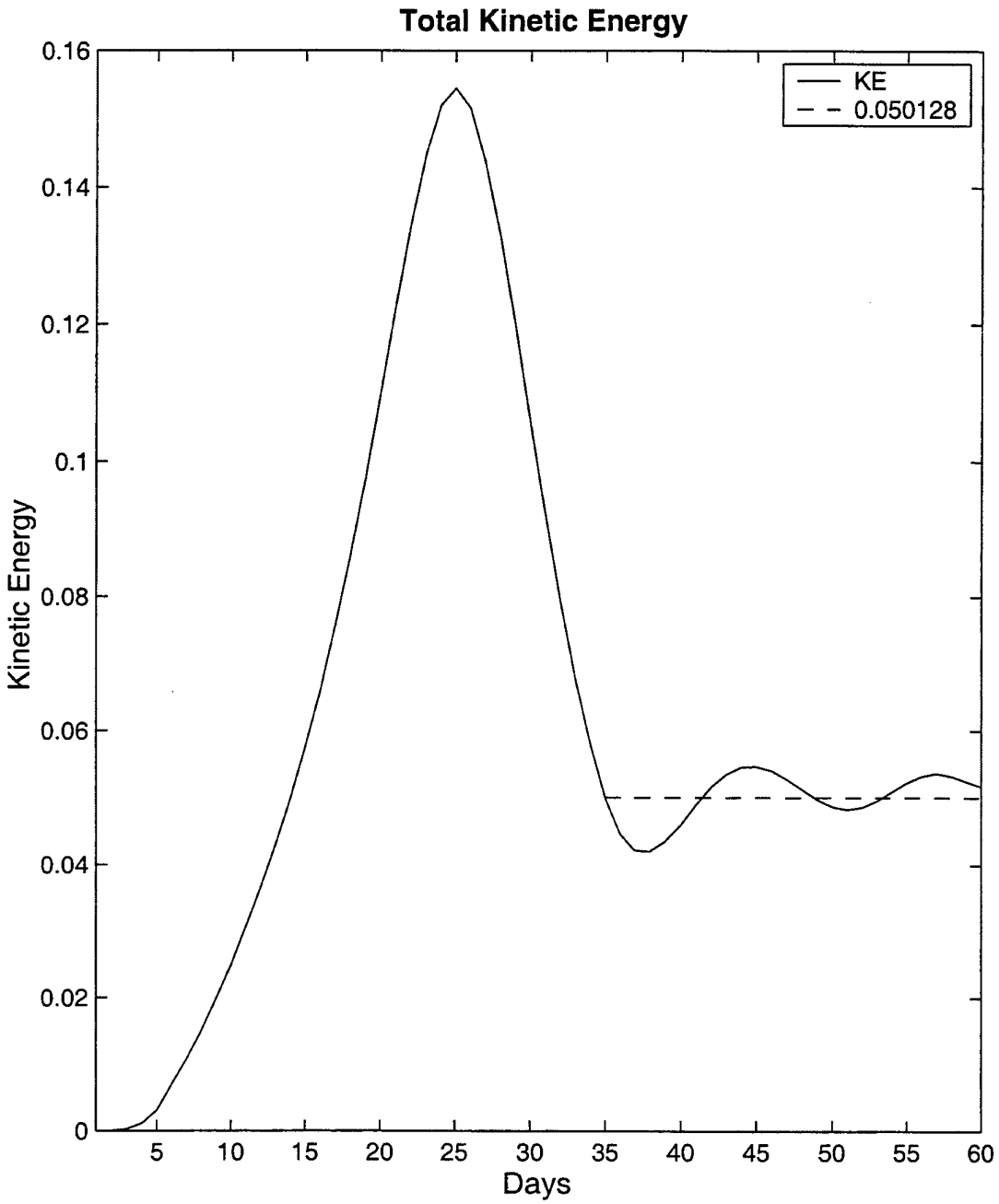

Figure 20a. Plot of the total kinetic energy integrated over the whole domain versus time.

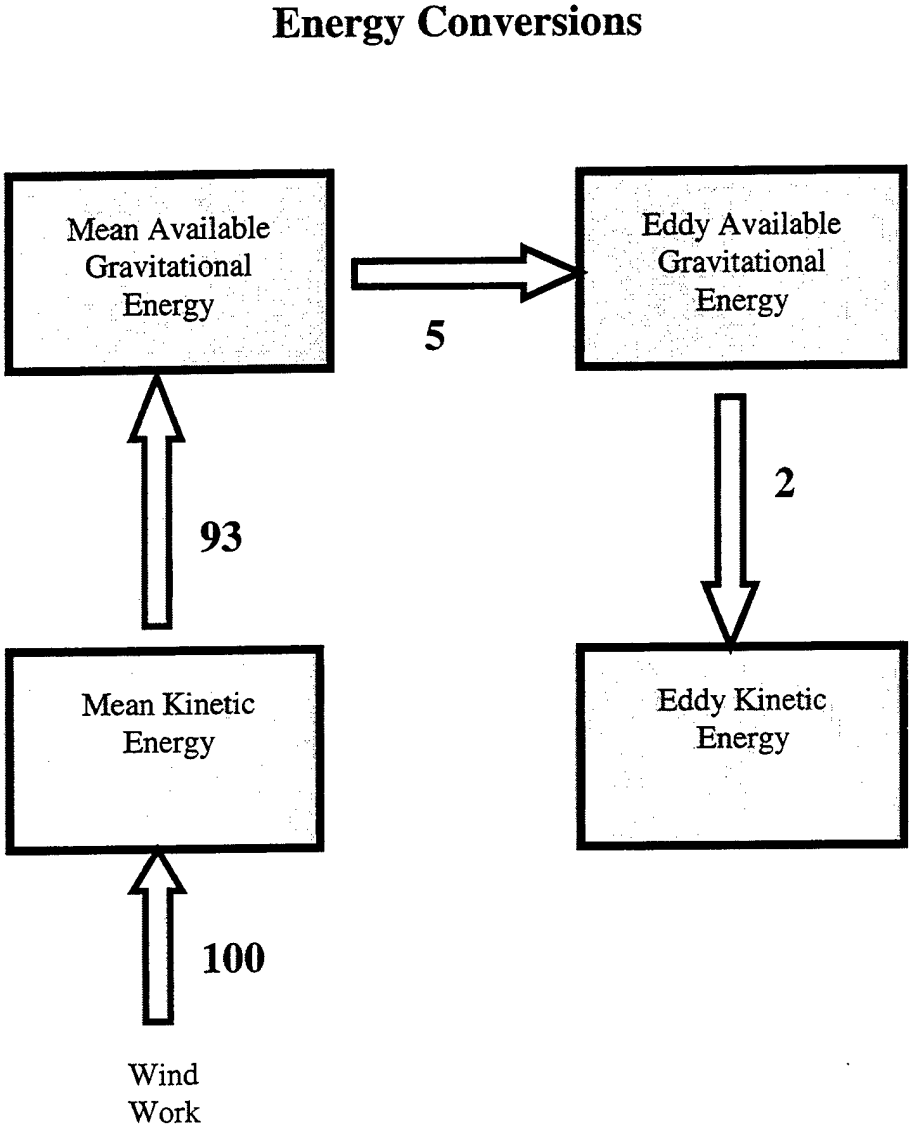

Figure 20b. Energy conversions in percentage of the wind work from Roed (2000).

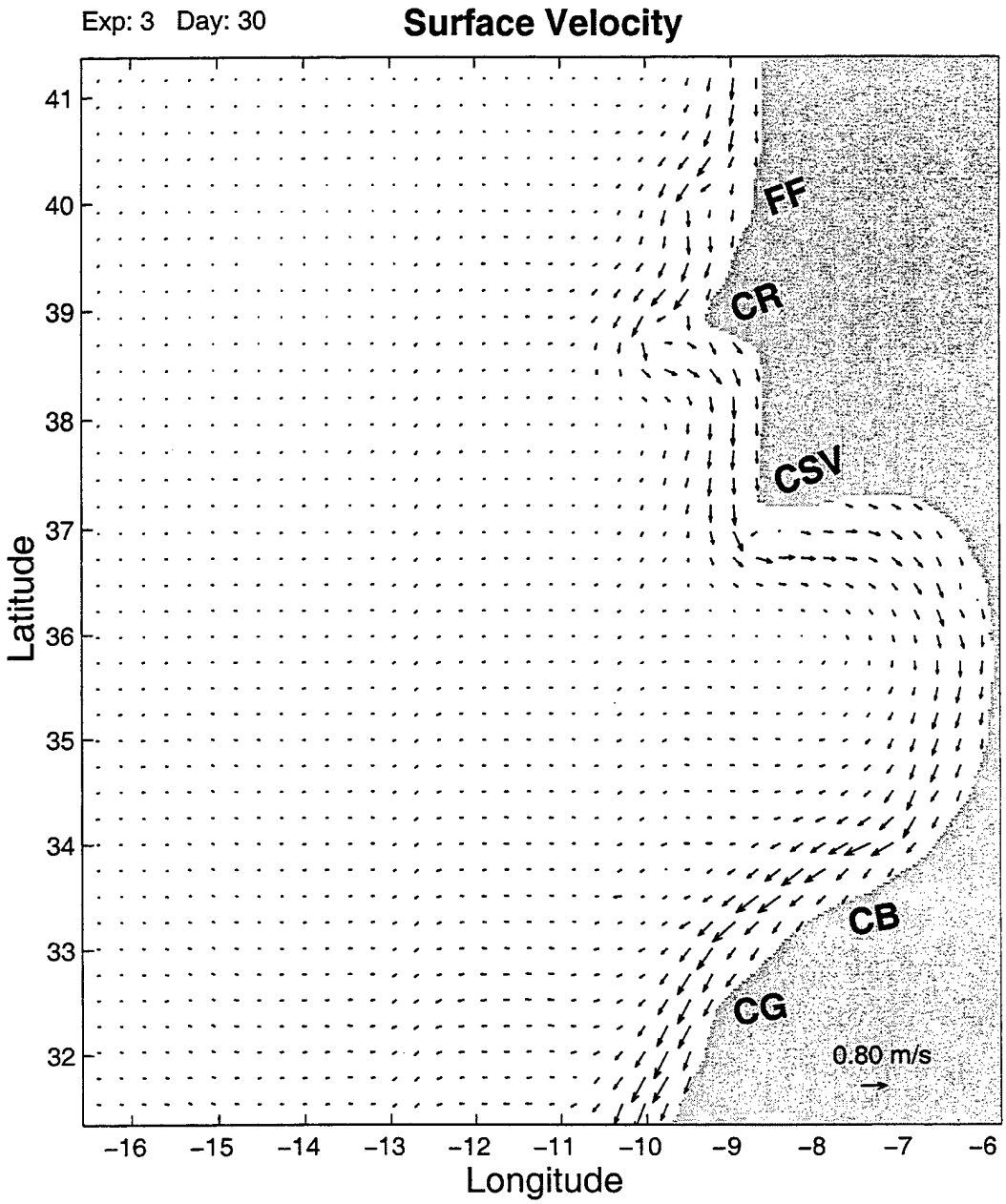

Figure 21. Surface velocity vectors for Experiment 3 on day 30.

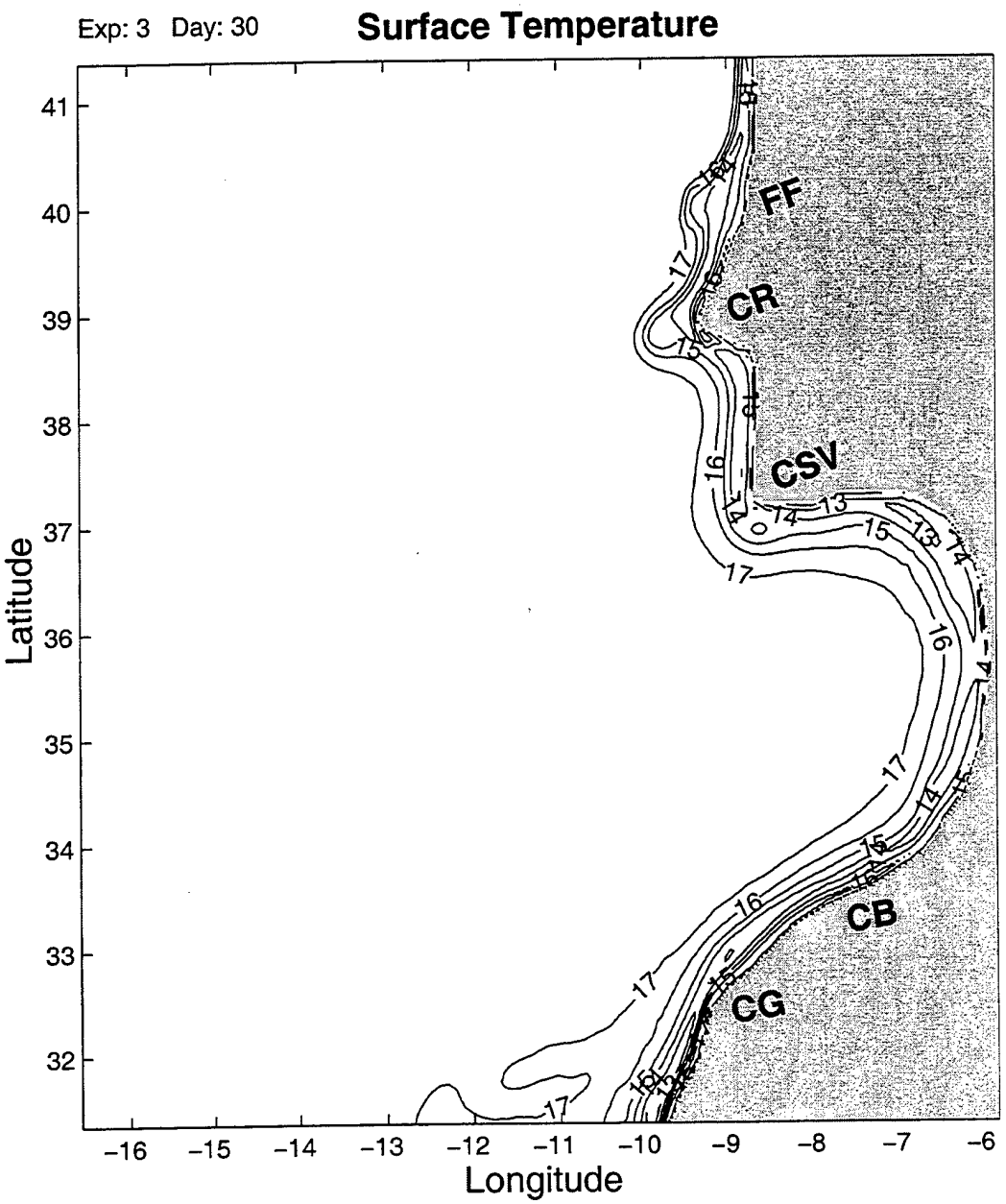

Figure 22. Surface temperature contours for Experiment 3 on day 30. Contour interval is 1°C.

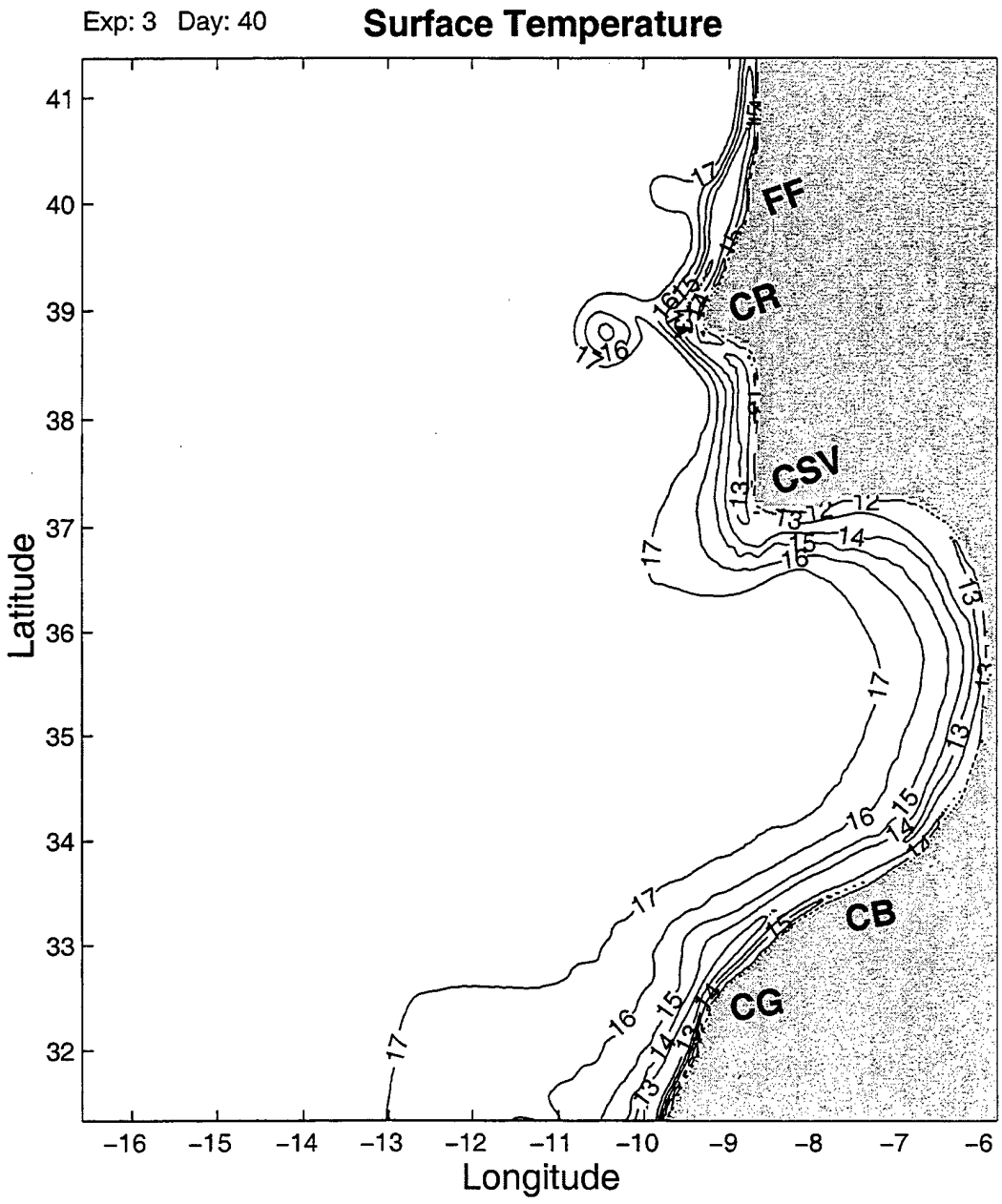

Figure 23a. Surface temperature contours for Experiment 3 on day 40. Contour interval is 1°C.

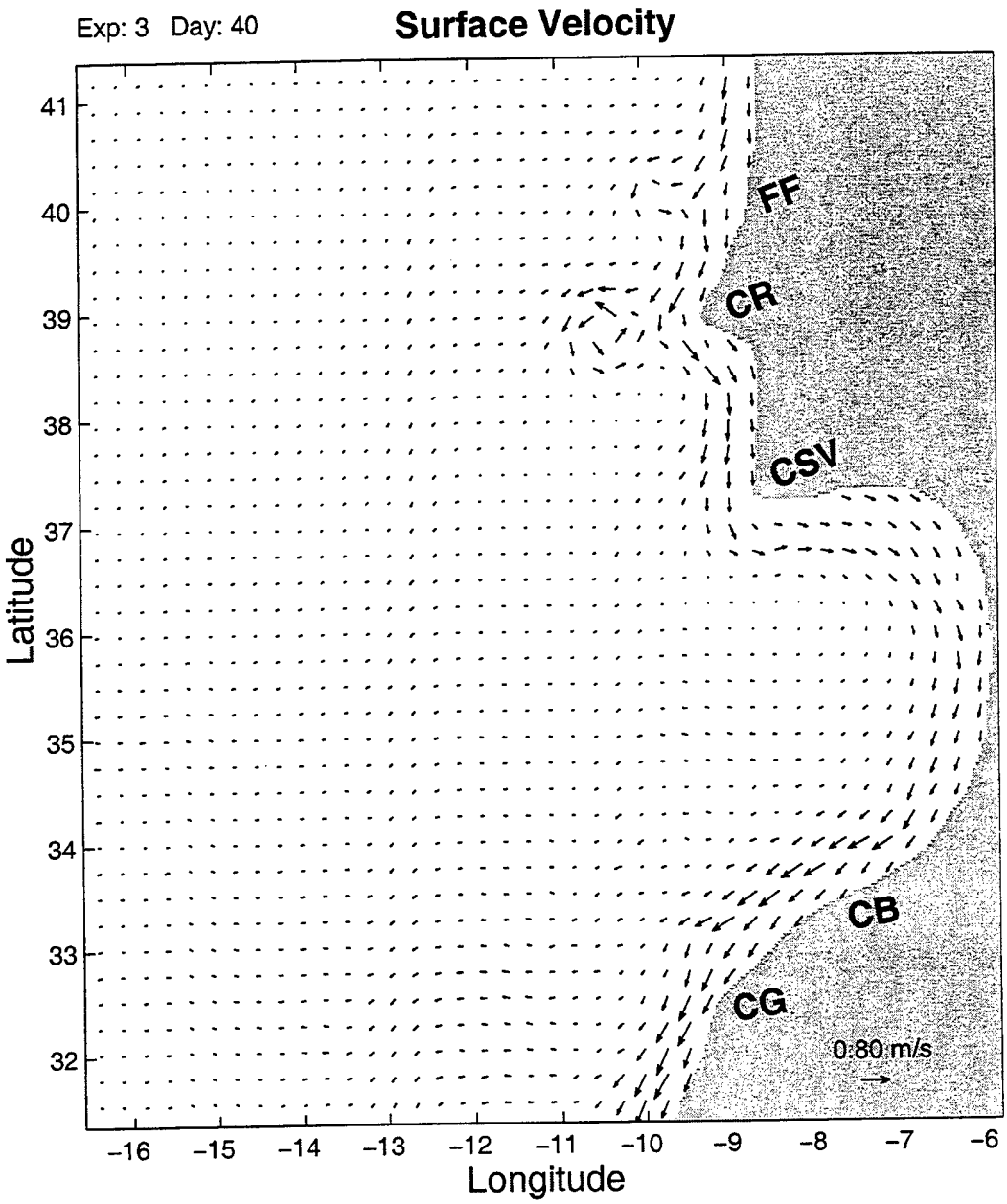

Figure 23b. Surface velocity vectors for Experiment 3 on day 40.

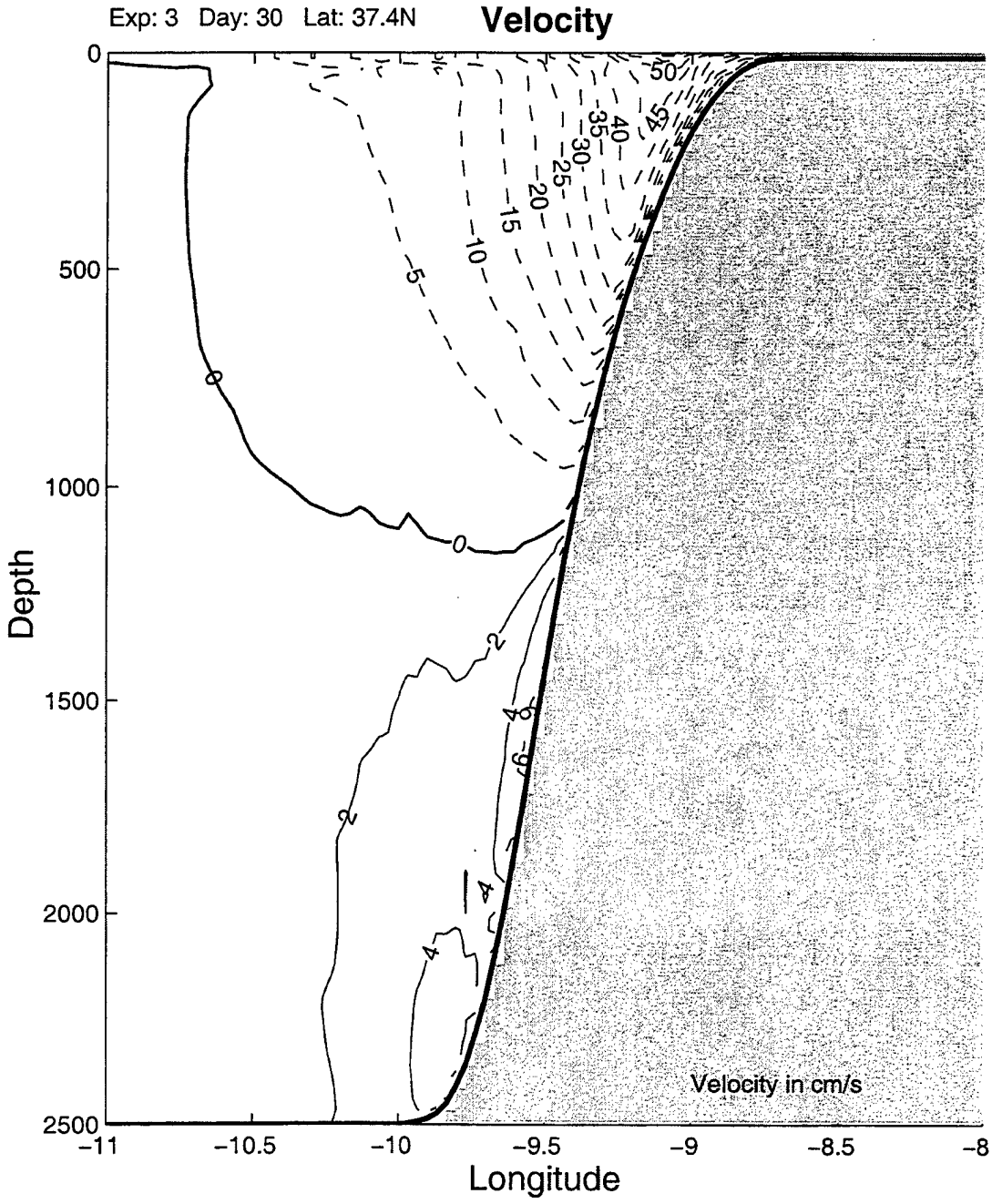

Figure 24a. Cross-section of meridional velocity (v) at 37.4°N for Experiment 3 on day 30. Equatorward (poleward) flow is denoted by dashed (solid) lines with contour intervals of 5 cm/s (2cm/s).

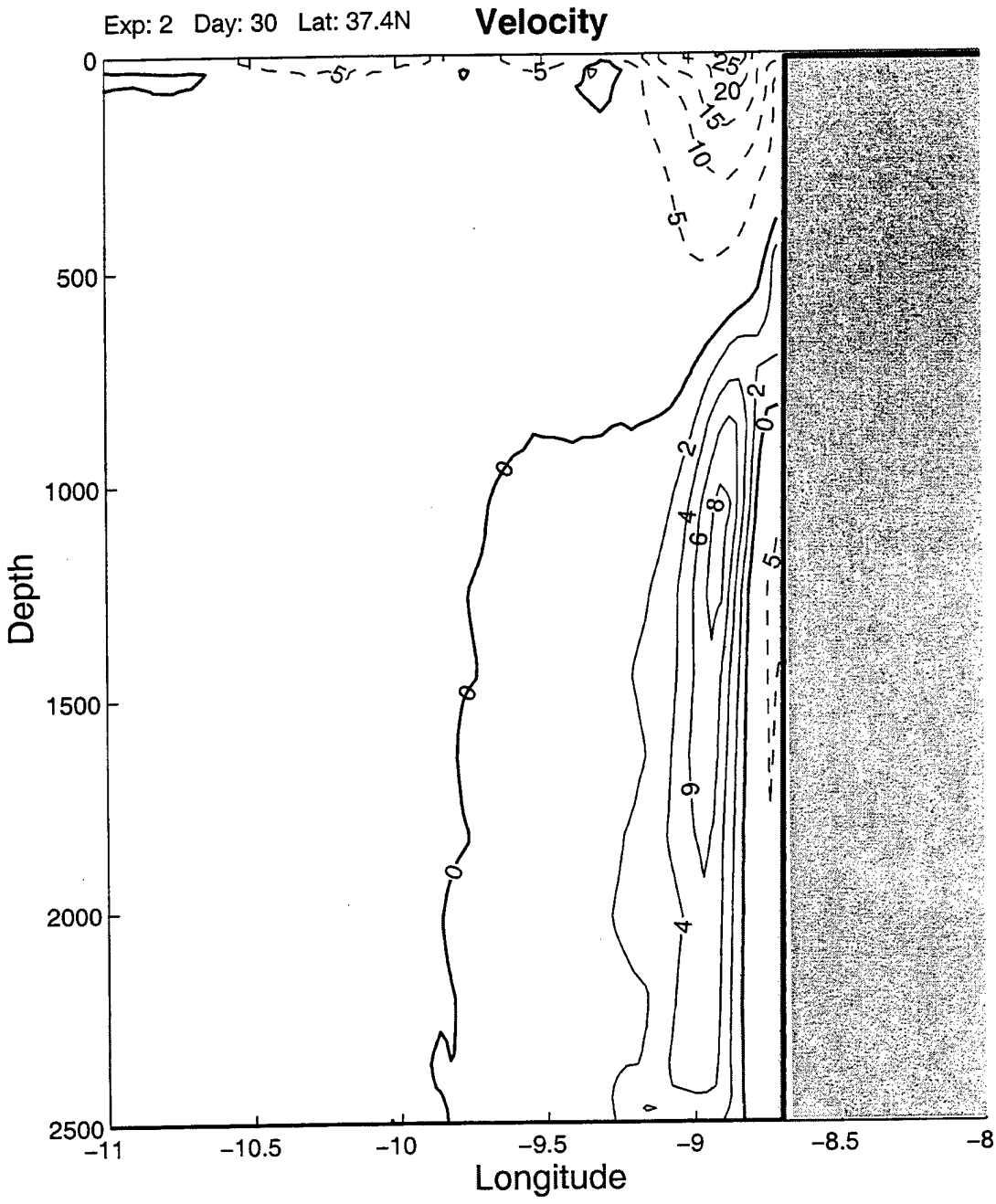

Cross-section of meridional velocity (v) at 37.4°N for Experiment 2 on day 30. Equatorward (poleward) flow is denoted by dashed (solid) lines with contour intervals of 5 cm/s (2cm/s).

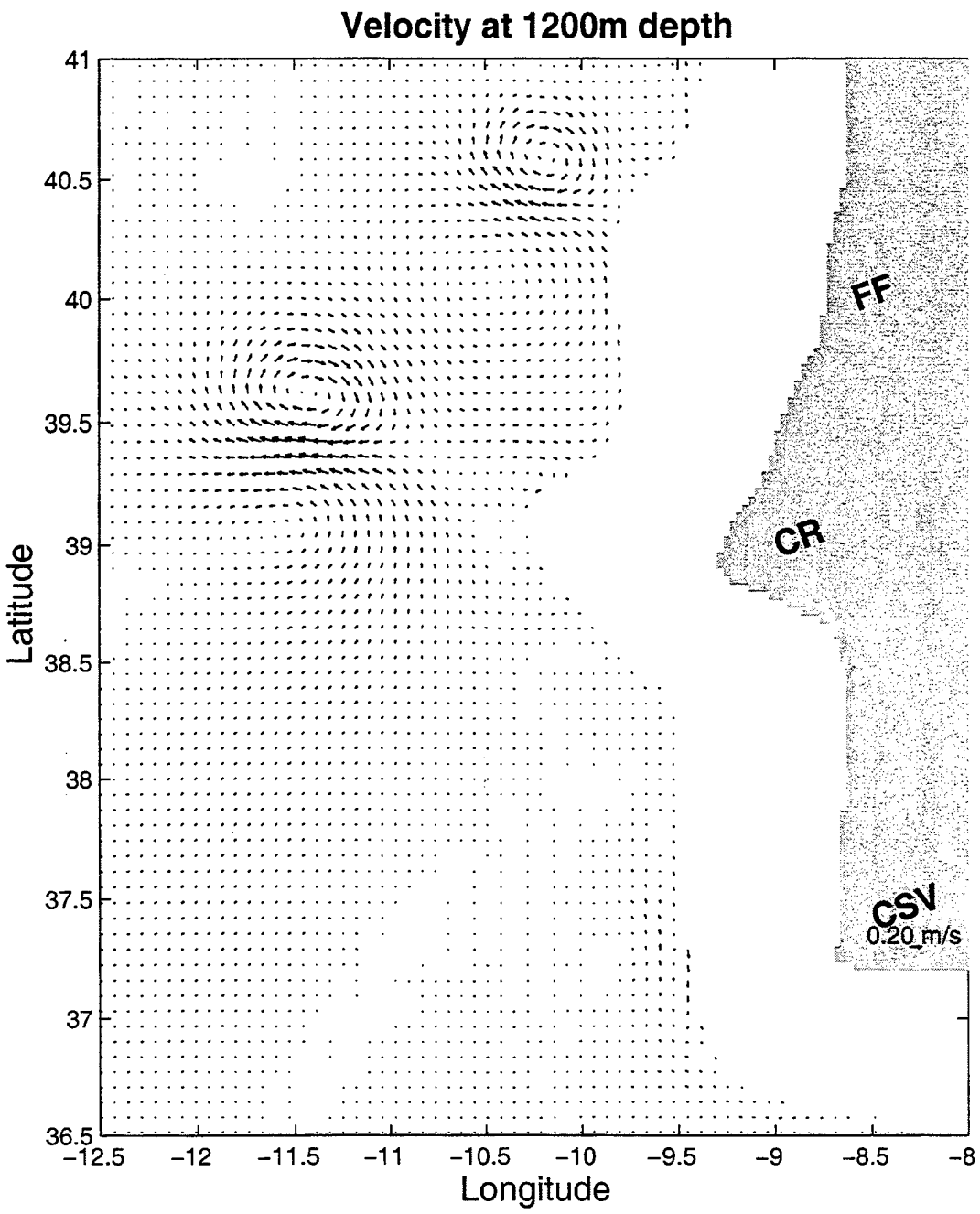

Figure 25. Velocity vectors at 1200 m depth for Experiment 3 on day 60.

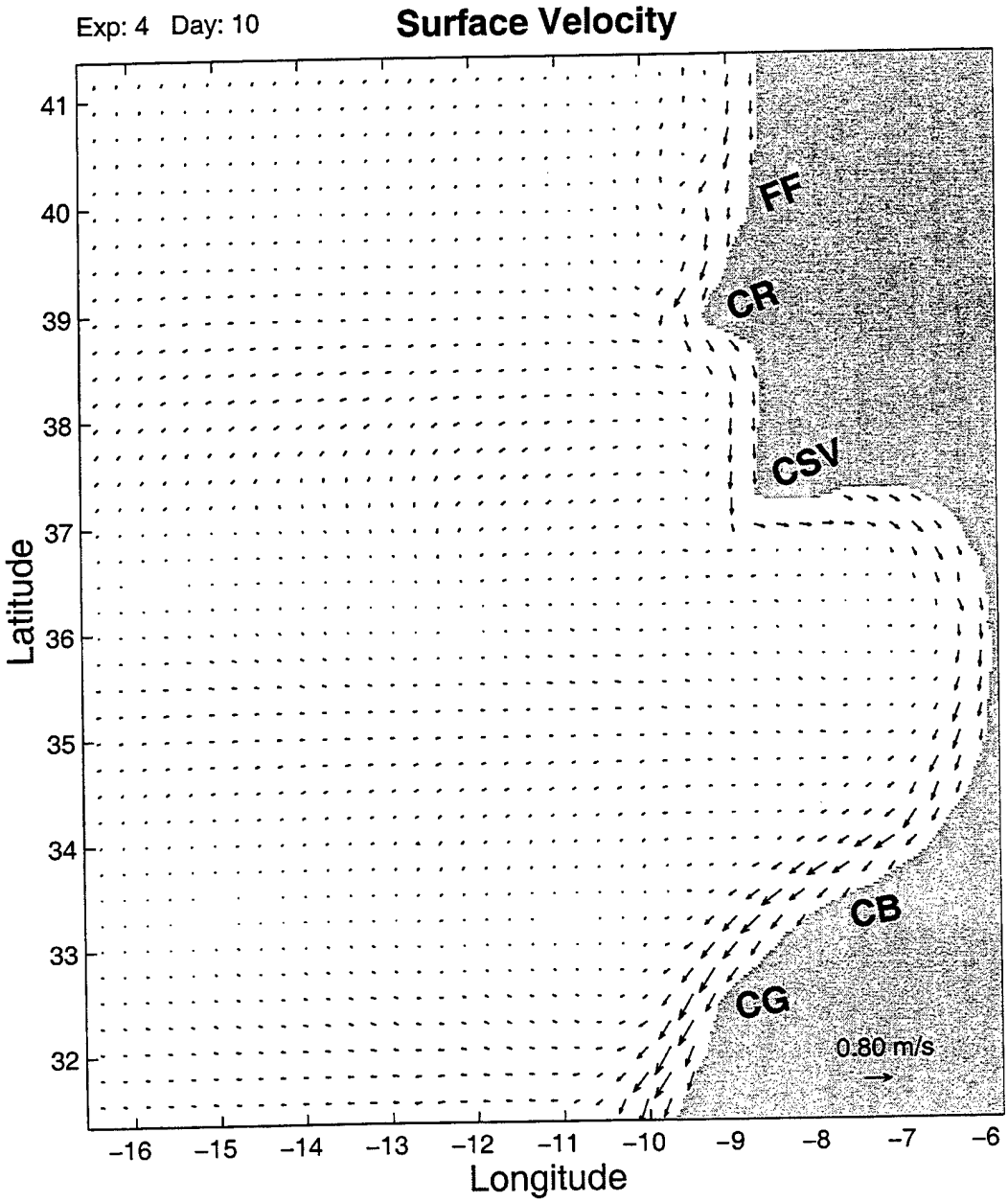

Figure 26. Surface velocity vectors for Experiment 4 on day 10.

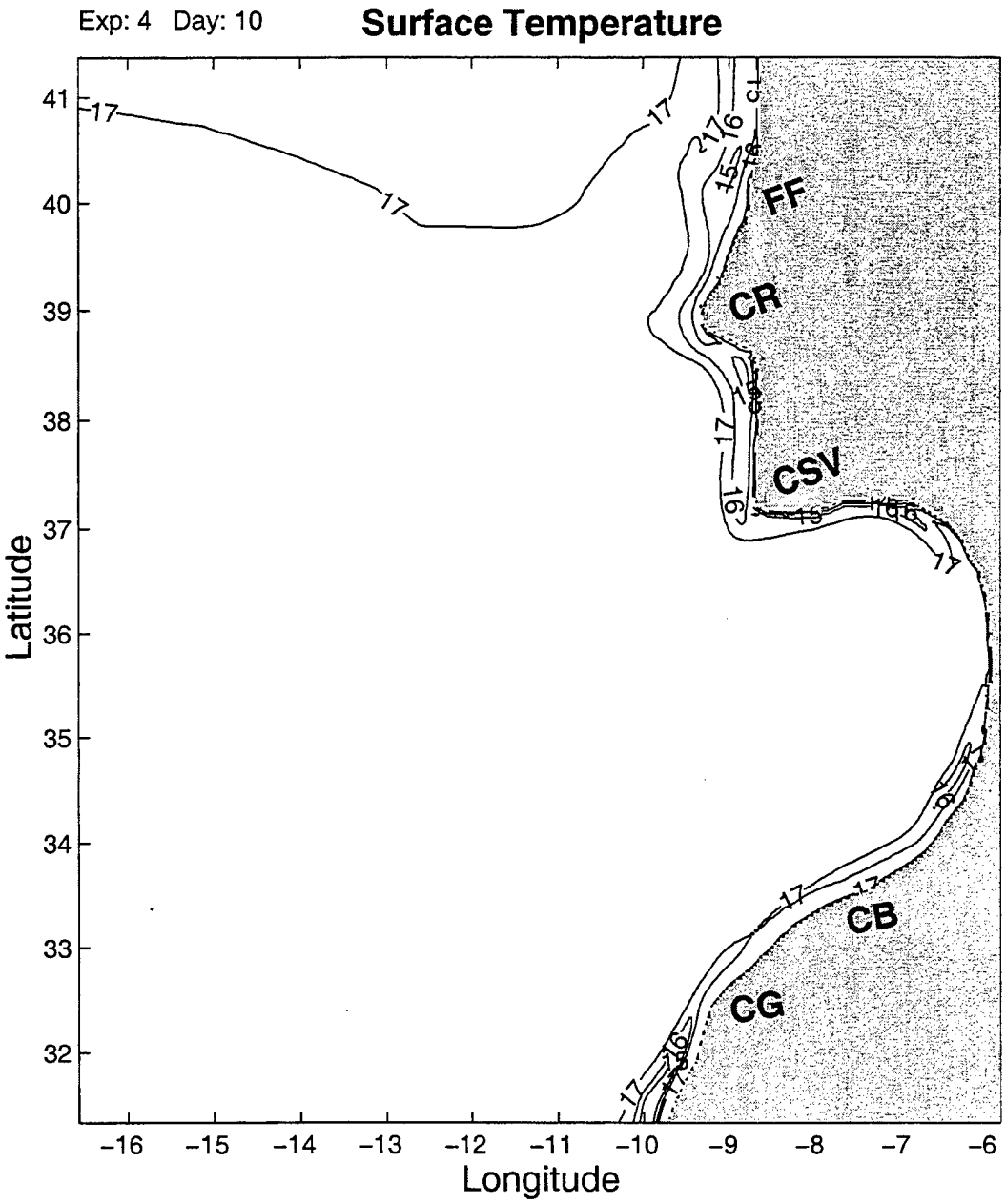

Figure 27. Surface temperature contours for Experiment 4 on day 10. Contour interval is 1°C.

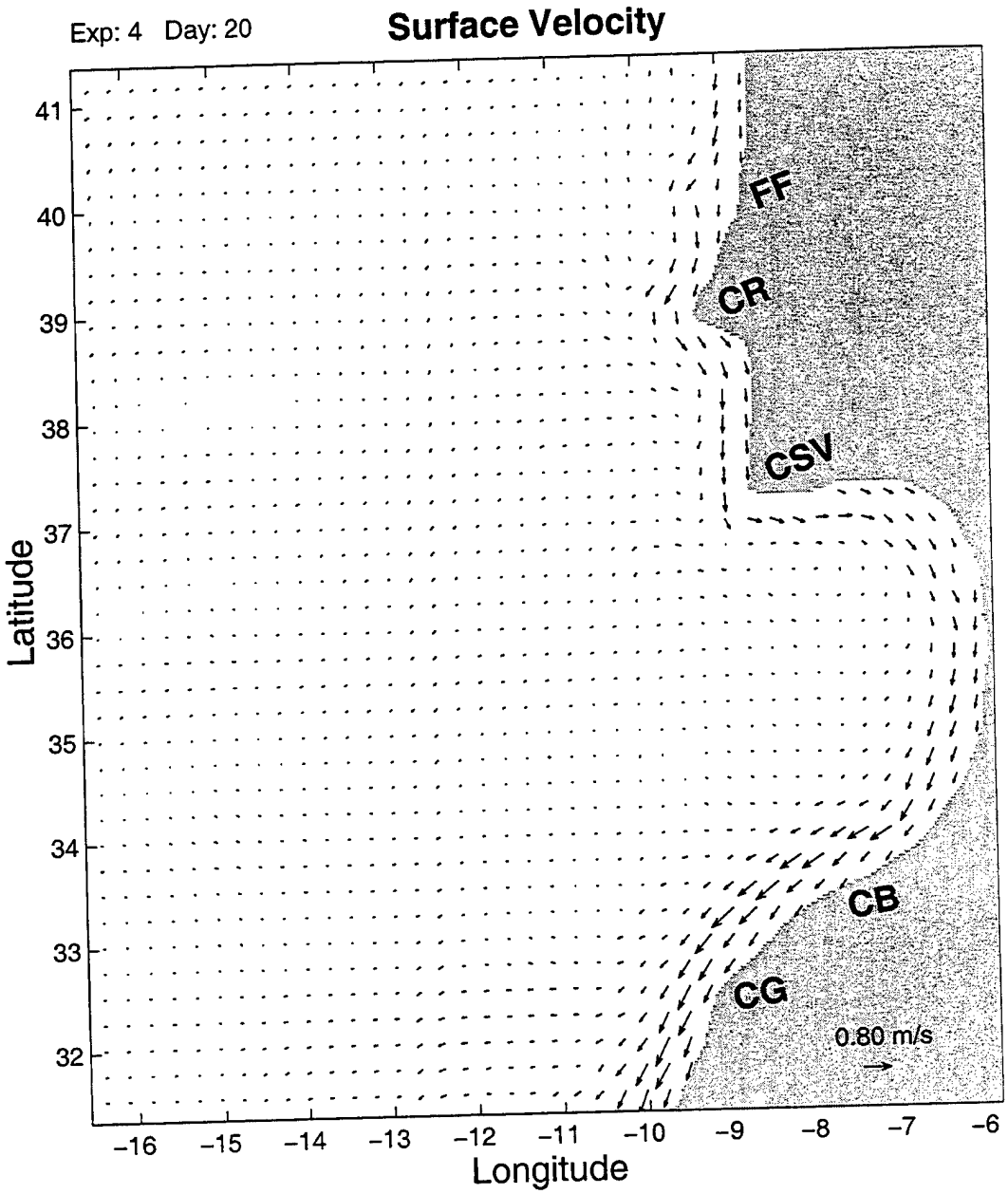

Figure 28. Surface velocity vectors for Experiment 4 on day 20.

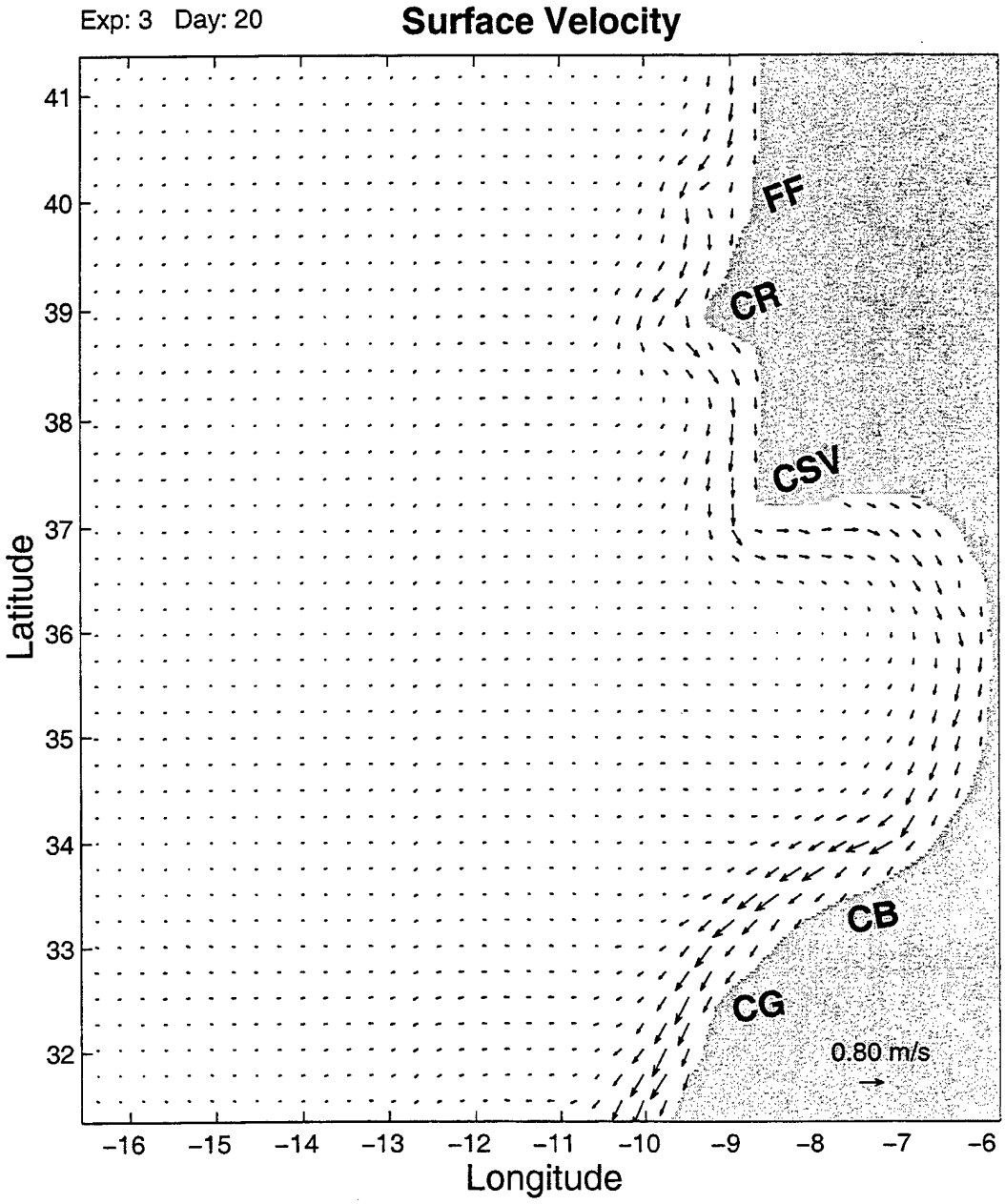

Figure 29. Surface velocity vectors for Experiment 3 on day 20.

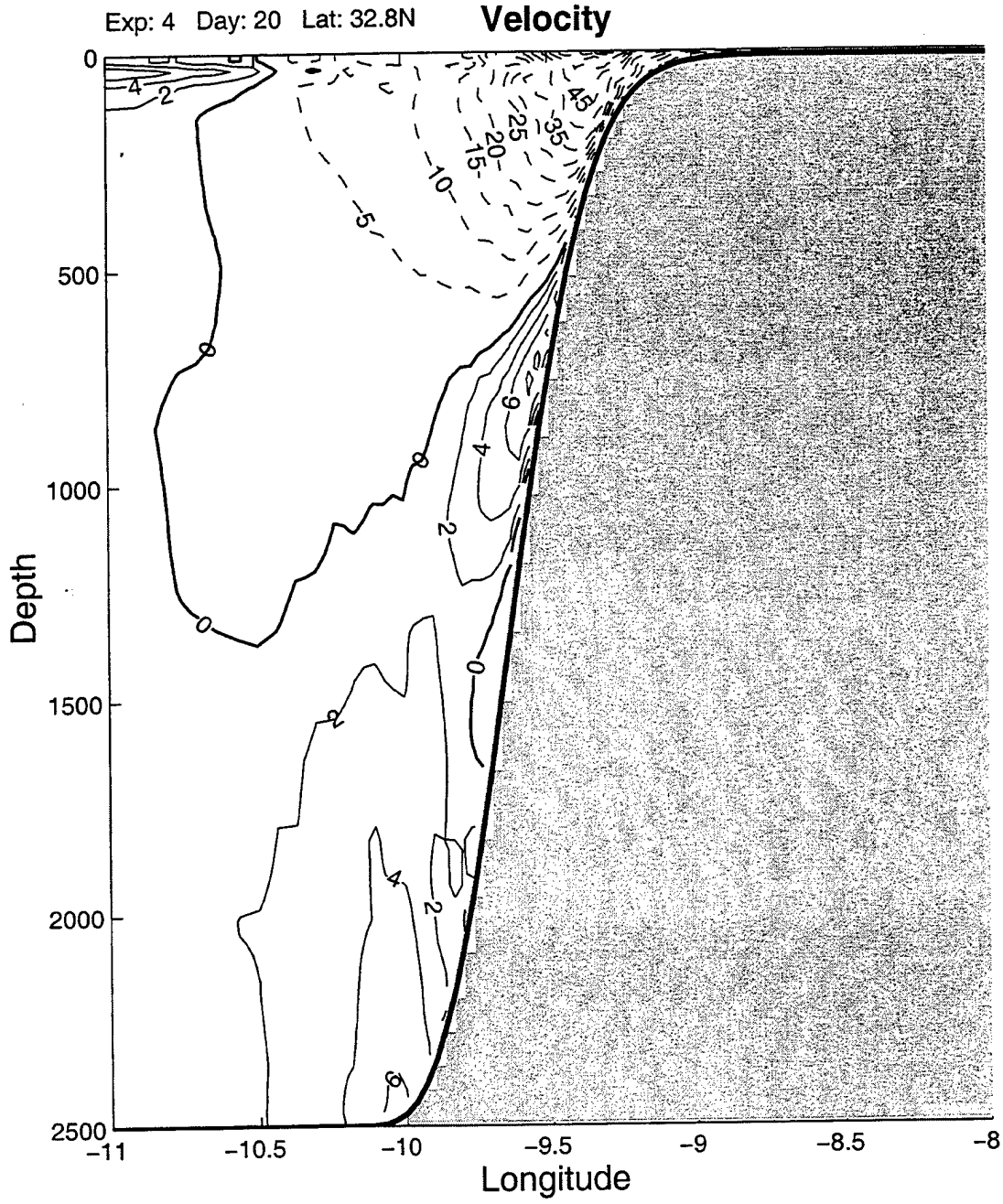

Figure 30. Cross-section of meridional velocity (v) at 32.8°N for Experiment 4 on day 20. Equatorward (poleward) flow is denoted by dashed (solid) lines with contour intervals of 5 cm/s (2cm/s).

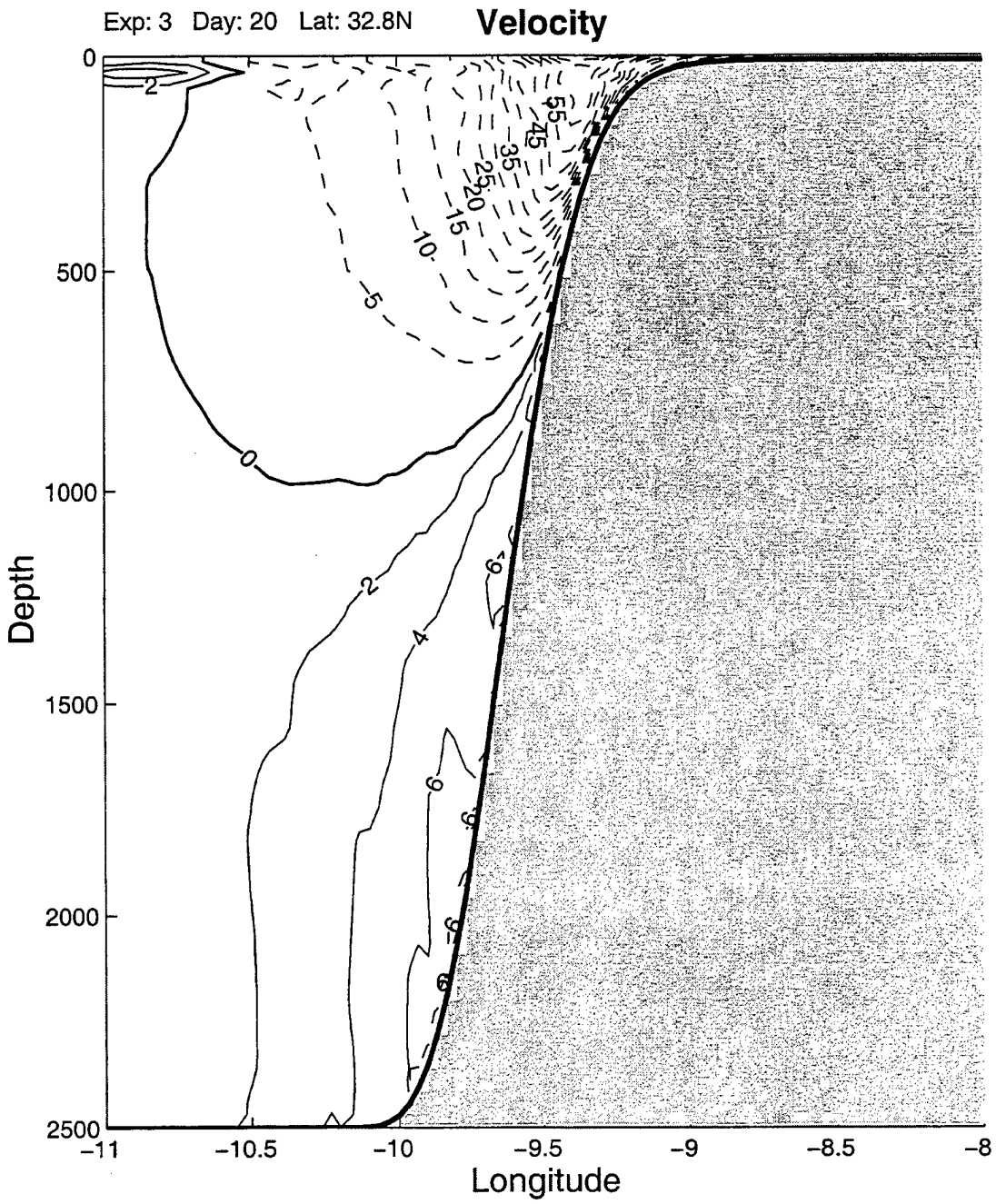

Figure 31. Cross-section of meridional velocity (v) at 32.8°N for Experiment 3 on day 20. Equatorward (poleward) flow is denoted by dashed (solid) lines with contour intervals of 5 cm/s (2cm/s).

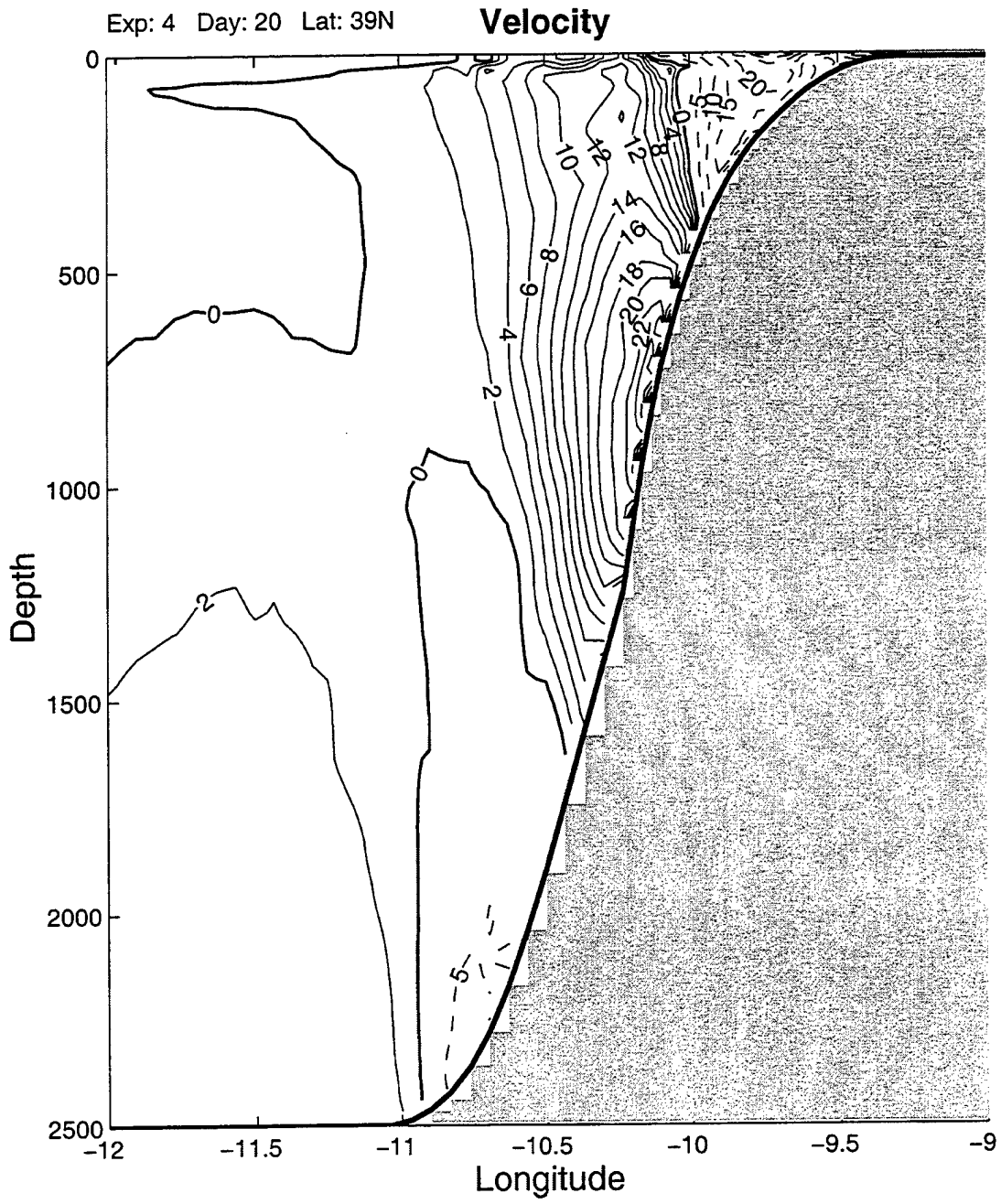

Figure 32. Cross-section of meridional velocity (v) at 39°N for Experiment 4 on day 20. Equatorward (poleward) flow is denoted by dashed (solid) lines with contour intervals of 5 cm/s (2cm/s).

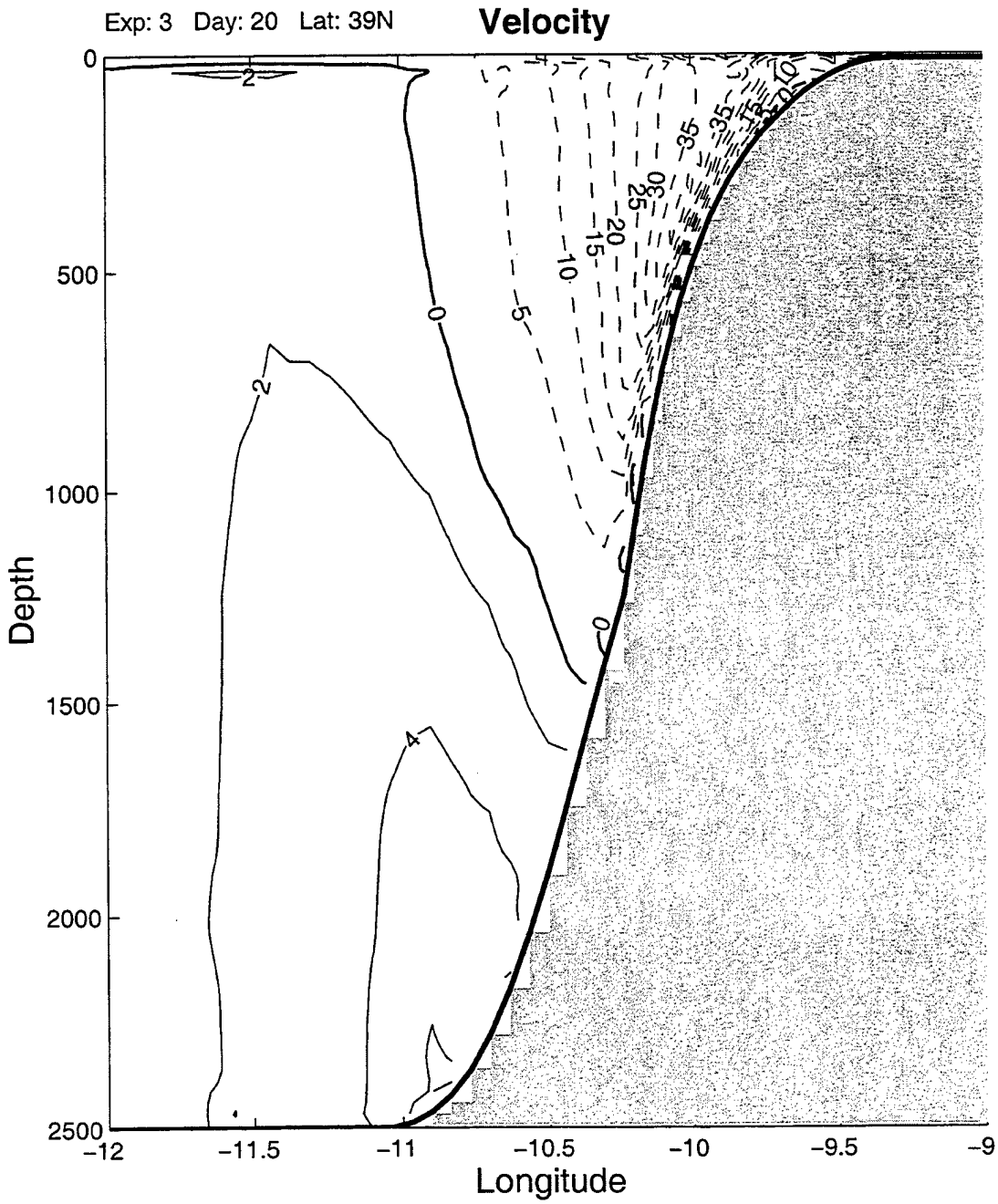

Figure 33. Cross-section of meridional velocity (v) at 39°N for Experiment 3 on day 20. Equatorward (poleward) flow is denoted by dashed (solid) lines with contour intervals of 5 cm/s (2cm/s).

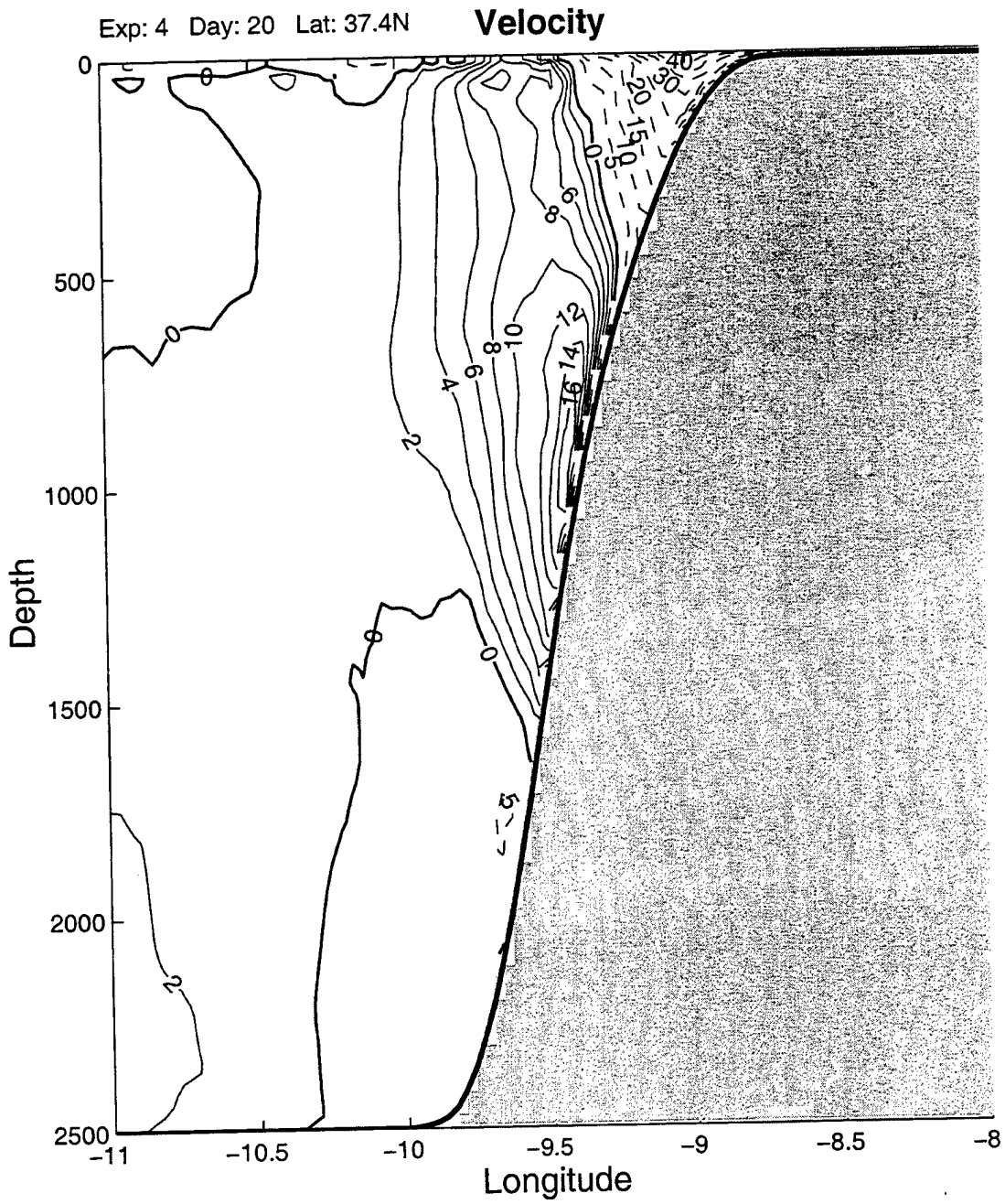

Figure 34. Cross-section of meridional velocity (v) at 37.4°N for Experiment 4 on day 20. Equatorward (poleward) flow is denoted by dashed (solid) lines with contour intervals of 5 cm/s (2cm/s).

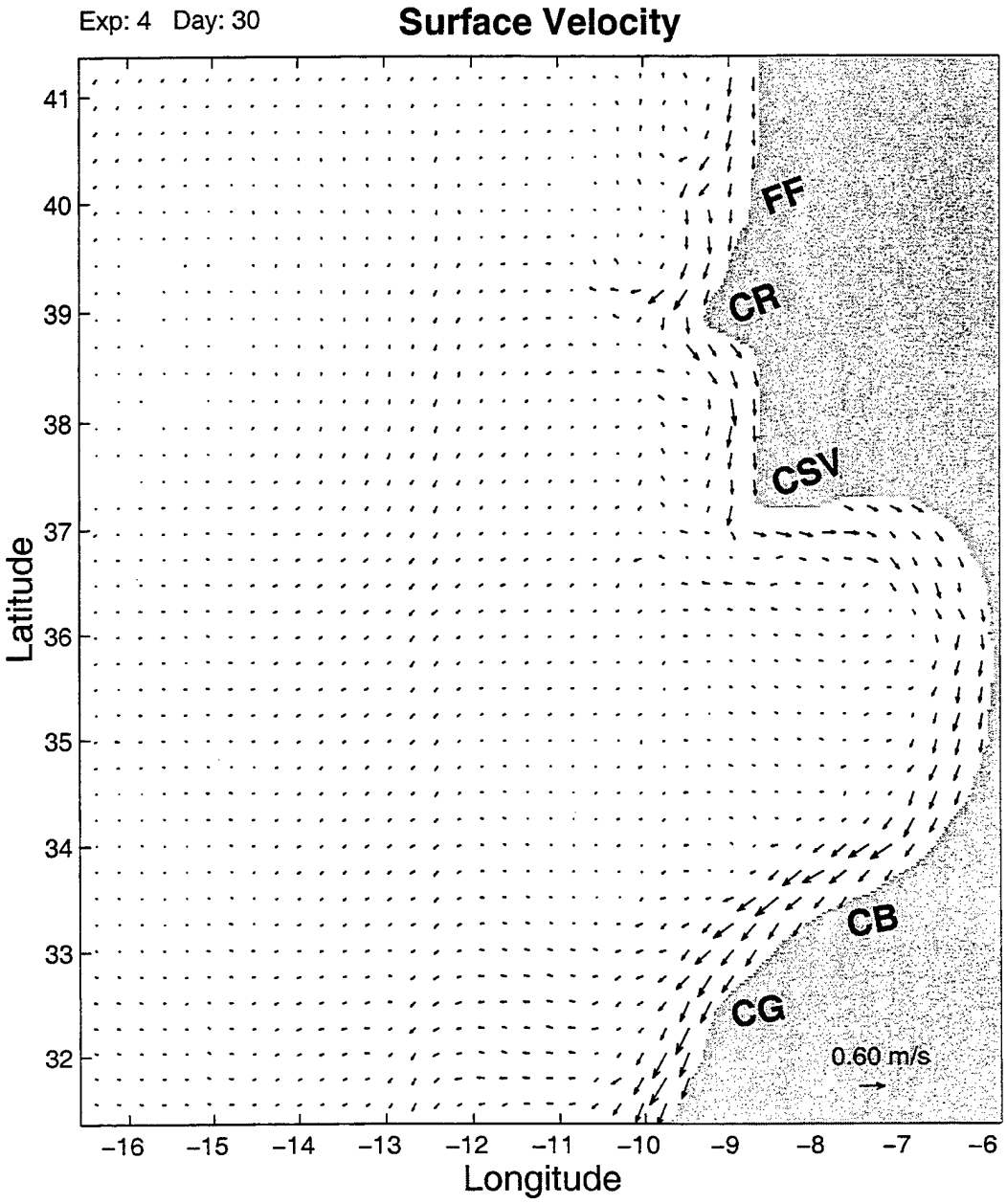

Figure 35. Surface velocity vectors for Experiment 4 on day 30.

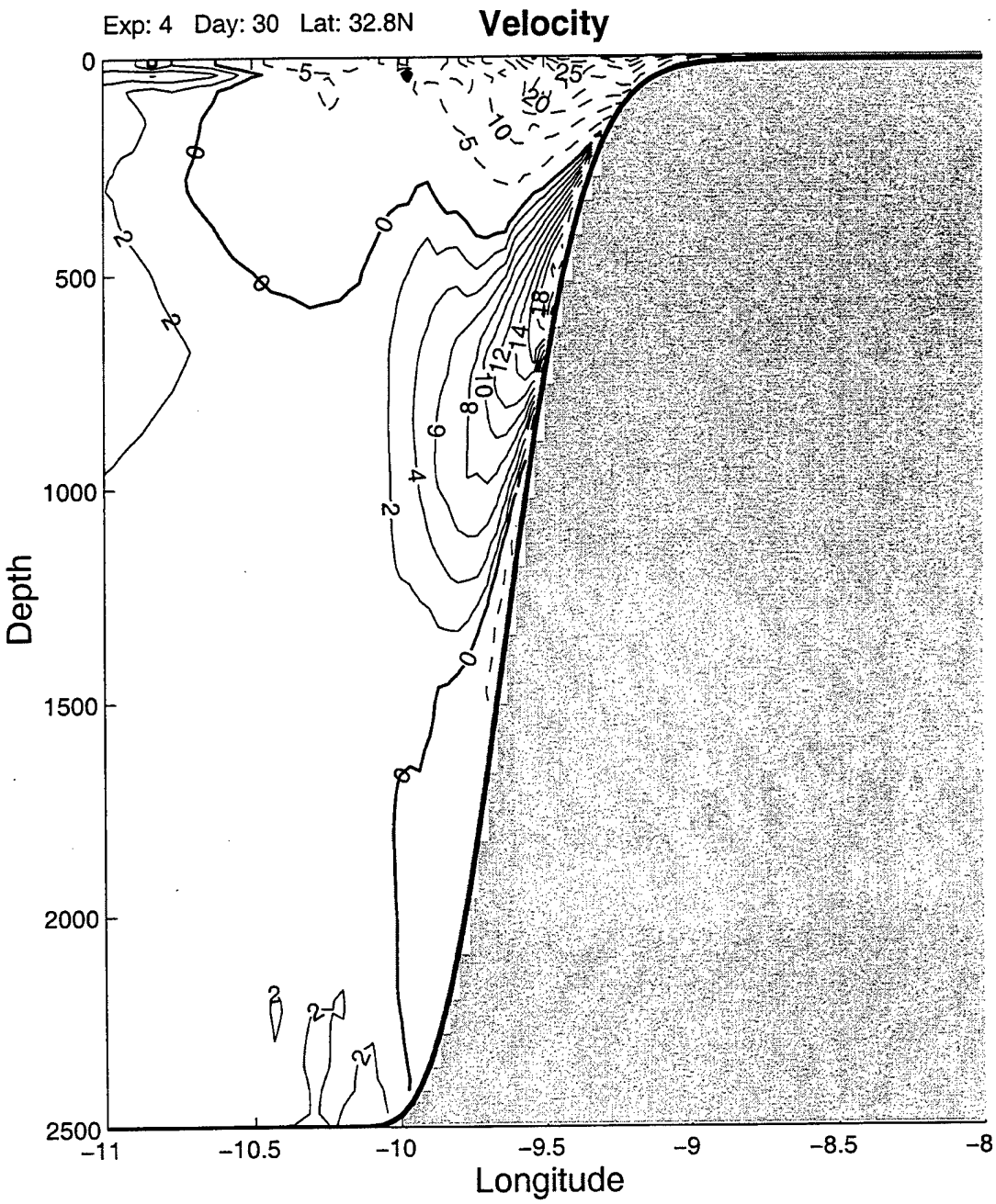

Cross-section of meridional velocity (v) at 32.8°N for Experiment 4 on day 30. Equatorward (poleward) flow is denoted by dashed (solid) lines with contour intervals of 5 cm/s (2cm/s).

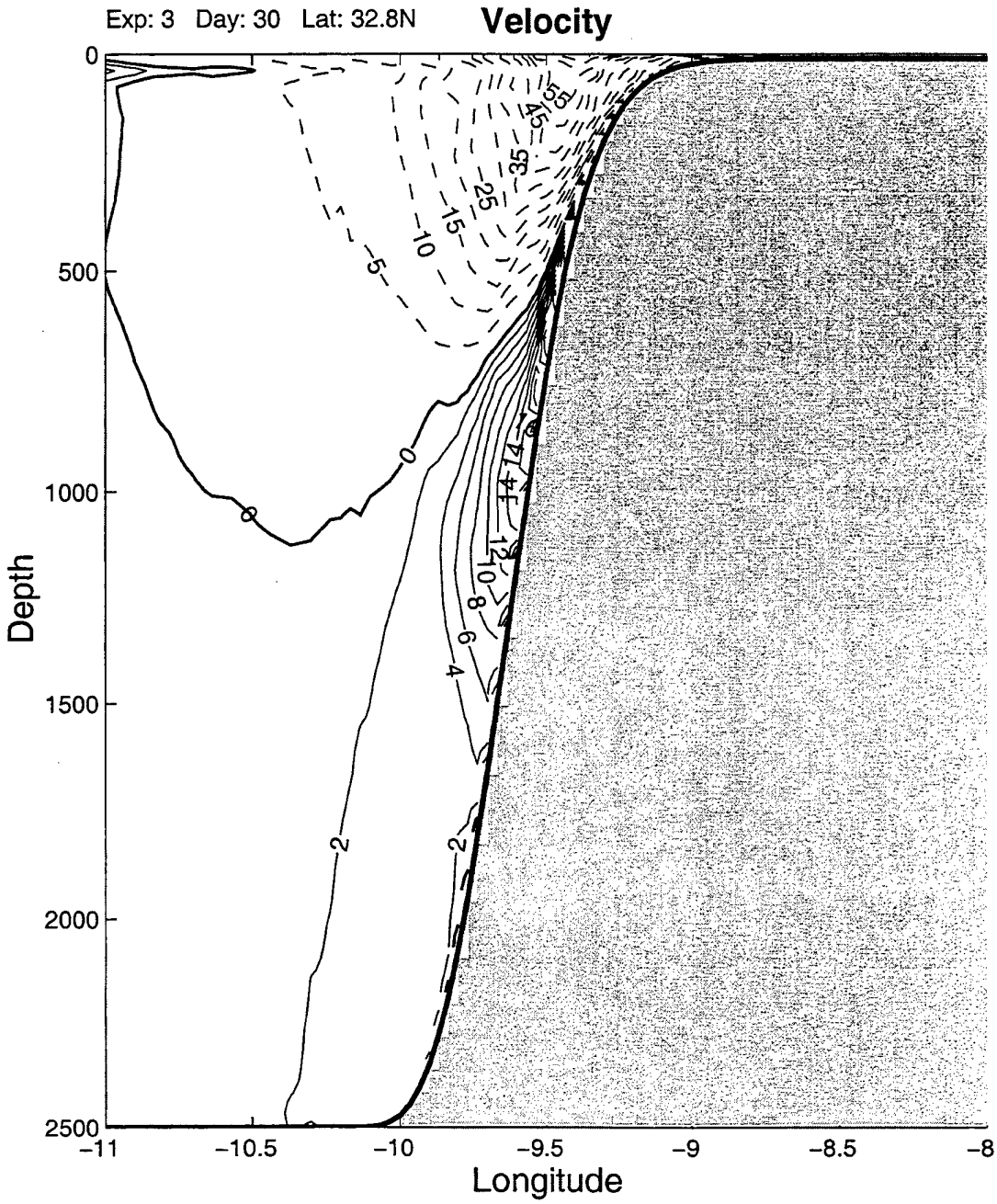

Figure 37. Cross-section of meridional velocity (v) at 32.8°N for Experiment 3 on day 30. Equatorward (poleward) flow is denoted by dashed (solid) lines with contour intervals of 5 cm/s (2cm/s).

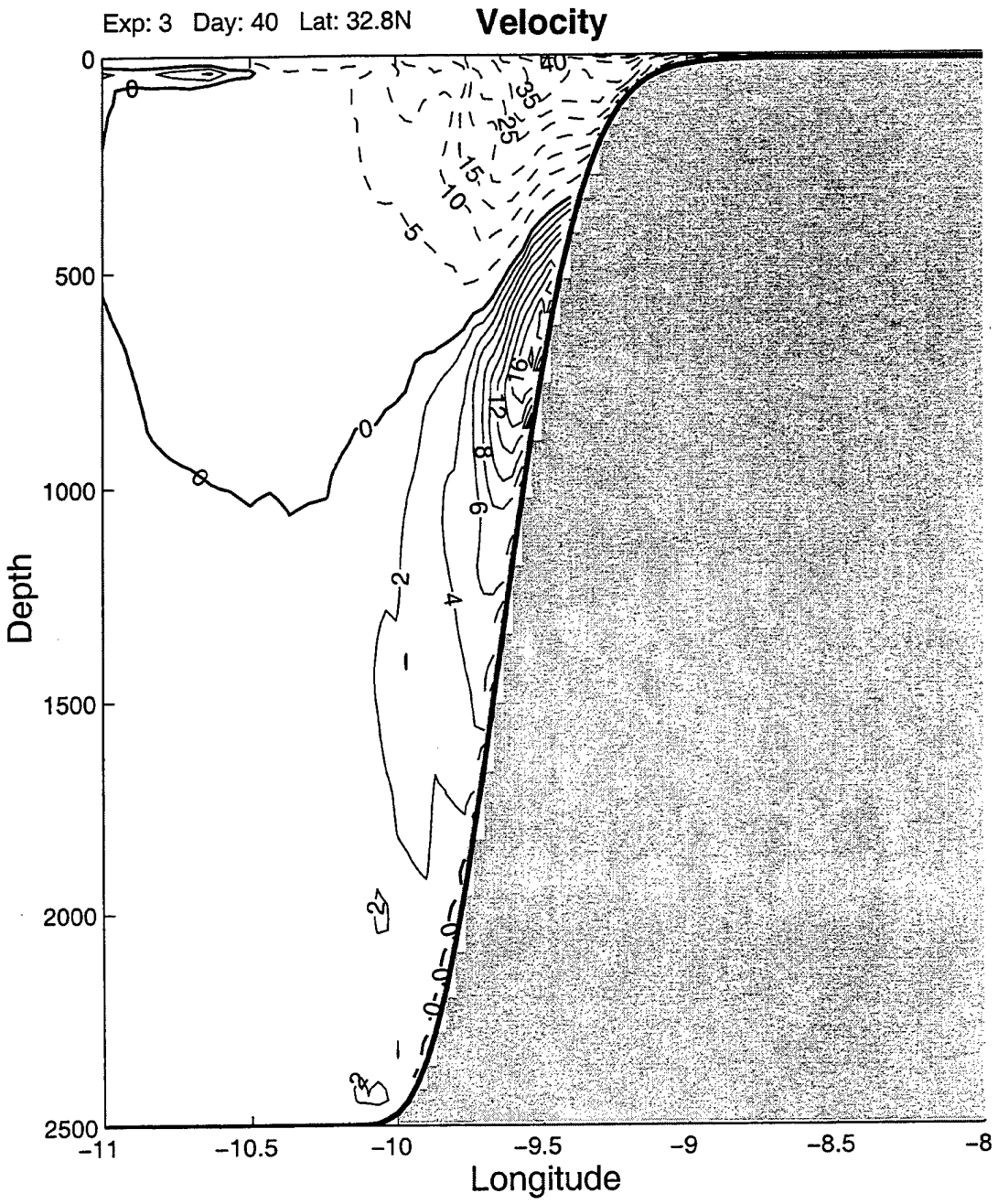

Figure 38. Cross-section of meridional velocity (v) at 32.8°N for Experiment 3 on day 40. Equatorward (poleward) flow is denoted by dashed (solid) lines with contour intervals of 5 cm/s (2cm/s).

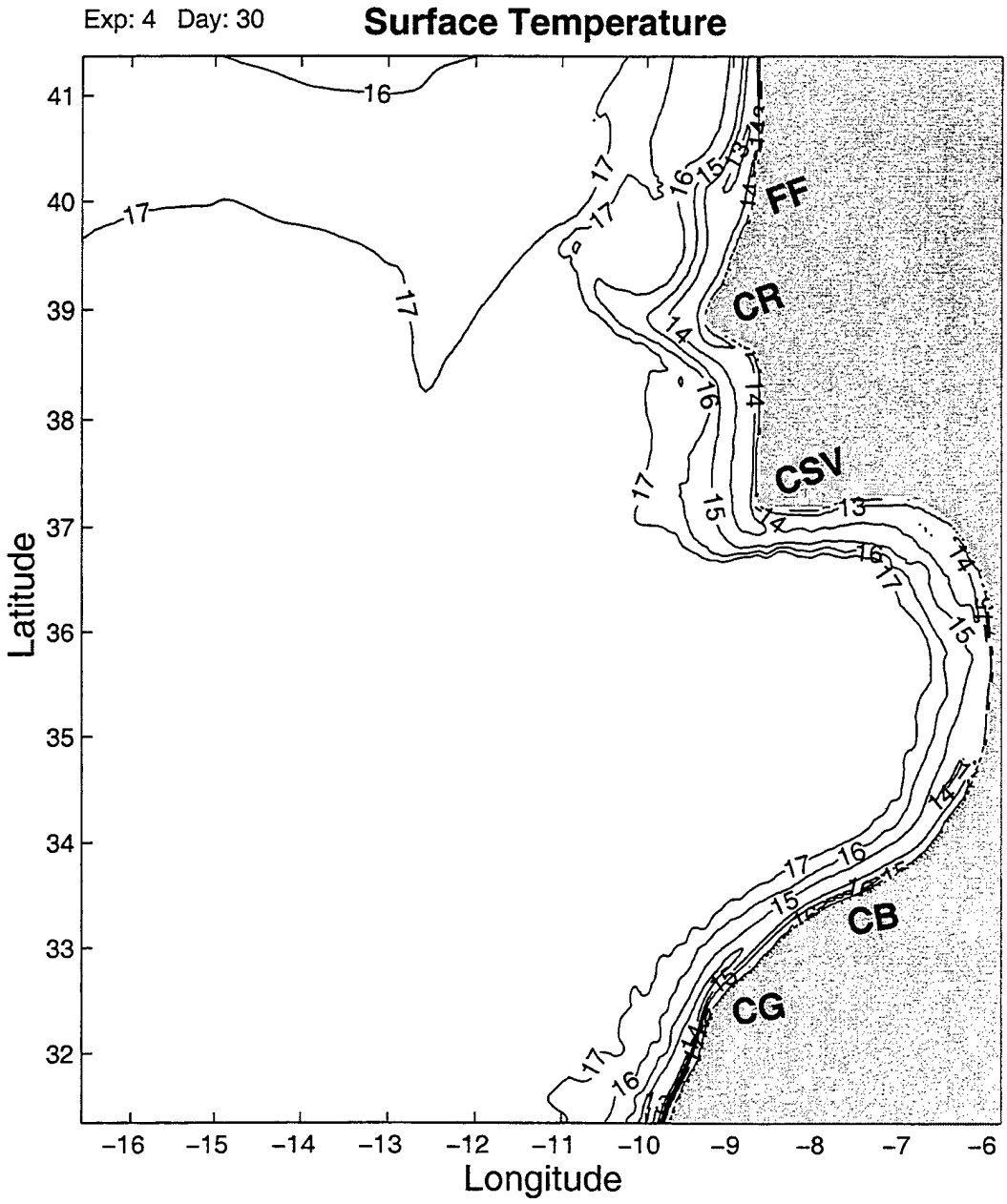

Figure 39. Surface temperature contours for Experiment 4 on day 30. Contour interval is 1°C.

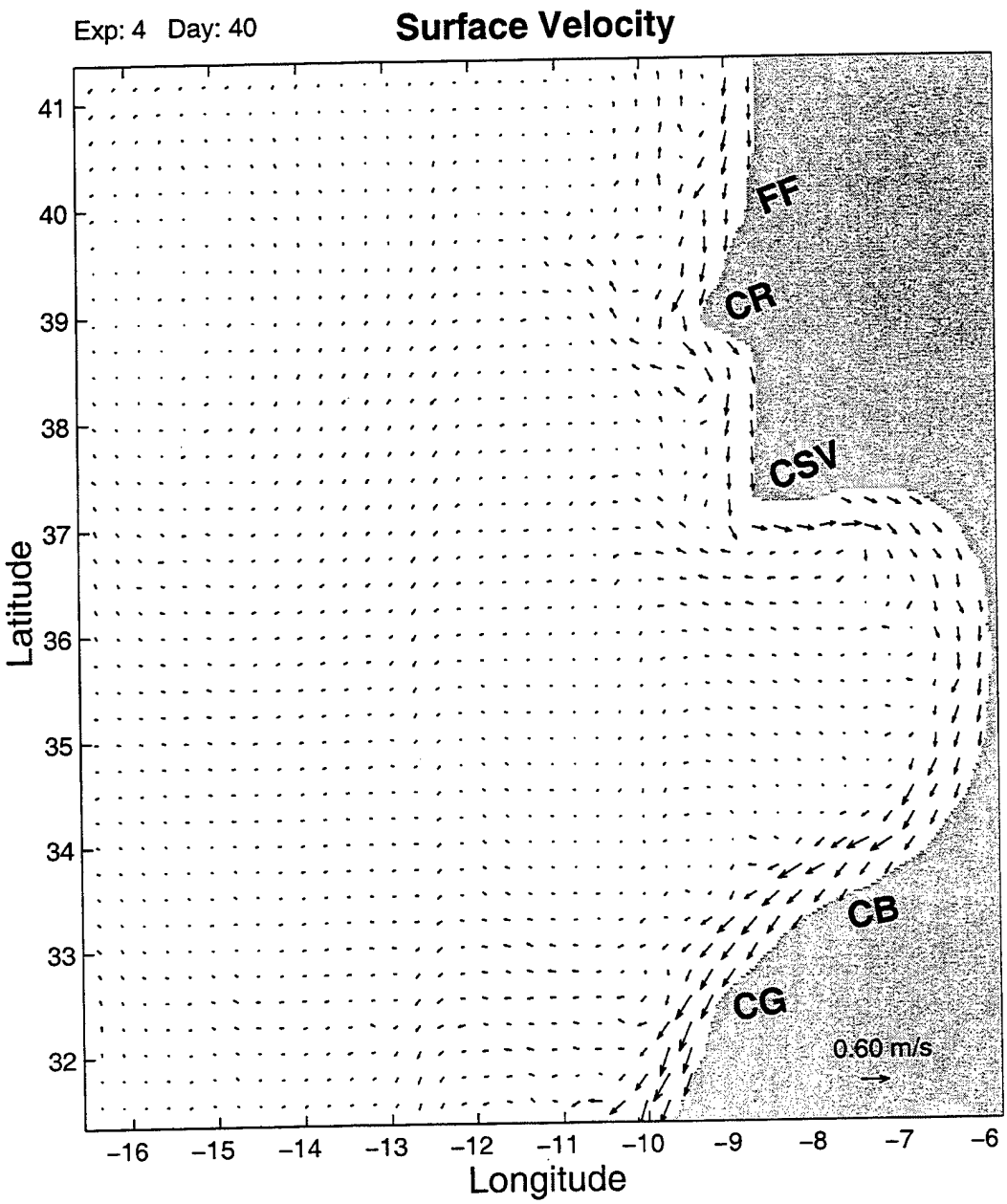

Figure 40. Surface velocity vectors for Experiment 4 on day 40.

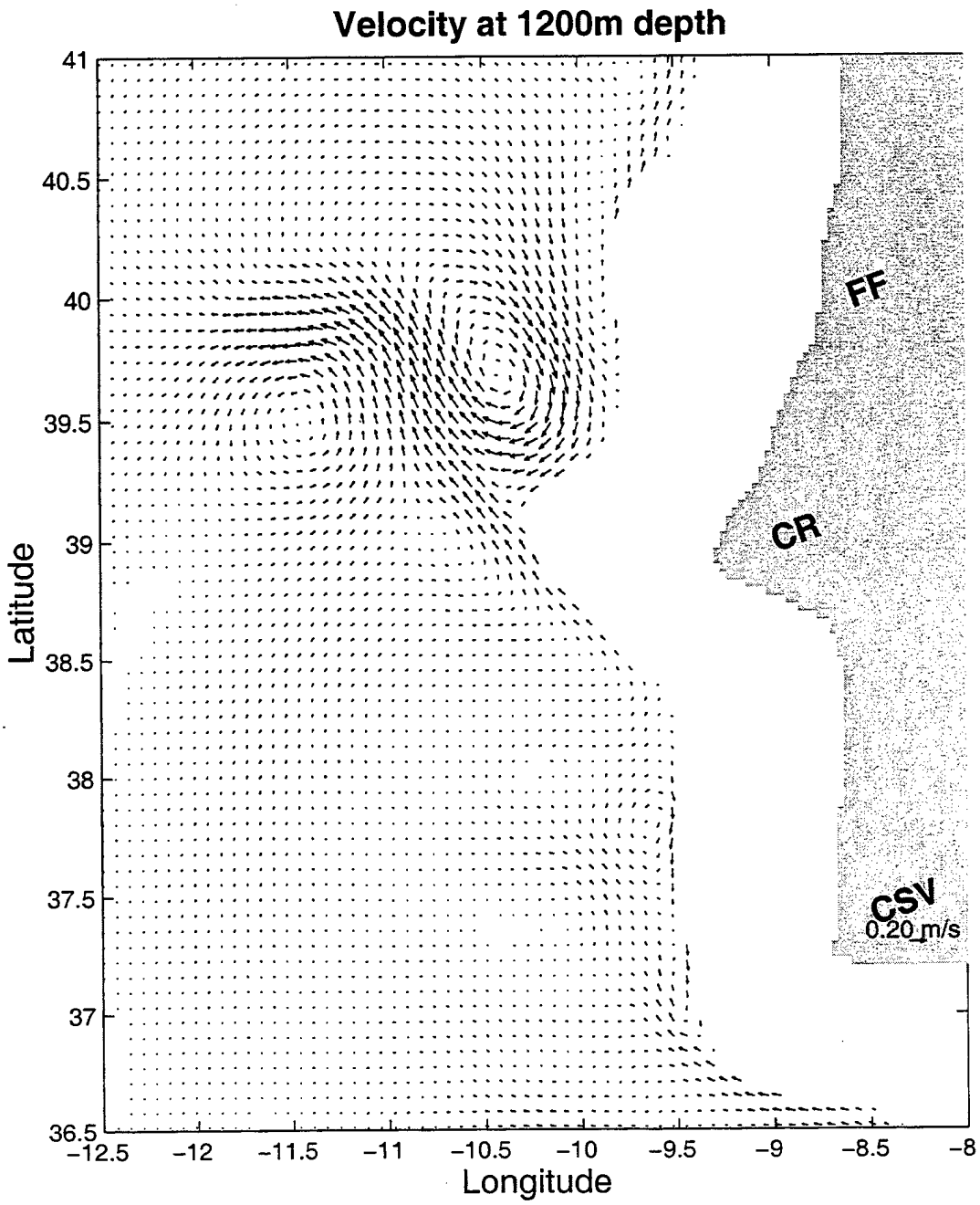

Figure 41. Velocity vectors at 1200 m depth for Experiment 4 on day 60.

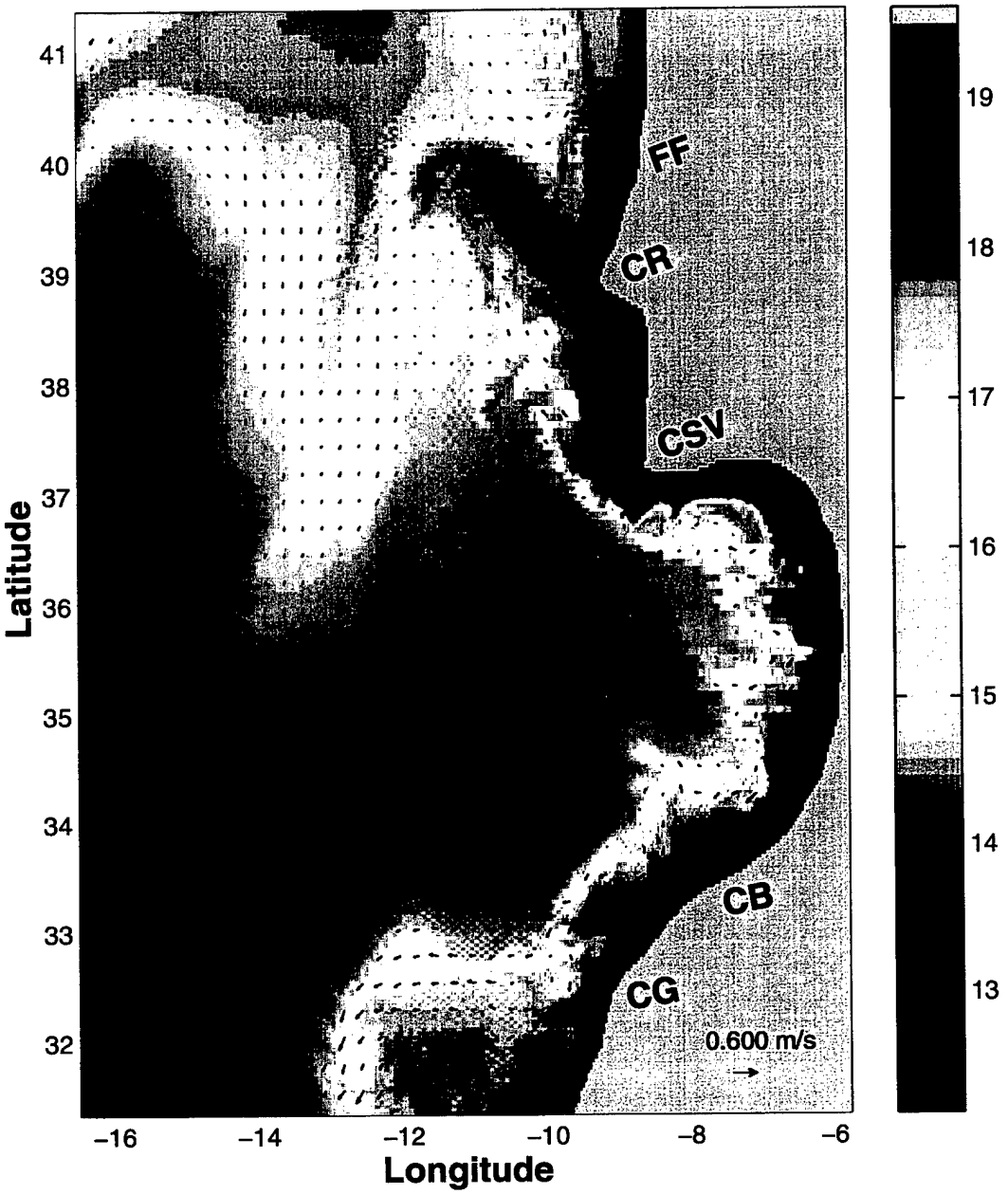

Figure 41. Surface velocity vectors (arrows) and temperatures (in color) for Experiment 4 on day 60.

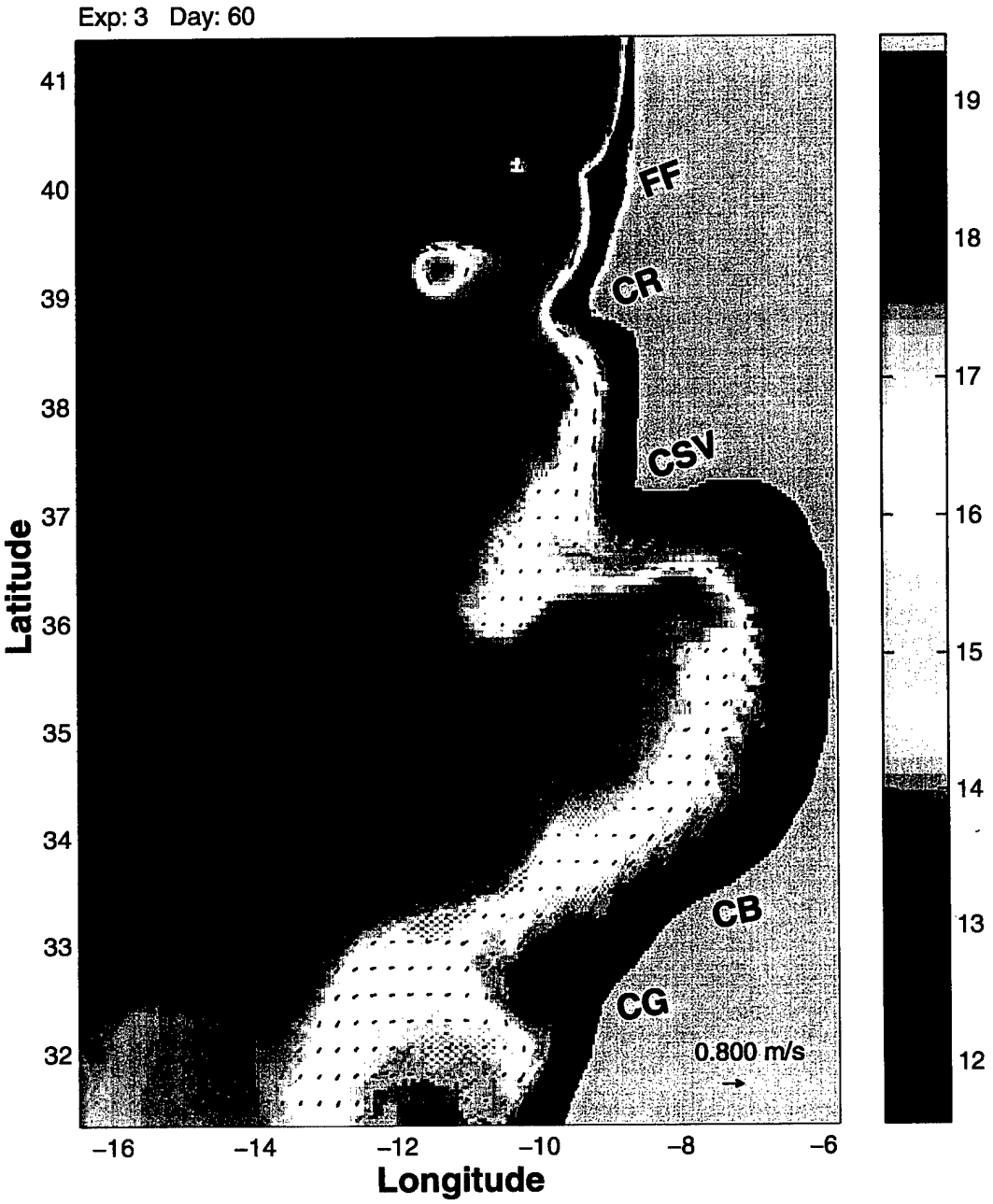

Figure 43. Surface velocity vectors (arrows) and temperatures (in color) for Experiment 3 on day 60.

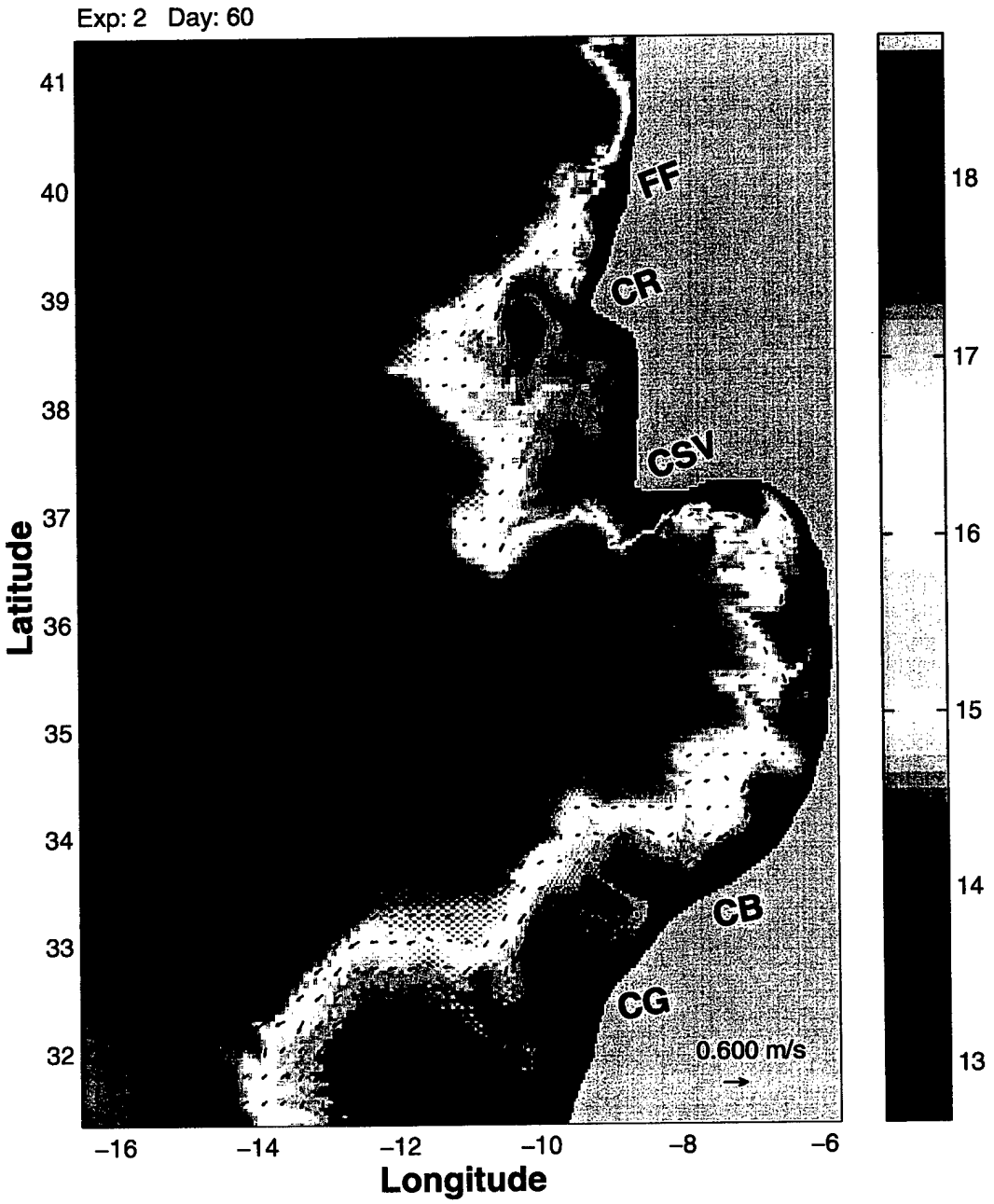

Figure 43. Surface velocity vectors (arrows) and temperatures (in color) for Experiment 2 on day 60.

THIS PAGE INTENTIONALLY LEFT BLANK

	EXPERIMENT 1	EXPERIMENT 2	EXPERIMENT 3	EXPERIMENT 4
ANNUAL WINDS	No	Yes	Yes	Yes
TOPOGRAPHY	Yes	No	Yes	Yes
TYPE OF ANNUAL CLIMATOLOGY	Horizontally Averaged	Horizontally Averaged	Horizontally Averaged	Full

Table 1. Summary of specific experimental design in this study

Level	Depth (m)	Level	Depth (m)	Level	Depth (m)
1	0	12	300	23	1400
2	10	13	400	24	1500
3	20	14	500	25	1750
4	30	15	600	26	200
5	50	16	700	27	2500
6	75	17	800	28	3000
7	100	18	900	29	3500
8	125	19	1000	30	4000
9	150	20	1100	31	4500
10	200	21	1200	32	5000
11	250	22	1300	33	5500

Table 2. Vertical levels and depths used by Levitus and Boyer (1994) and Levitus et al. (1994)

Level	Sigma Value	Level	Sigma Value
1	0	12	-0.61538
2	-0.00961	13	-0.69231
3	-0.01923	14	-0.76923
4	-0.03846	15	-0.84615
5	-0.07692	16	-0.92308
6	-0.15385	17	-0.96154
7	-0.23077	18	-0.98077
8	-0.30769	19	-0.99038
9	-0.38462	20	-0.99519
10	-0.46154	21	-1.0
11	-0.53846		

Table 3. Values of sigma levels

LIST OF REFERENCES

Ambar, I., and M.R. Howe. Observations of the Mediterranean Outflow – 1. Mixing in the Mediterranean Outflow. *Deep-Sea Res.*, 26, 535-554, 1979.

Barton, E.D., Eastern Boundary of the North Atlantic: Northwest Africa and Iberia. In *The Sea, Vol. 11, The Global Coastal Ocean: Regional Studies and Syntheses*, K.H. Brink and A.R. Robinson, eds., Wiley, New York, Chap.22, 633-657, 1998.

Batteen, M. L. and Y. -J. Han, On the Computational Noise of Finite Difference Schemes Used in Ocean Models, *Tellus,* 33, 387-396, 1981.

Batteen, M. L., R. L. Haney, T. A. Tielking, and P. G. Renaud, A Numerical Study of Wind Forcing of Eddies and Jets in the California Current System, *J. Mar. Res.*, 47, 493-523, 1989.

Batteen, M. L., Wind-Forced Modeling Studies of Currents, Meanders, and Eddies in the California Current System, *J. Geophys. Res.*, 102, 985-1009, 1997.

Batteen, M. L., J. R. Martinez, D. W. Bryan, and E. J. Buch, A Modeling Study of the Coastal Eastern Boundary Current System off Iberia and Morocco, *J. Geophys. Res*, 105 (C6), 14,173-14,195, 2000.

Batteen, M. L., and P. M. Murray, The Role of the Planetary Beta Effect on Currents and Meddies in the Northern Canary Current System, submitted, 2000.

Blumberg, A. F., and G. L. Mellor, A Description of a Three-Dimensional Coastal Ocean Circulation Model, *Three-Dimensional Coastal Ocean Models, Coastal Estuarine Sci.*, 4, edited by N. Heaps, pp 1-16, AGU, Washingtown, D. C., 1987.

Blumberg, A. F., and L. H. Khanta, Open Boundary Conditions for Circulation Models, *J. Hydraul. Eng.*, 11, 237-255, 1985.

Chapman, D. C., Numerical Treatement of Cross-Shelf Open Boundaries in a Barotropic Coastal Ocean Model, *Journal of Physical Oceanography*, 25, 1060-1075, 1985.

Ezer, T., On the Seasonal Mixed Layer Simulated by a Basin-Scale Ocean Model and the Mellor-Yamada Turbulence Scheme, *Journal of Geophysical Research*, 105 (C7), 16,843-16,855, 2000.

Ezer, T. and G. L. Mellor, Diagnostic and Prognostic Calculations of the North Atlantic Circulation and Sea Level Using a Sigma Coordinate Ocean Model, *Journal of Geophysical Research*, 99 (C7), 14,159-14,171, 1994.

Ezer, T. and G. L. Mellor, Simulations of the Atlantic Ocean With a Free Surface Sigma Coordinate Ocean Model, *Journal of Geophysical Research*, 102 (C7), 15,647-15,657, 1997.

Fiuza, A. F. de G., The Portuguese Coastal Upwelling System, in *Actual problems of Oceanography in Portugal, Junta Nacional de Investigacao Cientifica e Tecnologica, Lisboa,* 45-71, 1980.

Fiuza, A. F. de G., M. E. de Macedo, M. R. Guerreiro, Climatological Space and Time Variation of the Portuguese Coastal Upwelling, *Oceanologica Acta*, Vol. 5, No. 1, 31-40, 1982.

Fiuza, A. F. de G., Hidrologia e Dinamica das Aguas Costeiras de Portugal. Dissertacao apresentada a Universidade de Lisboa para obtencao do grau de Doutor em Fisica, especializacao em Ciencias Geofisicas. Univ Lisboa, 294pp., 1984.

Fiuza, A. F. de G. and F. M. Sousa, Preliminary Results of a CTD Survey in the Coastal Transition Zone off Portugal During 1-9 September 1988, *Coastal Transition Zone Newsletter,* 4, 2-9, 1989.

Frouin, R., A. F. G. Fiuza, I. Ambar, and T. J. Boyd, Observations of a Poleward Surface Current off the Coasts of Portugal and Spain During Winter, *J. Geophys. Res.,* 95, 679-691, 1990.

Gerdes, R., C. Köberle, A. Beckmann, P. Herrmann, and J. Willebrand, Mechanisms for Spreading of Mediterranean Water in Coarse-Resolution Numerical Models, *Journal of Physical Oceanography*, 29, 1682-1700, 1999.

Hagen, E., C. Zulicke, and R. Feistel, Near-Surface Structures in the Cape Ghir Filament off Morocco, *Oceanol. Acta*, 19, 6, 577-598, 1996.

Haynes, R. and E. D. Barton, A Poleward Flow Along the Atlantic Coast of the Iberian Peninsula, *J. Geophys. Res.,* 95, 11425-11441, 1990.

Haynes, R., E. D. Barton, and I. Pilling, Development, Persistence and Variability of Upwelling Filaments off the Atlantic Coast of Iberia, *J. Geophys. Res.,* 98, 22681-22692, 1993.

Haney, Robert L., On the Pressure Gradient Force Over Steep Topography in Sigma Coordinate Models, *Journal of Physical Oceanography*, 21, 610-619, 1991.

Iorga, M. C., and M. S. Lozier, Signatures of the Mediterranean Outflow From a North Atlantic Climatology, 1. Salinity and Density Fields, *J. Geophys. Res, 104,* 25,985-26,009, 1999.

Johnson, J., and I. Stevens, A Fine Resolution Model of the Eastern North Atlantic Between the Azores, the Canary Islands and the Gibraltar Strait, *Deep-Sea Research,* 47, 875-899, 2000.

Levitus, S., and T. P. Boyer, World Ocean Atlas 1994, Vol. 4: Temperature, *NOAA Atlas NESDI 4*, 117 pp., U. S. Dept. of Commerce, Washington, D.C., 1994.

Levitus, S., R. Burgett, and T.P. Boyer, World Ocean Atlas, 1994, Vol. 3: Salinity, *NOAA Atlas NESDI 3*, 99 pp., U.S. Dept. of Commerce, Washington, D.C., 1994.

Li, Z., and R. H. Weisberg, West Florida Shelf Response to Upwelling Favorable Wind Forcing: Kinematics, *Journal of Geophysical Research*, 104 (C6), 13,507-13,527, 1999.

Li, Z., and R. H. Weisberg, West Florida Shelf Response to Upwelling Favorable Wind Forcing 2. Dynamics, *Journal of Geophysical Research*, 104 (C10), 23,427-23,442, 1999.

Martisen, E. A., and H. Engedhal, Implementation and Testing of a Lateral Boundary Scheme as an Open Boundary Condition in a Barotropic Ocean Model, *Coastal Eng.*, 11, 603-627, 1987.

Meincke, J., G. Siedler, and W. Zenk,. Some cCurrent Observations Near the Continental Slope off Portugal, *"Meteor" Forsch.-Ergebn.*, A, 16, 15-22, 1975.

Mellor, G.L., User's Guide for a Three-Dimensional, Primitive Equation, Numerical Ocean Model, 40 pp, Program in Atmos. and Ocean Sci. report, Princeton Univ., Princeton, N. J. 1996.

Mellor, G.L., A. F. Blumberg, Modeling Vertical and Horizontal Diffusivities With the Sigma Coordinate System, *Mon. Weather Rev.*, 113, 1380-1383, 1985.

Mellor, G.L., L.Y. Oey, and T. Ezer, Sigma Coordinate Pressure Gradient Errors and the Seamount Problem, *Journal of Atmospheric and Ocean Technology*, 15, 1122-1131, 1998.

Mellor, G. L., and T. Yamada, Development of a Turbulence Closure Model for Geophysical Fluid Problems, *Rev. Geophys. Space Phys.*, 20, 851-875, 1982.

Mellor, G. L., and X. H. Wang, Pressure Compensation and the Bottom Boundary Layer, *Journal of Physical Oceanography*, 26, 2214-2222, 1996.

Nelson, C. S., Wind Stress and Wind Stress Curl Over the California Current, NOAA Tech Rep. NMFS SSFR-714, U. S. Dept. Commerce, 87 pp., 1977.

Palma E.D., and R. P. Matano, On the Implementation of Passive Open Boundary Conditions for a General Circulation Model: the Barotropic Mode, *Journal of Geophysical Research*, 103 (C1), 1319-1341, 1998.

Palma, E. D., and R. P. Matano, On the Implementation of Open Boundary Conditions for a General Circulation Model: the Three-Dimensional Case, *Journal of Geophysical Research*, 105 (C4), 8605-8627, 2000.

Sandwell, D.T., and W. F. Smith, Global Bathymetric Prediction for Ocean Modelling and Marine Geophysics, 1996.

Stammer, D., H. H. Hinrichsen, and R. H. Kase, Can Meddies Be Detected By Satellite Altimetry?, *J. Geophys. Res, 96*, 7005-7014, 1991.

Stevens, D. P., On Open Boundary Conditions for Three-Dimensional Primitive Equation Ocean Circulation Models, *Geophys. Astrophys. Fluid Dynamics*, 51, 103-133, 1990.

Tomczak, M. and J. S. Godfrey, *Regional Oceanography: An Introduction*, Pergamon Press, New York, 422 pp., 1994.

Van Camp, L., L. Nykjaer, E. Mittelstaedt, and P. Schlittenhardt, Upwelling and Boundary Circulation off Northwest Africa as Depicted by Infrared and Visible Satellite Observations, *Prog. Oceanog.*, 26, 357-402, 1991.

Wooster, W. S., A. Bakun, and D. R. McLain, The seasonal Upwelling Cycle Along the Eastern Boundary of the North Atlantic, *J. Mar. Res.*, 34, 131-140, 1976.

Yang,H., R. H. Weisberg, Response of the West Florida Shelf Circulation to Climatological Wind Stress Forcing, *Journal of Geophysical Research*, 104 (C3), 5301-5320, 2000.

Yanli, J., Formation of an Azores current Due to Mediterranean Overflow in a Modeling Study of the North Atlantic, *Journal of Physical Oceanography*, 30, 2342-2358, 2000.

INITIAL DISTRIBUTION LIST

No. Copies

1. Defense Technical Information Center.....2
   8725 John J. Kingman Rd, STE 0944
   Ft. Belvoir, VA 22060-6218

2. Dudley Knox Library.....2
   Naval Postgraduate School
   411 Dyer Rd
   Monterey, CA 93943-5101

3. Chairman (Code OC/Gd).....1
   Department of Oceanography
   Naval Postgraduate School
   Monterey, CA 93943-5122

4. Chairman (Code MR/Wx).....1
   Department of
   Naval Postgraduate School
   Monterey, CA 93943-5114

5. Dr. Mary L. Batteen, (Code OC/Bv).....3
   Department of Oceanography
   Naval Postgraduate School
   Monterey, CA 93943-5122

6. Dr. R. T. Williams, (Code OC/Co) 1
   Department of Meteorology
   Naval Postgraduate School
   Monterey, CA 93943-5122

7. LT Antonio Martinho, PON.....5
   5200 Coe Avenue, Apt. 1155
   Seaside, CA 93955

THIS PAGE INTENTIONALLY LEFT BLANK